

①

AFIT/GA/ENY/93D-4

**AD-A275 413**



**DTIC**  
**S** **E** **D**  
ELECTE  
FEB 03 1994

**ORBITAL APPLICATIONS OF  
ELECTRODYNAMIC PROPULSION**

**THESIS**  
**Troy Irwin**  
**Captain, USAF**

AFIT/GA/ENY/93D-4

125 PD

**93-30418**



Approved for public release; distribution unlimited

93 12 1508

**Best  
Available  
Copy**

AFIT/GA/ENY/93D-4

**ORBITAL APPLICATIONS OF  
ELECTRODYNAMIC PROPULSION**

**THESIS**

**Presented to the Faculty of the Graduate School of Engineering  
of the Air Force Institute of Technology  
Air University**

**In Partial Fulfillment of the  
Requirements for the Degree of  
Master of Science in Astronautical Engineering**

**DTIC QUALITY INSPECTED 8**

**Troy Irwin, B.S., M.S.  
Captain, USAF**

**December, 1993**

Accession For	
NTIS	CRA&I <input checked="" type="checkbox"/>
DTIC	TAB <input type="checkbox"/>
Unannounced <input type="checkbox"/>	
Justification .....	
By .....	
Distribution /	
Availability Codes	
Dist	Avail and/or Special
A-1	

**Approved for public release; distribution unlimited**

### *Acknowledgements*

I thank Dr. Curtis Spenny, my thesis advisor, for suggesting another research topic and allowing it to diverge to this challenging investigation of electrodynamic propulsion. His office door was always open, and he always found a way to convert my pessimism into optimism any time I came to talk to him.

Special thanks go the faculty of the University of Dayton School of Law, who kept my wife sufficiently occupied with her studies so she did not have a chance to notice how much she was neglected these past eighteen months. Even so, Vicki was a constant source of encouragement and support.

Troy Irwin

## *Table of Contents*

	<b>Page</b>
<b>Acknowledgements . . . . .</b>	<b>ii</b>
<b>List of Figures . . . . .</b>	<b>vi</b>
<b>List of Tables . . . . .</b>	<b>vii</b>
<b>List of Symbols . . . . .</b>	<b>ix</b>
<b>Abstract . . . . .</b>	<b>xiii</b>
 <b>I. Background and Problem Statement . . . . .</b>	 <b>1</b>
 <b>II. Theory &amp; Approach . . . . .</b>	 <b>4</b>
<b>2.1 Coordinate Systems . . . . .</b>	<b>4</b>
2.1.1 Geocentric Equatorial Frame . . . . .	4
2.1.2 Greenwich Equatorial Frame . . . . .	4
2.1.3 Geomagnetic Equatorial Frame . . . . .	5
2.1.4 Spherical Magnetic Frame . . . . .	5
2.1.5 Orbital Frame . . . . .	5
2.1.6 Orbital Reference Frame . . . . .	5
<b>2.2 Rotation Matrices . . . . .</b>	<b>6</b>
2.2.1 Orbital Frame to Geocentric Equatorial Frame . . . . .	6
2.2.2 Geocentric Equatorial Frame to Greenwich Equatorial Frame . . . . .	7
2.2.3 Greenwich Equatorial Frame to Geomagnetic Equatorial Frame . . . . .	7
2.2.4 Spherical Geomagnetic Frame to Geomagnetic Equatorial Frame . . . . .	7

	Page
2.3 Orbital Motion . . . . .	8
2.4 Lagrange's Planetary Equations . . . . .	9
2.5 Clohessy-Wiltshire Equations . . . . .	12
2.6 Electrodynamics . . . . .	13
2.6.1 Geomagnetic Field . . . . .	13
2.6.2 Electrodynamic Forces . . . . .	14
2.6.3 Specific Power & Energy . . . . .	17
2.7 Approach . . . . .	20
III. Orbital Plane Change . . . . .	22
3.1 Inclination Change . . . . .	22
3.1.1 Inclination Forcing Function . . . . .	22
3.1.2 Inclination Change Results . . . . .	25
3.2 Right Ascension of the Ascending Node Change . . . . .	32
3.2.1 Right Ascension of the Ascending Node Forcing Function . . . . .	34
3.2.2 Right Ascension of the Ascending Node Change Results . . . . .	37
3.3 Summary of Orbital Plane Change Results . . . . .	46
IV. Molniya Orbit Stationkeeping . . . . .	48
4.1 Effects of the Earth's Oblateness . . . . .	48
4.2 Desired Forcing Function . . . . .	49
4.3 Results . . . . .	53
V. Rendezvous & Docking . . . . .	62
5.1 Solutions to the Clohessy-Wiltshire Equations . . . . .	62
5.1.1 Decaying Solution . . . . .	63
5.1.2 Polynomial Solution . . . . .	65
5.2 Methodology of the Rendezvous & Docking Study . . . . .	66
5.3 Results . . . . .	68

	Page
VI. Conclusions & Recommendations . . . . .	78
Appendix A. File Listings . . . . .	80
Appendix B. Survey of Conducting Metals . . . . .	107
Bibliography . . . . .	108
Vita . . . . .	110

# *List of Figures*

Figure	Page
1. Closed Loop Conductor . . . . .	16
2. Geometry of the $\kappa$ Vector . . . . .	24
3. Case 2: Inclination Change . . . . .	26
4. Case 2: Right Ascension of the Ascending Node Change . . . . .	27
5. Case 1: $\kappa$ Profile (Amp·m/kg) . . . . .	28
6. Case 1: $P_r$ Profile (W/kg) . . . . .	29
7. Case 2: $\kappa$ Profile (Amp·m/kg) . . . . .	30
8. Case 2: $P_r$ Profile (W/kg) . . . . .	31
9. Case 2: $i^2 R$ and $iV_i$ Power . . . . .	32
10. Case 2: Accelerations (m/s <sup>2</sup> ) . . . . .	33
11. Case 2: Magnetic Field Near Revolution 4 . . . . .	34
12. Magnetic Field Components (Tesla) . . . . .	35
13. Case 2: Semi-major Axis Change . . . . .	36
14. Case 6: Semi-major Axis Change . . . . .	36
15. Case 4: Right Ascension of the Ascending Node Change . . . . .	39
16. Case 4: Inclination Change . . . . .	39
17. Case 4: $\kappa$ Profile (Amp·m/kg) . . . . .	40
18. Case 4: $P_r$ Profile (W/kg) . . . . .	41
19. Case 4: Accelerations (m/s <sup>2</sup> ) . . . . .	43
20. Case 4: Semi-major Axis Change . . . . .	44
21. $\bar{P}_r$ Required for $\Delta\Omega$ ( $m/m_e = 10$ ) . . . . .	44
22. $\bar{P}_r$ Required for $\Delta\Omega$ ( $m/m_e = 6$ ) . . . . .	45
23. $\bar{P}_r$ Required for $\Delta\Omega$ ( $m/m_e = 3$ ) . . . . .	46
24. Effect of Earth Oblateness on 24 Hour Polar Molniya Orbit . . . . .	49
25. Geomagnetic Field Strength for 24 Hour Polar Molniya Orbit, $\Omega_o = 141^\circ$ . . . . .	52

Figure	Page
26. Specific Energy Required for Molniya Stationkeeping . . . . .	54
27. Geomagnetic Field Strength for 24 Hour Polar Molniya Orbit, $\Omega_0 = 89^\circ$ .	54
28. Change in Semi-major Axis Due to Molniya Stationkeeping . . . . .	55
29. Change in Argument of Perigee for Molniya Stationkeeping . . . . .	56
30. Change in $I$ Due to Molniya Stationkeeping . . . . .	56
31. Change in $\Omega$ Due to Molniya Stationkeeping . . . . .	57
32. Electrodynamic Accelerations for Molniya Stationkeeping . . . . .	57
33. Change in $a$ for Molniya Stationkeeping . . . . .	58
34. Change in $e$ for Molniya Stationkeeping . . . . .	58
35. $\kappa$ Profile for Molniya Stationkeeping . . . . .	59
36. Power Profile for Molniya Stationkeeping . . . . .	59
37. Case 1: Decaying Solution . . . . .	70
38. Case 2: Polynomial Solution . . . . .	71
39. Case 3: Decaying Solution . . . . .	72
40. Case 4: Polynomial Solution . . . . .	73
41. Case 6: V-BAR Approach with Polynomial Solution . . . . .	75
42. Case 13: V-BAR Approach with Decaying Solution . . . . .	76

*List of Tables*

Table		Page
1.	Inclination Change Study Results . . . . .	26
2.	Right Ascension of the Ascending Node Change Study Results . . . . .	38
3.	Additional $\Delta\Omega$ Cases . . . . .	42
4.	Specific Power Requirements for a 24 Hour Polar Molniya Satellite . . . . .	61
5.	Rendezvous Power Results ( $m/m_e = 10$ ) . . . . .	68
6.	Rendezvous Final Position and Velocity Results . . . . .	69
7.	Additional Rendezvous Power Results . . . . .	74

### *List of Symbols*

Symbol	Units	Definition
$A$	$m^2$	Cross sectional area of conductor
$A_E$	$kg \cdot m^2$	Earth's moment of inertia about an axis perpendicular to the polar axis
$A_I$	$m/sec^2$	Acceleration constant for inclination change
$\hat{a}$		Orbital frame
$a$	$m$	Semi-major axis
$a_0$	$1/sec^2$	Constant of the decaying solution
$a_1$	$1/sec$	Constant of the decaying solution
$a_x$	$m$	Constant of the polynomial solution
$a_y$	$m$	Constant of the polynomial solution
$\underline{B}$	Tesla	Magnetic field vector
$B$	Tesla	Magnitude of $\underline{B}$
$B_\Omega$	$m/sec^2$	Acceleration constant for $\Omega$ change
$\hat{b}$		Geomagnetic equatorial frame
$b$	$m$	Constant of the decaying solution
$b_x$	$m/sec$	Constant of the polynomial solution
$b_y$	$m/sec$	Constant of the polynomial solution
$C_E$	$kg \cdot m^2$	Earth's moment of inertia about the polar axis
$\hat{c}$		Orbital reference frame
$c$	$m/sec$	Constant of the decaying solution
$c_x$	$m/sec^2$	Constant of the polynomial solution
$c_y$	$m/sec^2$	Constant of the polynomial solution
$d_x$	$m/sec^3$	Constant of the polynomial solution
$d_y$	$m/sec^3$	Constant of the polynomial solution

Symbol	Units	Definition
$E$	rad	Eccentric anomaly
$\mathcal{E}$	$\text{kg}\cdot\text{m}^2/\text{sec}^2$	Energy
$e$		Eccentricity
$e_x$	$\text{m}/\text{sec}^4$	Constant of the polynomial solution
$e_y$	$\text{m}/\text{sec}^4$	Constant of the polynomial solution
$\underline{F}$	$\text{kg}\cdot\text{m}/\text{sec}^2$	Force vector
$\underline{f}$	$\text{m}/\text{sec}^2$	Acceleration vector
$f$	$\text{m}/\text{sec}^2$	Acceleration
$G$	$\text{m}^3/\text{kg}\cdot\text{sec}^2$	Gravitational constant
$g$	rad/sec	Constraint function
$\hat{g}$		Greenwich equatorial frame
$\mathcal{H}$	$\text{Amp}^2\cdot\text{m}^2/\text{kg}^2$	Minimize function
$\overline{\mathcal{H}}$	$\text{Amp}^2\cdot\text{m}^2/\text{kg}^2$	Constrained minimize function
$h$		Equinoctial element equal to $e \sin \omega$
$I$	rad	Inclination
$\dot{I}$	rad/sec	Average inclination change rate
$i$	Ampere	Electrical current
$\hat{i}$		Geocentric equatorial frame
$k$		Equinoctial element equal to $e \cos \omega$
$k_1$	sec/m	Constraint function coefficient
$k_2$		Constraint function coefficient
$\underline{L}$	m	Conductor vector
$L$	m	Length of conductor exposed to $\underline{B}$ field
$\mathcal{L}$	m	Total conductor length
$M$	rad	Mean anomaly
$\mathcal{M}$	$\text{kg}\cdot\text{m}^3/\text{coul}\cdot\text{sec}$	Magnetic moment
$\hat{m}$		Spherical magnetic frame
$m$	kg	Total vehicle mass
$m_c$	kg	Conductor mass

Symbol	Units	Definition
$N$		Number of conductor turns
$\mathcal{N}$		Order
$n$	rad/sec	Mean motion
$\mathcal{O}$		Truncated Taylor series terms
$P$	Watts	Power
$P_s$	Watts/kg	Specific power
$\bar{P}_s$	Watts/kg	Average specific power
$p$	rad/sec	Poles of the characteristic equation
$q$	coul	Electric charge
$R$	Ohms	Resistance
$\mathcal{R}$		Rotation matrix
$\underline{r}$	m	Satellite radius vector
$r$	m	Satellite's distance from center of the Earth
$s$	rad	mean argument of latitude
$T$	sec	Orbital period
$t$	sec	Time
$t_f$	sec	Final time
$u$	rad	Argument of latitude
$V_i$	Volts	Induced voltage
$\mathcal{V}$	m <sup>3</sup>	Conductor volume
$\underline{v}$	m/sec	Velocity vector
$\underline{v}_B$	m/sec	$\underline{B}$ field velocity vector
$\underline{v}_{rel}$	m/sec	Relative velocity vector between satellite and $\underline{B}$ field
$x$	m	Radial distance from target to chase vehicle
$y$	m	In-track distance from target to chase vehicle
$z$	m	Out-of-plane distance from target to chase vehicle

Symbol	Units	Definition
$\delta$		Infinitesimal change
$\theta_s$	rad	Sidereal time
$\kappa$	Amp·m/kg	Current-length/mass parameter
$\underline{\kappa}$	Amp·m/kg	Current-length/mass vector
$\hat{\kappa}$		Unit vector in direction of $\underline{\kappa}$
$\lambda_m$	rad	Magnetic longitude
$\lambda$	Amp·m <sup>2</sup> /kg·sec·Tesla	Lagrange multiplier
$\mu$	m <sup>3</sup> /sec <sup>2</sup>	Gravitational parameter
$\nu$	rad	True anomaly
$\underline{\rho}$	m	Relative position vector from target to chase vehicle
$\rho_c$	kg/m <sup>3</sup>	Conductor mass density
$\rho_R$	Ohm·m	Resistivity
$\phi_m$	rad	Magnetic latitude
$\Omega$	rad	Right ascension of the ascending node
$\bar{\Omega}$	rad/sec	Average $\Omega$ change rate
$\omega$	rad	Argument of perigee
$\bar{\omega}$	rad/sec	Average $\omega$ change rate
$\omega_\oplus$	rad/sec	Angular velocity of Earth's rotation
Superscript $T$		Matrix transpose
Subscript $r$		Radial direction
Subscript $\theta$		In-track direction
Subscript $3$		Out of plane direction
Subscript $j$		$j$ th direction, $j = r, \theta, 3$
Subscript $o$		Initial condition
Subscript $f$		Final condition
$\dot{\phantom{x}}$		First derivative with respect to time
$\ddot{\phantom{x}}$		Second derivative with respect to time

*Abstract*

This thesis studies the feasibility of applying electrodynamic propulsion to three different orbital applications: orbital plane change, Molniya stationkeeping, and rendezvous and docking. Electrodynamic propulsion uses the forces resulting from electric currents flowing through conductors as a spacecraft travels through the Earth's magnetic field. A vehicle-independent expression for the specific power required for any maneuver is derived and used to assess the feasibility of electrodynamic propulsion. Analytical expressions for the desired accelerations and combined current-conductor vector for the plane change and Molniya studies are developed based on Lagrange's planetary equations. Solutions to the forced Clohessy-Wiltshire equations are developed to study in-plane rendezvous and docking. Results show electrodynamic propulsion can be used to change either inclination or right ascension of the ascending node at rates of approximately 0.4 degrees/day or higher with current spacecraft specific power technology. Electrodynamic propulsion can also be used to negate the effects of the Earth's oblateness on a 24 hour Molniya orbit at 90° inclination. The energy required for this maneuver is very sensitive to the right ascension of the ascending node, which determines the orientation of the orbital plane with respect to the magnetic field. Specific power requirements of the non-optimized acceleration and current-conductor algorithms are more than required for conventional electric rocket propulsion, but can be met by current spacecraft specific power technology. Rendezvous and docking are possible with electrodynamic propulsion, which offers the advantages of allowing a soft dock - relative velocities and accelerations decay to zero as the chase vehicle approaches the target - and lack of a thruster plume to impart momentum or contaminate the target vehicle. Approaches along the target velocity vector with no altitude change are possible with current spacecraft specific power. Approaches involving changes in altitude will be possible when modest improvements in spacecraft power are made.

# ORBITAL APPLICATIONS OF ELECTRODYNAMIC PROPULSION

## *I. Background and Problem Statement*

The concept of *electrodynamic propulsion* — using the earth's magnetic field as a source of spacecraft propulsion — has been described by NASA (12) and studied in depth by Lawrence (8) and Spenny (14). Lawrence and Spenny created a preliminary design for a large spacecraft, called the Precision Orbital Tracking Vehicle (POTkV), which was capable of precisely tracking other vehicles, docking, and performing gross orbital maneuvers. The POTkV used electrodynamic propulsion as its main propulsion source.

The fundamental theory behind the Lawrence design is the Lorentz equation, which states the force on a current conductor in a magnetic field is (12:131):

$$\underline{F}_B = i \underline{L} \times \underline{B} \quad (1)$$

where  $\underline{F}$  is the force exerted on the conductor by the magnetic field,  $i$  is the current flowing through the conductor,  $\underline{L}$  is a vector with magnitude equal to the conductor length which points in the direction of positive current flow, and  $\underline{B}$  is the geomagnetic field vector.

The POTkV conductors must make electrical contact with the plasma in the earth's ionosphere to close the current loop. Lawrence placed plasma-generating hollow cathodes (12:120-121) at the ends of POTkV conductors to make electrical contact with the plasma because this technology is the most promising for high current densities (8:1-2).

One of the drawbacks of the Lawrence/Spenny design is the large power requirement (14:19). One way to reduce the power requirement is to conduct the current through some medium with less resistance than the ionosphere. Ladouceur's *closed loop circuit* is just such a system (7). In Ladouceur's concept, one half of a continuous conductor loop is shielded from the magnetic field. Theoretically, the current inside the shielded half of the conductor loop will be unable to interact with both the magnetic field of the Earth and

the magnetic field of the unshielded half. The torque usually associated with a current flowing through a loop in a magnetic field will not exist (17:204-205); instead, there will be a non-zero resultant force which can be used for thrust.

The POTkV design can be modified to incorporate the closed loop circuit, but are there other feasible applications for electrodynamic propulsion and the closed loop circuit? That is the question this thesis attempts to answer. We will derive a general equation for the electrical power and energy required to perform an orbital maneuver. Power and energy will then be used to evaluate the potential performance of the closed loop conductors for several candidate applications.

Several criteria can be used to select - or eliminate - potential applications for electrodynamic propulsion. The first criterion is to perform thrusting at low altitude, since the magnitude of  $B$  drops off with the inverse cube of the distance from the center of the Earth, as we shall see later. The second criterion is to use relatively small thrust. As elegant as the Lorentz equation is, the resulting forces for any reasonable current level are small, and there is no value in studying high thrust applications. A third criterion is for an application to exploit the unique feature of electrodynamic propulsion: during rendezvous and docking there is no exhaust plume to impart momentum to a target vehicle from a chase vehicle (8:3).

A recent survey of electric rocket propulsion (thrust which is dependent upon the expulsion of mass) by Janson and others identifies near and far term applications (4). Several of these applications meet the first two criteria, and have been selected for further study in this thesis. These include stationkeeping the argument of perigee ( $\omega$ ) of a  $90^\circ$  inclination Molniya orbit (4:9) and controlling the right ascension of the ascending node ( $\Omega$ ) of a sun synchronous low Earth orbit.

Other potential applications were inspired by Lawrence and Spenny. The POTkV design assumed a low inclination orbit, and classical electric propulsion was used for out of plane thrusts (8:4-16). Therefore, another potential application is the control of inclination. For this thesis, controlling inclination of a low Earth orbit in the vicinity of  $90^\circ$  will be studied. The methodology will be nearly identical to the sun synchronous  $\Omega$  control case

discussed above, and we will refer to the two collectively as orbital plane change. To satisfy the third criterion, we will study rendezvous between two spacecraft in low altitude, low inclination orbit.

For each application we will model the electrodynamic accelerations and their resulting effects on the orbit, then compute the power and energy required for each maneuver. Janson reports the current state of the art in spacecraft specific power is four Watts/kilogram (W/kg) (4:3), and we will use this as a benchmark in evaluating the applications we study. We will determine whether each application is feasible for electrodynamic propulsion based on a) ability to perform the stated objective, b) the electrical power required compared to the four W/kg benchmark, and c) the existence any undesirable side effects.

We will not attempt to optimize the implementation of electrodynamic propulsion — our goal is to show it *can* be done, not how it *can best* be done. Optimization is left as a challenge for future researchers.

In this chapter we have discussed the recent history of studies in electrodynamic propulsion and identified the potential new applications for electrodynamic propulsion we will study. Chapter two introduces all the necessary definitions and theory we will use to study each application. Chapters three through five study the areas of orbital plane change, polar Molniya stationkeeping, and rendezvous respectively, and may be read independent of each other. The final chapter summarizes important results and makes recommendations for further research. The appendices contain computer file listings, and information about potential conducting metals for the closed circuit conductor.

## II. Theory & Approach

In this chapter we develop the theory necessary to study the proposed applications of electrodynamic propulsion. We will define the various coordinate frames and the rotation matrices between each frame. The unforced orbital motion will be described, and then we will introduce Lagrange's planetary equations as a tool to use in studying the Molniya and plane change applications. The Clohessy-Wiltshire equations will be presented for use in the rendezvous problem. We will model the magnetic field and the electrodynamic forces, and derive an expression for the specific power required for each maneuver. Finally, we integrate all the theory into an overall approach to each study.

### 2.1 Coordinate Systems

This section defines the coordinate systems used in this thesis.

**2.1.1 Geocentric Equatorial Frame.** The origin of the geocentric equatorial frame ( $\hat{i}$ ) is at the center of the earth. The fundamental plane is the equator and the  $\hat{i}_1$  unit vector points in the vernal equinox direction. The  $\hat{i}_3$  unit vector points in the direction of the north pole. The  $\hat{i}_2$  unit vector completes the right-handed orthogonal set (1:55) of this Cartesian frame. The  $\hat{i}$  frame is the inertial reference frame for this study.

**2.1.2 Greenwich Equatorial Frame.** The Greenwich equatorial frame ( $\hat{g}$ ) frame differs from the  $\hat{i}$  frame by a single rotation about  $\hat{i}_3$ . The angle of rotation  $\theta_g$  locates the Greenwich prime meridian with respect to  $\hat{i}_1$ . This angle is called the sidereal time and is calculated using the following simple formula (1:99):

$$\theta_g = \theta_{g_0} + \omega_{\oplus}(t - t_0) \quad (2)$$

where  $\theta_{g_0}$  is the value of  $\theta_g$  at reference time  $t_0$  and  $\omega_{\oplus}$  is the angular velocity of the earth's rotation. Although  $\theta_{g_0}$  for a given  $t_0$  is readily available from a source such as The Astronomical Almanac (16), we will use  $\theta_{g_0} = 0$  for all cases in this study without changing the significance of the results.

**2.1.3 Geomagnetic Equatorial Frame.** For this study, we place the origin of the geomagnetic equatorial frame ( $\hat{b}$ ) at the center of the Earth, and the fundamental plane is the geomagnetic equator. The  $\hat{b}_3$  unit vector points to the geomagnetic north pole, which we locate at  $78.3^\circ$  north and  $69^\circ$  west in the  $\hat{g}$  frame. The  $\hat{b}_1$  unit vector points to  $11.7^\circ$  south and  $69^\circ$  west in the  $\hat{g}$  frame. The  $\hat{b}_2$  unit vector completes the right hand coordinate system. This definition of the  $\hat{b}$  frame is based on Tascione's description of a dipole model of the Earth's magnetic field (15:33-34).

**2.1.4 Spherical Magnetic Frame.** The origin of the spherical magnetic frame ( $\hat{m}$ ) is at the center of the Earth. The  $\hat{m}_r$  unit vector is collinear with the satellite's radius vector  $\underline{r}$ . The unit vector  $\hat{m}_{\lambda_m}$  is perpendicular to  $\underline{r}$ , lies parallel to the geomagnetic equator, and points in the direction of increasing geomagnetic longitude. The unit vector  $\hat{m}_{\phi_m}$  completes the right handed coordinate system, pointing in the direction of increasing geomagnetic latitude.

**2.1.5 Orbital Frame.** The origin of the orbital frame  $\hat{a}$  is at the center of the Earth. The fundamental plane of the orbital frame is the orbital plane. The unit vector  $\hat{a}_r$  is fixed to  $\underline{r}$  and points radially outward. The unit vector  $\hat{a}_3$  is perpendicular to the orbital plane and collinear with the satellite's angular momentum vector. The  $\hat{a}_\theta$  unit vector lies in the orbital plane perpendicular to  $\underline{r}$  to complete the right handed coordinate system. The  $\hat{a}$  frame rotates with respect to the  $\hat{i}$  frame with angular velocity  $\underline{\omega}_a = \dot{\nu}\hat{a}_3$  where  $\dot{\nu}$  is the satellite's instantaneous angular velocity.

**2.1.6 Orbital Reference Frame.** The orbital reference frame ( $\hat{c}$ ) is parallel to the  $\hat{a}$  frame and the origin is at the end of  $\underline{r}$ . If the orbit is circular, the  $\hat{c}_\theta$  unit vector will coincide with the satellite's velocity vector. In that special case, this  $\hat{c}$  frame is the same as Lawrence's  $\hat{c}$  frame (8:2-1). The  $\hat{c}$  frame also rotates with respect to the  $\hat{i}$  frame with angular velocity  $\underline{\omega}_c = \dot{\nu}\hat{a}_3$ .

## 2.2 Rotation Matrices

In this section we will derive the rotation matrices we will need to transform vectors between the different coordinate systems defined in section 2.1. We use the notation  $\mathcal{R}^{12}$ , where  $\mathcal{R}^{12}$  is a matrix which transforms a vector basis from frame 2 to frame 1.

**2.2.1 Orbital Frame to Geocentric Equatorial Frame.** The orientation of a satellite's radius vector in space at any time is defined by three parameters:

- the right ascension of the ascending node,  $\Omega$ , the angle between the vernal equinox and line of nodes.
- inclination,  $I$ , the angle between the orbital plane and the equatorial plane.
- argument of latitude,  $u$ , the sum of the argument of perigee  $\omega$  and true anomaly  $\nu$ .

The process of rotating from the  $\hat{i}$  frame to the  $\hat{a}$  frame is described by rotating an angle  $\Omega$  about the inertial  $\hat{i}_3$  axis, then rotating an angle  $I$  about the new  $\hat{i}_1$  axis, and finally rotating an angle  $u$  about the newest  $\hat{i}_3$  axis. The rotation matrix  $\mathcal{R}^{ia}$  is formed by the product of three intermediate rotation matrices:

$$\mathcal{R}^{ia} = \mathcal{R}_3(\Omega)\mathcal{R}_1(I)\mathcal{R}_3(u)$$

where

$$\mathcal{R}_3(\Omega) = \begin{bmatrix} \cos \Omega & -\sin \Omega & 0 \\ \sin \Omega & \cos \Omega & 0 \\ 0 & 0 & 1 \end{bmatrix}$$

$$\mathcal{R}_1(I) = \begin{bmatrix} 1 & 0 & 0 \\ 0 & \cos I & -\sin I \\ 0 & \sin I & \cos I \end{bmatrix}$$

$$\mathcal{R}_3(u) = \begin{bmatrix} \cos u & -\sin u & 0 \\ \sin u & \cos u & 0 \\ 0 & 0 & 1 \end{bmatrix}$$

The resulting rotation matrix is:

$$\mathcal{R}^{ia} = \begin{bmatrix} \cos \Omega \cos u - \sin \Omega \cos I \sin u & -\cos \Omega \sin u - \sin \Omega \cos I \cos u & \sin \Omega \sin I \\ \sin \Omega \cos u + \cos \Omega \cos I \sin u & -\sin \Omega \sin u + \cos \Omega \cos I \cos u & -\cos \Omega \sin I \\ \sin I \sin u & \sin I \cos u & \cos I \end{bmatrix}$$

**2.2.2 Geocentric Equatorial Frame to Greenwich Equatorial Frame.** As mentioned in section 2.1.2, the  $\hat{g}$  frame differs from the  $\hat{i}$  by a rotation about  $\hat{i}_3$  through the angle  $\theta_g$ . Thus the matrix  $\mathcal{R}^{gi}$  which rotates a vector from the  $\hat{i}$  frame to the  $\hat{g}$  frame is:

$$\mathcal{R}^{gi} = \begin{bmatrix} \cos \theta_g & \sin \theta_g & 0 \\ -\sin \theta_g & \cos \theta_g & 0 \\ 0 & 0 & 1 \end{bmatrix}$$

**2.2.3 Greenwich Equatorial Frame to Geomagnetic Equatorial Frame.** Transforming a vector from the  $\hat{g}$  frame to the  $\hat{b}$  frame first requires a negative rotation about  $\hat{g}_3$  through  $69^\circ$  to the intermediate frame  $\hat{g}'$ . Then another negative rotation about  $\hat{g}'_2$  of  $11.7^\circ$  completes the transformation to the  $\hat{b}$  frame. The result is:

$$\begin{aligned} \mathcal{R}^{bg} &= \begin{bmatrix} \cos 11.7 & 0 & -\sin 11.7 \\ 0 & 1 & 0 \\ \sin 11.7 & 0 & \cos 11.7 \end{bmatrix} \begin{bmatrix} \cos 69 & -\sin 69 & 0 \\ \sin 69 & \cos 69 & 0 \\ 0 & 0 & 1 \end{bmatrix} \\ &= \begin{bmatrix} \cos 11.7 \cos 69 & -\cos 11.7 \sin 69 & -\sin 11.7 \\ \sin 69 & \cos 69 & 0 \\ \sin 11.7 \cos 69 & -\sin 11.7 \sin 69 & \cos 11.7 \end{bmatrix} \end{aligned}$$

**2.2.4 Spherical Geomagnetic Frame to Geomagnetic Equatorial Frame.** We transform vectors from the  $\hat{m}$  frame to the  $\hat{b}$  frame by making a negative rotation about  $\hat{m}_2$  through the magnetic latitude  $\phi_m$  to the intermediate frame  $\hat{m}'$ . Another negative rotation through the magnetic longitude  $\lambda_m$  about  $\hat{m}'_3$  completes the transformation to the  $\hat{b}$  frame.

The result is:

$$\begin{aligned}\mathcal{R}^{bm} &= \begin{bmatrix} \cos \lambda_m & -\sin \lambda_m & 0 \\ \sin \lambda_m & \cos \lambda_m & 0 \\ 0 & 0 & 1 \end{bmatrix} \begin{bmatrix} \cos \phi_m & 0 & -\sin \phi_m \\ 0 & 1 & 0 \\ \sin \phi_m & 0 & \cos \phi_m \end{bmatrix} \\ &= \begin{bmatrix} \cos \lambda_m \cos \phi_m & -\sin \lambda_m & -\cos \lambda_m \sin \phi_m \\ \sin \lambda_m \cos \phi_m & \cos \lambda_m & -\sin \lambda_m \sin \phi_m \\ \sin \phi_m & 0 & \cos \phi_m \end{bmatrix}\end{aligned}$$

We compute  $\lambda_m$  and  $\phi_m$  from the components of  $\underline{r}$  when expressed in the  $\hat{b}$  frame, denoted by  ${}^b\underline{r}$ , in the following manner. By definition

$${}^a\underline{r} = \begin{pmatrix} r \\ 0 \\ 0 \end{pmatrix}$$

Then

$${}^b\underline{r} = \mathcal{R}^{b'a'}\mathcal{R}^{a'i}\mathcal{R}^{is}{}^a\underline{r} = r_1\hat{b}_1 + r_2\hat{b}_2 + r_3\hat{b}_3$$

$\lambda_m$  and  $\phi_m$  are found by taking the inverse trigonometric functions of

$$\tan \lambda_m = \frac{r_2}{r_1}$$

and

$$\tan \phi_m = \frac{r_3}{\sqrt{r_1^2 + r_2^2}}$$

### 2.3 Orbital Motion

In this section we will describe the Keplerian motion of  $\underline{r}$  in the orbital plane (1:72-73, 185). The magnitude of  $\underline{r}$  is

$$r = \frac{a(1 - e^2)}{1 + e \cos \nu} \quad (3)$$

where  $a$  is the semi-major axis of the orbit,  $e$  is the eccentricity, and  $\nu$  is the true anomaly.

Write  $\underline{r} = r\hat{a}_r$ , treat  $a$  and  $e$  as constants, and differentiate to find  $\dot{\underline{r}}$  to be

$$\dot{\underline{r}} = \sqrt{\frac{\mu}{a(1-e^2)}} (e \sin \nu \hat{a}_r + (1 + e \cos \nu) \hat{a}_\theta) \quad (4)$$

To find  $\nu$  we first define the mean motion ( $n$ ) according to Kepler's third law:

$$n = \sqrt{\frac{\mu}{a^3}} = \frac{2\pi}{T} = \frac{dM}{dt} \quad (5)$$

where  $\mu$  is the gravitational parameter of the central body, and  $T$  is the period of the orbit. Integration of Equation (5) with respect to time yields the mean anomaly ( $M$ ):

$$M = n(t - t_o) + M_o \quad (6)$$

After numerically solving Kepler's transcendental equation

$$M = E - e \sin E \quad (7)$$

for the eccentric anomaly ( $E$ ), the inverse trigonometric function of

$$\cos \nu = \frac{\cos E - e}{1 - e \cos E} \quad (8)$$

gives  $\nu$ .

## 2.4 Lagrange's Planetary Equations

The foci of the plane change and Molniya studies will be how a force, besides the two body force, changes the orbital elements. For this, we turn to the force form of Lagrange's planetary equations. These equations describe the time derivatives of the classical elements  $a$ ,  $e$ ,  $I$ ,  $\Omega$ ,  $\omega$ , and  $M_o$  due to a perturbing acceleration,  $f_p$ , defined in  $\hat{a}$  frame components as:

$$\underline{f}_p \equiv f_r \hat{a}_r + f_\theta \hat{a}_\theta + f_3 \hat{a}_3$$

They are (18:37-38):

$$\frac{da}{dt} = \frac{2e \sin \nu}{n\sqrt{1-e^2}} f_r + \frac{2a\sqrt{1-e^2}}{nr} f_\theta \quad (9)$$

$$\frac{de}{dt} = \frac{\sqrt{1-e^2} \sin \nu}{na} f_r + \frac{\sqrt{1-e^2}}{na^2 e} \left( \frac{a^2(1-e^2)}{r} - r \right) f_\theta \quad (10)$$

$$\frac{dI}{dt} = \frac{r \cos u}{na^2 \sqrt{1-e^2}} f_3 \quad (11)$$

$$\frac{d\Omega}{dt} = \frac{r \sin u}{na^2 \sqrt{1-e^2} \sin I} f_3 \quad (12)$$

$$\frac{d\omega}{dt} = -\frac{\sqrt{1-e^2} \cos \nu}{nae} f_r + \frac{\sqrt{1-e^2}}{nae} \left( 1 + \frac{1}{1+e \cos \nu} \right) \sin \nu f_\theta - \frac{r \cot I \sin u}{na^2 \sqrt{1-e^2}} f_3 \quad (13)$$

$$\begin{aligned} \frac{dM_o}{dt} = & -\frac{1}{na} \left( \frac{2r}{a} - \frac{1-e^2}{e} \cos \nu \right) f_r - \frac{1-e^2}{nae} \left( 1 + \frac{r}{a(1-e^2)} \right) \sin \nu f_\theta \\ & + \frac{3}{2} t \sqrt{\frac{\mu}{a^5}} \frac{da}{dt} \end{aligned} \quad (14)$$

Unfortunately, Lagrange's planetary equations in this form pose several problems because of the way we intend to use them. First, notice  $dM_o/dt$  has a secular term. We will be integrating over an entire day, and this secular term will eventually become a nuisance. Battin shows how to eliminate this problem from the potential form of Lagrange's planetary equations (2:487-488), and the same procedure will eliminate  $t$  in Equation (14). Recall  $M = nt + M_o$  and differentiate with respect to time:

$$\frac{dM}{dt} = \frac{dn}{dt} t + n + \frac{dM_o}{dt} \quad (15)$$

Differentiate  $n = \sqrt{\mu/a^3}$  to find

$$\frac{dn}{dt} = -\frac{3n}{2a} \frac{da}{dt} \quad (16)$$

Substitute Equations (14) and (16) into Equation (15) and simplify:

$$\frac{dM}{dt} = n - \frac{1}{na} \left( \frac{2r}{a} - \frac{1-e^2}{e} \cos \nu \right) f_r - \frac{1-e^2}{nae} \left( 1 + \frac{r}{a(1-e^2)} \right) \sin \nu f_\theta \quad (17)$$

Thus we have a new time-independent expression for the mean motion as a function of the two body mean motion and the perturbing accelerations.

Equations (10), (13), and (17) pose a problem because they are singular in  $e$ . This is undesirable because we intend to study the orbital plane change of initially circular orbits. The problem is solved for  $dM/dt$  in this manner: for our circular orbit, which is perturbed to a near circular orbit, we can say  $\nu \approx M$  and  $\dot{\nu} \approx \dot{M}$ . Define a new angle called the *mean argument of latitude* as

$$s = \omega + M \quad (18)$$

and its derivative as

$$\frac{ds}{dt} = \frac{d\omega}{dt} + \frac{dM}{dt} \quad (19)$$

If we substitute Equations (3), (13), and (17) into Equation (19), simplify, and then expand in a Taylor series to first order in  $e$ , we find the  $ds/dt$  term of Lagrange's planetary equations to be

$$\frac{ds}{dt} = n - \frac{2}{an} f_r - \frac{\sin u}{an \tan I} f_s + \mathcal{O}(e) \quad (20)$$

The last problem to solve, and the most tedious, is the singularity in  $e$  of Equation (10). To do this we introduce two of the equinoctial elements (18:22):

$$h = e \sin \omega$$

$$k = e \cos \omega$$

Note we easily recover  $e$  from  $e = \sqrt{h^2 + k^2}$ . If we differentiate, substitute in Equations (10) and (13), neglect  $e^2$  terms, and simplify the resulting expressions are:

$$\begin{aligned} h &= e \sin \omega \\ \frac{dh}{dt} &= \frac{de}{dt} \sin \omega + e \cos \omega \frac{d\omega}{dt} \end{aligned} \quad (21)$$

$$= -\frac{\cos u}{na} f_r + \frac{(r+a) \sin u + hr}{na^2} f_\theta - \frac{kr \cot I \sin u}{na^2} f_3 \quad (22)$$

$$\begin{aligned} k &= e \cos \omega \\ \frac{dk}{dt} &= \frac{de}{dt} \cos \omega - e \sin \omega \frac{d\omega}{dt} \end{aligned} \quad (23)$$

$$= \frac{\sin u}{na} f_r + \frac{(r+a) \cos u + kr}{na} f_\theta + \frac{hr \cot I \sin u}{na^2} f_3 \quad (24)$$

Equations (9), (11), (12), (17), (20), (22), and (24) will be used in the plane change study. The Molniya study will use Equations (9-13) and (17).

## 2.5 Clohessy-Wiltshire Equations

We will use the Clohessy-Wiltshire equations to study the application of electrodynamic propulsion to rendezvous and docking. The Clohessy-Wiltshire equations are a linearized set of equations which describe the motion of one body with respect to another body in a nearby circular orbit. We will use the results of Kaplan's derivation (5:105-108).

Consider a body in a circular orbit with the  $\hat{c}$  frame attached to it as defined in section 2.1.6. We will refer to this orbit as the reference orbit or the target orbit, and the origin of the  $\hat{c}$  frame as the target. The position of another body orbiting near the target  $\underline{\rho}$  is given by

$$\underline{\rho} = x\hat{c}_1 + y\hat{c}_2 + z\hat{c}_3$$

and the relative translational equations of motion are:

$$\ddot{x} - 2n\dot{y} - 3n^2x = \frac{F_r}{m} = f_r \quad (25)$$

$$\ddot{y} + 2n\dot{x} = \frac{F_\theta}{m} = f_\theta \quad (26)$$

$$\ddot{z} + n^2z = \frac{F_3}{m} = f_3 \quad (27)$$

where  $f_r$ ,  $f_\theta$ ,  $f_3$  are the  $\hat{c}$  frame components of the non-gravitational accelerations acting on the vehicle. When  $f_r = f_\theta = f_3 = 0$ , Equations (25-27) can be solved in closed form to yield:

$$x(t) = -\left(\frac{2}{n}\dot{y}_o + 3x_o\right)\cos nt + \frac{1}{n}\dot{x}_o\sin nt + 4x_o + \frac{2}{n}\dot{y}_o \quad (28)$$

$$y(t) = y_o - (3\dot{y}_o + 6nx_o)t + \left(\frac{4}{n}\dot{y}_o + 6x_o\right)\sin nt + \frac{2}{n}\dot{x}_o\cos nt - \frac{2}{n}\dot{x}_o \quad (29)$$

$$z(t) = z_o\cos nt + \frac{1}{n}\dot{z}_o\sin nt \quad (30)$$

where  $x_o$ ,  $y_o$ , and  $z_o$  are the components of  $\underline{\rho}$  at time  $t = 0$ .

## 2.6 Electrodynamics

In this section we will describe our model of the geomagnetic field, model the forces, define a new vector  $\underline{\kappa}$  and derive an expression for the specific power required for any maneuver.

**2.6.1 Geomagnetic Field.** For this thesis we will use Tascione's simplified dipole geomagnetic field model (15:33-34). Tascione defines the magnetic field vector as

$$\underline{B} = \frac{2\mathcal{M}\sin\phi_m}{r^3}\hat{m}_r - \frac{\mathcal{M}\cos\phi_m}{r^3}\hat{m}_3 \quad (31)$$

where  $\mathcal{M}$  is the magnetic moment,  $\phi_m$  is the geomagnetic latitude as defined by section 2.2.4, and  $r$  is the distance from the center of the Earth.  $\mathcal{M}$  for the Earth is approximately  $8.05 \times 10^{15}$  kg-meters<sup>3</sup>/(coulomb-sec). To express  $\underline{B}$  in the  $\hat{a}$  frame we multiply by the

appropriate rotation matrices:

$${}^a\mathbf{B} = \mathcal{R}^{ia^T} \mathcal{R}^{j^T} \mathcal{R}^{b^T} \mathcal{R}^{bm} {}^m\mathbf{B} \quad (32)$$

**2.6.2 Electrodynamic Forces.** To determine the electrodynamic force, we return to Equation (1) and explore its derivation, which we find in Orear (11:350,374). We begin with the definition of force acting on a charge  $q$  moving through the magnetic field  $\mathbf{B}$  with velocity  $\mathbf{v}$ :

$$\mathbf{F} = q\mathbf{v} \times \mathbf{B} \quad (33)$$

Now consider the differential force  $d\mathbf{F}$  due to a differential charge  $dq$ , and replace  $\mathbf{v}$  with  $d\mathbf{L}/dt$ :

$$\mathbf{F} = dq \frac{d\mathbf{L}}{dt} \times \mathbf{B}$$

Rearrange terms and recognize the definition of current is  $i = dq/dt$ :

$$d\mathbf{F} = \frac{dq}{dt} d\mathbf{L} \times \mathbf{B} = i d\mathbf{L} \times \mathbf{B}$$

Finally, we assume the conductor  $\mathbf{L}$  is a straight line and integrate over the appropriate limits to obtain Equation (1)

$$\int_0^F d\mathbf{F} = i \int_0^L d\mathbf{L} \times \mathbf{B}$$

$$\mathbf{F} = i\mathbf{L} \times \mathbf{B}$$

The product  $i\mathbf{L}$  can be combined into one vector. Consider a vehicle with three mutually perpendicular conductors fixed parallel to the  $\hat{a}$  frame. Let positive current  $i$ , flow through conductor  ${}^a\mathbf{L} = \{N_r L_r, 0, 0\}$  in the plus  $\hat{a}_r$  direction, where  $N_r$  is the number of turns of a coiled conductor and  $L_r$  is the length of one loop of the conductor exposed to the  $\mathbf{B}$  field as shown in Figure 1. Then

$$\mathbf{F} = i_r \mathbf{L} \times \mathbf{B} = \begin{Bmatrix} 0 \\ -i_r N_r L_r B_3 \\ i_r N_r L_r B_0 \end{Bmatrix}$$

Divide by the satellite mass  $m$  so the acceleration due to the radial current/conductor becomes

$$\underline{f} = \frac{\underline{F}}{m} = \begin{pmatrix} 0 \\ -\frac{i_r N_r L_r}{m} B_3 \\ \frac{i_r N_r L_r}{m} B_\theta \end{pmatrix} \quad (34)$$

Define the parameter

$$\kappa_r \equiv \frac{i_r N_r L_r}{m}$$

and rewrite Equation (34) as

$$\underline{f} = \begin{pmatrix} 0 \\ -\kappa_r B_3 \\ \kappa_r B_\theta \end{pmatrix}$$

Similarly for currents  $i_\theta$  and  $i_3$  flowing in a positive direction through conductors  $\underline{L}_\theta = \{0 \ N_\theta L_\theta \ 0\}$  and  $\underline{L}_3 = \{0 \ 0 \ N_3 L_3\}$  respectively, define

$$\kappa_\theta \equiv \frac{i_\theta N_\theta L_\theta}{m}$$

and

$$\kappa_3 \equiv \frac{i_3 N_3 L_3}{m}$$

Then the accelerations due to  $\kappa_\theta$  and  $\kappa_3$  are

$$\underline{f} = \begin{pmatrix} \kappa_\theta B_3 \\ 0 \\ -\kappa_\theta B_r \end{pmatrix} \quad (35)$$

and

$$\underline{f} = \begin{pmatrix} -\kappa_3 B_\theta \\ \kappa_3 B_r \\ 0 \end{pmatrix} \quad (36)$$

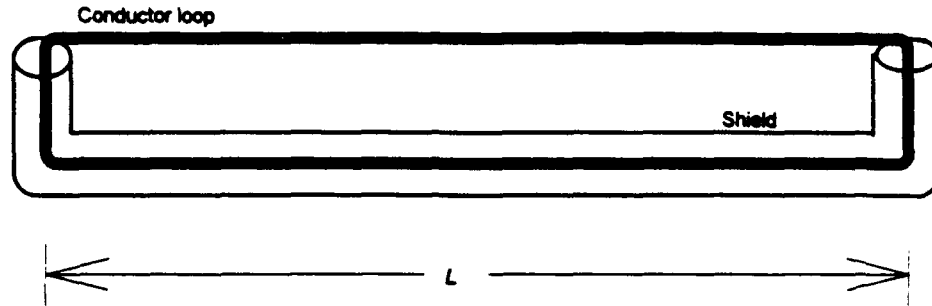


Figure 1. Closed Loop Conductor

Equations (34-36) can be combined to obtain the total acceleration resulting from  $\kappa_r$ ,  $\kappa_\theta$ , and  $\kappa_3$ :

$$\underline{f} = \begin{Bmatrix} \kappa_\theta B_3 - \kappa_3 B_\theta \\ \kappa_3 B_r - \kappa_r B_3 \\ \kappa_r B_\theta - \kappa_\theta B_r \end{Bmatrix} = \underline{\kappa} \times \underline{B} \quad (37)$$

where  $\underline{\kappa}$  is a vector defined by

$$\underline{\kappa} = \kappa_r \hat{a}_r + \kappa_\theta \hat{a}_\theta + \kappa_3 \hat{a}_3 \quad (38)$$

The new nomenclature  $\underline{\kappa}$  allows us to refer to the combined product of  $iNL$  in any one conductor without regard to the actual value of either  $i$ ,  $N$ , or  $L$ , and retains the 'per unit mass' definition we desire.

Note that although  $\underline{\kappa}$  can be specified in any direction, we cannot accelerate in any direction. Accelerations resulting from  $\underline{\kappa} \times \underline{B}$  are constrained to be perpendicular to both  $\underline{\kappa}$  and  $\underline{B}$  due to the nature of the cross product. Unless  $\underline{B}$  is perpendicular to the desired acceleration direction, Equation (37) will generate unwanted accelerations perpendicular to the desired acceleration direction. We will see the impact of this phenomenon in the orbital plane change and Molniya stationkeeping applications.

**2.6.3 Specific Power & Energy.** Now we will derive an expression for the specific power required to deliver the accelerations which result from Equation (37). The total power ( $P$ ) required to drive a current through the circuit which describes the motor/generator action of electrodynamic propulsion is (8:C-3)

$$P = iV_i + i^2 R \quad (39)$$

where  $V_i$  is the voltage induced across the conductor as it moves through the magnetic field and  $R$  is the total resistance of the conductor. Resistance is defined by (11:337-341)

$$R = \rho_r \frac{\mathcal{L}}{\mathcal{A}} \quad (40)$$

where  $\rho_r$  is the resistivity in Ohm-meters,  $\mathcal{L}$  is the entire length of conductor the current flows through in meters, and  $\mathcal{A}$  is the cross sectional area of the conductor in meters<sup>2</sup>. Note  $\mathcal{L} = 2NL$ , assuming the length of the portion of the conductor perpendicular to  $L$  is negligibly small compared to  $L$ , because the resistance dissipates power as the current flows through the entire conductor, including the shielded part. If we treat each conductor as a separate circuit, the total power is  $P = P_r + P_\theta + P_3$ .

We return to our definition of a component of  $\underline{\kappa}$ , which we now denote by  $\kappa_j$  ( $j = r, \theta, 3$ ), and solve for  $i_j$  to find

$$\begin{aligned} \frac{i_j N_j L_j}{m} &= \kappa_j \\ i_j &= \frac{\kappa_j m}{N_j L_j} \end{aligned}$$

Substituting this result, Equation (40), and  $\mathcal{L} = 2NL$  into  $i^2 R$  gives

$$i_j^2 R_j = \left( \frac{\kappa_j m}{N_j L_j} \right)^2 \left( \rho_r \frac{\mathcal{L}_j}{\mathcal{A}_j} \right) = 2\kappa_j^2 m^2 \frac{\rho_r}{N_j L_j \mathcal{A}_j} \quad (41)$$

Next, we assume a constant conductor cross sectional area  $\mathcal{A}_j$  and solve for the conductor volume  $\mathcal{V}_j = \mathcal{L}_j \mathcal{A}_j = 2N_j L_j \mathcal{A}_j$  in terms of the conductor mass  $m_c$ , and conductor mass density  $\rho_c$ :

$$\rho_c \equiv \frac{m_c}{\mathcal{V}_j} = \frac{m_c}{2N_j L_j \mathcal{A}_j}$$

$$N_j L_j A_j = \frac{m_{e_j}}{2\rho_c} \quad (42)$$

Replacing  $N_j L_j A_j$  in Equation (41) gives

$$i_j^2 R_j = 4\kappa_j^2 \frac{m^2}{m_{e_j}} \rho_n \rho_c \quad (43)$$

which is the power dissipated by the resistance in one conductor.

The induced voltage term of Equation (39) is given by (8:C-1)

$$V_i = -(\underline{v}_{rel} \times \underline{B}) \cdot (\underline{L}) \quad (44)$$

$\underline{v}_{rel} = \underline{v} - \underline{v}_B$  is the relative velocity of the conductor with respect to the magnetic field. The velocity of the satellite in  $\hat{a}$  frame components is given by Equation (4). To determine  $\underline{v}_B$  we begin in the  $\hat{g}$  frame, where  $\underline{B}$  is fixed. The velocity of  $\underline{B}$  due to the Earth's rotation then follows from

$$\begin{aligned} {}^g \underline{v}_B &= {}^g \underline{\omega}_\oplus \times {}^g \underline{r} \\ {}^a \underline{v}_B &= \mathcal{R}^{iaT} \mathcal{R}^{giT} {}^g \underline{v}_B \end{aligned} \quad (45)$$

where  ${}^g \underline{\omega}_\oplus = \{0 \ 0 \ \omega_\oplus\}^T$ . For the rest of the derivation we denote  $\underline{v}_{rel}$  by

$$\underline{v}_{rel} = v_{rel,r} \hat{a}_r + v_{rel,\theta} \hat{a}_\theta + v_{rel,z} \hat{a}_3$$

We proceed by expanding  $iV_i$  with our new expression for  $i$  and simplifying as follows:

$$\begin{aligned}
iV_i &= -i(\underline{v}_{rel} \times \underline{B}) \cdot \underline{L} \\
&= -i[N_r L_r (v_{rel\theta} B_3 - v_{rel3} B_\theta) + N_\theta L_\theta (v_{rel3} B_r - v_{relr} B_3) + N_3 L_3 (v_{relr} B_\theta - v_{rel\theta} B_r)] \\
&= -(i_r N_r L_r)(v_{rel\theta} B_3 - v_{rel3} B_\theta) - (i_\theta N_\theta L_\theta)(v_{rel3} B_r - v_{relr} B_3) \\
&\quad - (i_3 N_3 L_3)(v_{relr} B_\theta - v_{rel\theta} B_r) \\
&= -\kappa_r m (v_{rel\theta} B_3 - v_{rel3} B_\theta) - \kappa_\theta m (v_{rel3} B_r - v_{relr} B_3) - \kappa_3 m (v_{relr} B_\theta - v_{rel\theta} B_r) \\
&= -m [\kappa_r (v_{rel\theta} B_3 - v_{rel3} B_\theta) + \kappa_\theta (v_{rel3} B_r - v_{relr} B_3) + \kappa_3 (v_{relr} B_\theta - v_{rel\theta} B_r)] \quad (46)
\end{aligned}$$

Finally, we substitute Equations (43) and (46) into Equation (39), assume

$$m_{c_r} = m_{c_\theta} = m_{c_3} = m_c$$

and divide by the total satellite mass to obtain an expression for specific power ( $P_s$ ):

$$\begin{aligned}
P_s &= -\kappa_r (v_{rel\theta} B_3 - v_{rel3} B_\theta) - \kappa_\theta (v_{rel3} B_r - v_{relr} B_3) \\
&\quad - \kappa_3 (v_{relr} B_\theta - v_{rel\theta} B_r) + 4 \frac{m}{m_c} \rho_R \rho_c (\kappa_r^2 + \kappa_\theta^2 + \kappa_3^2) \quad (47)
\end{aligned}$$

Equation (47) provides insight to any system we might consider. First, Equation (47) is not configuration specific, although we must choose values of the conductor mass fraction  $m/m_c$  to study. Second, we see the  $\kappa_j^2$  terms will dominate  $P_s$  if  $\kappa_j$  is large, so it is important to minimize  $m/m_c$  and the product  $\rho_R \rho_c$ . The limiting value of  $m/m_c$  is 3, which implies the entire vehicle is consists of only the three conductors with no bus, power supply, or payload. For most of this study, we will use the value  $m/m_c = 10$ , meaning 30% of the vehicle mass is in the conductors. To show the affect of varying  $m/m_c$ ,  $m/m_c = 6$  (50% conductor mass) and  $m/m_c = 3$  (100% conductor mass) will also be investigated for several cases. The product  $\rho_R \rho_c$  depends on the conductor material we select. Appendix B presents the results of a survey of common conducting metals. Aluminum has the lowest  $\rho_R \rho_c$  product, so we use the value  $(\rho_R \rho_c)_{Al} = 7.2 \times 10^{-5}$  Ohms·kg/meter<sup>2</sup> for this study.

Although  $\rho_n \rho_c$  can potentially be made quite small with a superconductor, this was not investigated.

Note the last term in Equation (47) is always positive. Other terms can be negative, depending on the sign of  $\kappa_j$  and the sign of each bracketed quantity. A negative  $P_i$  implies regeneration, i.e. storage of energy rather than expenditure.

For particular orbits some terms in Equation (47) are small compared to others. For example, consider a low inclination circular orbit.  $B_r$  and  $B_\theta$  are small compared to  $B_\phi$ , and  $v_{rel,r} \approx 0$  and  $v_{rel,\theta} \approx 0$ . Therefore the second and third bracketed terms are small compared to the first. This leads to the conclusion that the  $\kappa_r$  conductor is the primary source of any regeneration which may occur in this special case.

In addition to the instantaneous power requirement given by Equation (47), we will be interested in the total energy ( $\mathcal{E}$ ) required to perform a given maneuver. To find energy we will simply integrate the power over the thrust duration, or

$$\mathcal{E} = \int_{t_0}^{t_f} P(t) dt$$

where  $t_0$  and  $t_f$  mark the beginning and end of the thrust period. We will perform this integration numerically using the trapezoidal rule (6:979).

Dividing the energy by the thrust time gives the average specific power  $\bar{P}_s$ :

$$\bar{P}_s = \frac{\mathcal{E}}{t_f - t_0}$$

## 2.7 Approach

In this section we describe how the theory we have presented is applied to each study. The general approach is as follows.

1. Specify all constants.
2. Specify initial values of all orbital elements.
3. Calculate  $\hat{r}$ .
4. Rotate  $\hat{r}$  from the  $\hat{a}$  frame to the  $\hat{b}$  frame.

5. Calculate  $\lambda_m$  and  $\phi_m$ .
6. Rotate  $\underline{r}$  from the  $\hat{b}$  frame to the  $\hat{m}$  frame.
7. Calculate  $\underline{B}$ .
8. Rotate  $\underline{B}$  from the  $\hat{m}$  frame to the  $\hat{a}$  frame.
9. Calculate  $\underline{\kappa}$ . This will be done with algorithms developed in later chapters specific to each case.
10. Calculate and store specific power.
11. Calculate  $\underline{f} = \underline{\kappa} \times \underline{B}$ .
12. Evaluate Lagrange's planetary equations.
13. Numerically integrate the orbital elements from  $t_1$  to  $t_2$  with the Euler method (6:1063-1064).
14. Repeat steps 3 through 13 until the final time.
15. Integrate specific power to obtain total specific energy.
16. Calculate average specific power.

This procedure was implemented with the MATLAB interactive software package (13). The script and function files are listed in Appendix A. Any case-specific deviations or simplifications to the procedure are described in Chapters 3-5.

### III. Orbital Plane Change

In this chapter we will investigate the applicability of electrodynamic propulsion to orbital plane change. First we will study inclination change, then we will look at changing the right ascension of the ascending node. In both studies we neglect plane changes due to any other accelerations, such as Earth oblateness or Sun-Moon perturbations.

#### 3.1 Inclination Change

Studying inclination change interests us for several reasons. First, Lawrence restricted his studies to in-plane thrusting and did not study inclination change. Second, classical inclination change maneuvers are relatively expensive in terms of fuel, so it may be advantageous to use electrodynamic propulsion rather than chemical or electrical thrusters.

**3.1.1 Inclination Forcing Function.** To change  $I$  we need to find a forcing function  $f_{3I}$  to substitute into Equation (11) to create a net change in  $I$ . Recall Equation (11) is

$$\frac{dI}{dt} = \frac{r \cos u}{na^2 \sqrt{1 - e^2}} f_{3I}$$

and simplifies to

$$\frac{dI}{dt} = \frac{\cos u}{na} f_{3I} \quad (48)$$

for a circular orbit. Note a constant  $f_{3I}$  is not a satisfactory forcing function because the  $\cos u$  function in the equation will result in zero average  $\dot{I}$ . Instead, assume  $f_{3I}$  is of the form  $A_I \cos u$ , where  $A_I$  is a constant we will derive shortly, and examine the average  $\dot{I}$  ( $\bar{\dot{I}}$ ) over one orbit:

$$\begin{aligned} \bar{\dot{I}} &= \frac{1}{2\pi} \int_0^{2\pi} \frac{A_I \cos^2 u}{na} du \\ &= \frac{A_I}{2\pi na} \int_0^{2\pi} \cos^2 u du \\ &= \frac{A_I}{2\pi na} \left( \frac{u}{2} + \frac{\sin 2u}{4} \right) \Big|_0^{2\pi} \\ &= \frac{A_I}{2na} \end{aligned} \quad (49)$$

Solving Equation (49) for  $A_I$  gives

$$A_I = 2na\bar{I}$$

and the forcing function

$$f_{3,} = 2na\bar{I} \cos u$$

where  $\bar{I}$  is a desired value we specify.

Similarly, we can check to ensure  $f_{3,}$  does not change  $\Omega$  by looking at the average  $\bar{\Omega}$  based on Equation (12):

$$\begin{aligned} \frac{d\Omega}{dt} &= \frac{r \sin u}{na^2 \sqrt{1-e^2} \sin I} f_3 \\ &= \frac{\sin u}{na \sin I} (2na\bar{I} \cos u) \\ &= \frac{2\bar{I}}{\sin I} \sin u \cos u \end{aligned}$$

If we assume  $I$  is a constant over one orbit, although not strictly correct, then  $\bar{\Omega}$  is

$$\bar{\Omega} = \frac{2\bar{I}}{2\pi \sin I} \int_0^{2\pi} \sin u \cos u \, du = 0$$

Now we must find the vector  $\underline{\kappa}$  which will result in the desired force vector

$$\underline{f}_A = \{0 \ 0 \ f_{3,}\}$$

To begin, find the unit vector  $\hat{\kappa}$  as depicted in Figure 2 by crossing  $\underline{B}$  into  $\underline{f}_A$  and normalizing the result:

$$\hat{\kappa} = \frac{\underline{B} \times \underline{f}_A}{\|\underline{B} \times \underline{f}_A\|} \quad (50)$$

$$= \frac{B_\theta f_3 \hat{a}_r - B_r f_3 \hat{a}_\theta}{\left[(B_\theta f_3)^2 + (B_r f_3)^2\right]^{1/2}} \quad (51)$$

$$= \frac{B_\theta \hat{a}_r - B_r \hat{a}_\theta}{(B_\theta^2 + B_r^2)^{1/2}} \quad (52)$$



and

$$\kappa = \frac{f_{3i}}{(B_{\theta}^2 + B_z^2)^{1/2}} \quad (57)$$

Equations (55-57) guarantee achievement of the desired  $f_{3i}$ . However, they will generally also produce  $f_r$  and  $f_{\theta}$  accelerations as well. We will see the effects of these unwanted accelerations in the next section.

This algorithm has another shortfall. The algorithm makes no assumptions about  $\underline{B}$ , and there are times in the orbit when the denominator of Equation (57) will be near 0, resulting in unreasonable values of  $\kappa$ . To avoid this problem, we will put a limit on the components of  $\underline{\kappa}$ . Since the algorithm does not consider the varying  $\underline{B}$  field, there may be an inefficient use of power. To correct this deficiency crosses the line into optimization, which is beyond the scope of this thesis.

**3.1.2 Inclination Change Results.** Average inclination change rates of  $\pm 1^\circ/\text{day}$  and  $\pm 0.1^\circ/\text{day}$  at the initial inclination  $I_o = 90^\circ$  were studied, as well as  $\pm 0.1^\circ/\text{day}$  at  $I_o = 45^\circ$ . Results of each case are summarized in Table 1.  $m/m_e = 10$  for all cases. To study the effects of the rotation of the  $\underline{B}$  field, the duration of each case was one sidereal day ( $86\ 160^\circ$ ). The other initial orbital elements of each case were

$$\begin{aligned} a &= 6\ 578 \text{ km} \\ h &= 0 \\ k &= 0 \\ \Omega &= 0 \\ u_o &= 0 \end{aligned}$$

In each case we were able to obtain the desired secular change in  $I$  with no net change in  $\Omega$ . Figures 3 and 4 are representative of the performance of  $I$  and  $\Omega$  in each case.

Figures 5 and 6 show the case 1  $\kappa$  and  $P_r$  profiles respectively, before we imposed a limit on  $\kappa$ . After case 1, we imposed the limit that the magnitude of no component of  $\underline{\kappa}$  exceed 200 Amp-m/kg. Figures 7 and 8 show  $P_r$  and  $\kappa$  for case 2. Note the effect of

Table 1. Inclination Change Study Results

Case	1	2	3	4	5	6	7
$I_0$ (deg)	90	90	90	90	90	45	45
$\kappa_{limit}$ (A·m/kg)	n/a	200	200	200	200	200	200
Target $\dot{I}$ (deg/day)	1.0	1.0	-1.0	.10	-.10	.10	-.10
$\mathcal{E}$ (J/kg $\times 10^4$ )	360	220	210	4.1	2.8	4.0	9.6
$P_s$ (W/kg)	42	26	24	.47	.33	.46	1.1
$P_{total}$ (W/kg)	6736	287	269	79	100	229	202
$\Delta a$ (km)	1.496	.349	.144	-.061	.109	-7.336	7.404

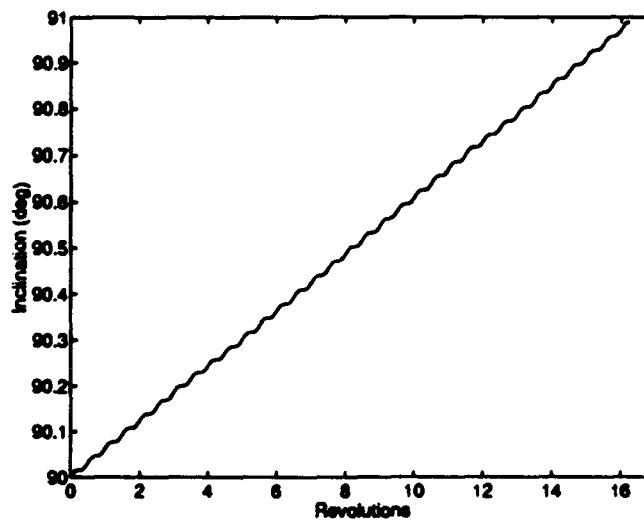


Figure 3. Case 2: Inclination Change

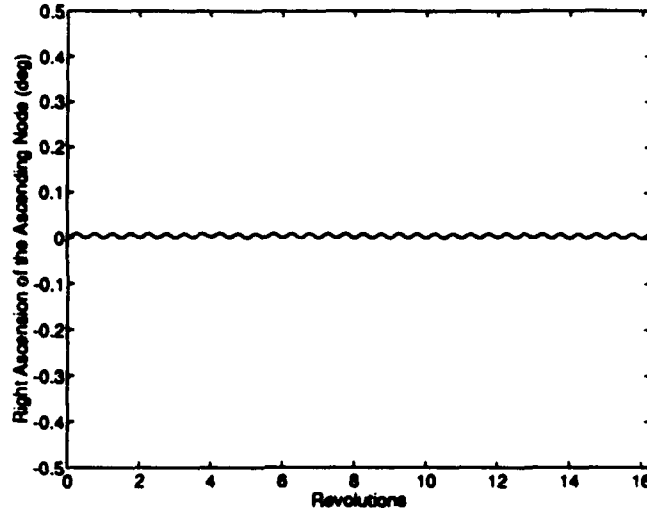


Figure 4. Case 2: Right Ascension of the Ascending Node Change

limiting  $\kappa$  in Figure 7. Further,  $\kappa_3$  is zero, as would be expected since the numerator of Equation (55) gives

$$\begin{Bmatrix} B_r \\ B_\theta \\ B_3 \end{Bmatrix} \times \begin{Bmatrix} 0 \\ 0 \\ f_{3r} \end{Bmatrix} = \begin{Bmatrix} B_\theta f_{3r} \\ -B_r f_{3r} \\ 0 \end{Bmatrix}$$

Referring back to Figure 3, note  $I$  does not quite reach the target value. This is because the limit on  $\kappa$  prevented achievement of the desired  $f_{3r}$  at times.  $\bar{I}$  can be adjusted to make up for the shortfall.

In Table 1 we see limiting  $\kappa$  resulted in 1/3 less energy required for case 2 compared to case 1. In cases 3-7 we changed the target  $\bar{I}$  to .1°/day. This one order of magnitude change resulted in two orders of magnitude change in  $E$  and  $\bar{P}_r$ , bringing  $\bar{P}_r$  in reach of current spacecraft specific power technology.

Figure 9 shows how the power is divided between  $i^2 R$  and  $iV_i$ . There is some negative  $iV_i$ , but overall the  $iV_i$  power is negligible compared to the  $i^2 R$  power, indicating the  $\kappa_j^2$  terms dominate Equation (47).

Figure 10 shows  $f_{3r}$  is a cosine function, as desired, except for several points near revolutions 4 and 12 where the limit on  $\kappa$  is invoked.  $\kappa$  must be limited in areas where

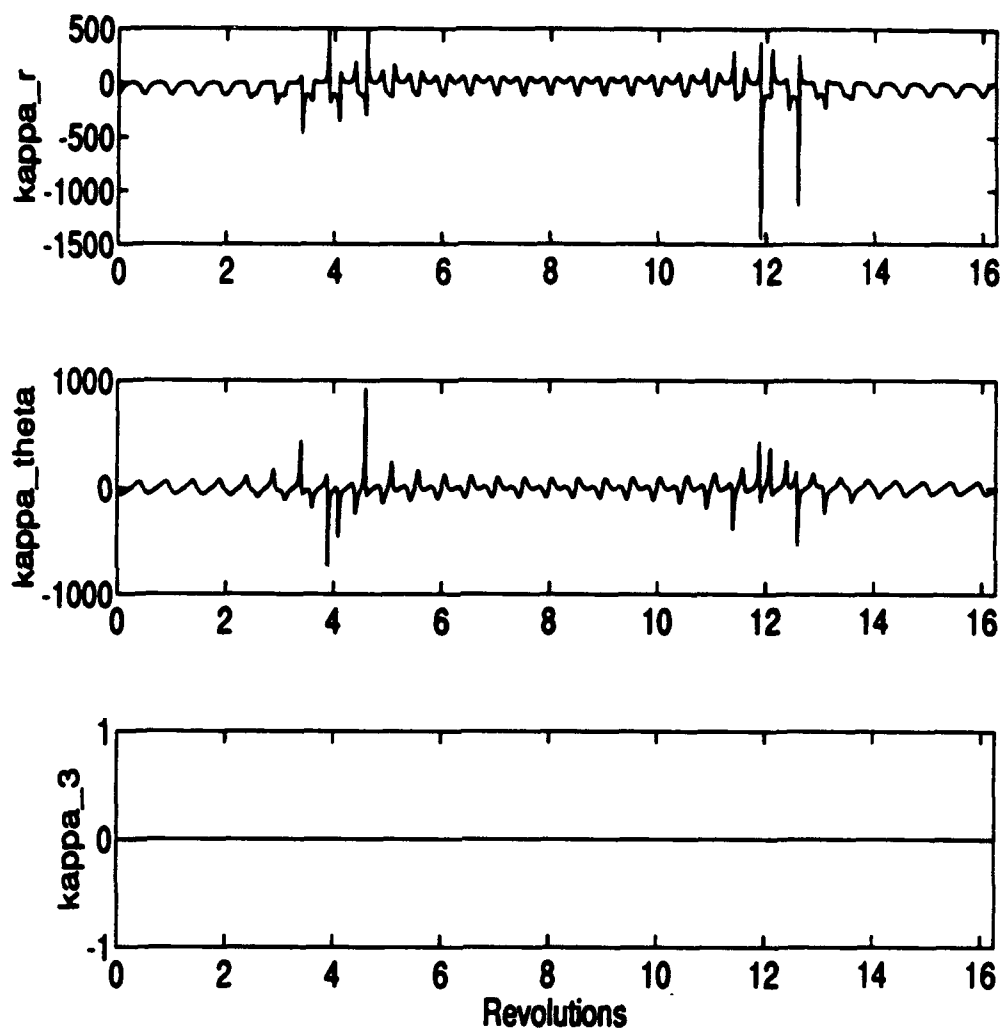


Figure 5. Case 1:  $\kappa$  Profile (Amp·m/kg)

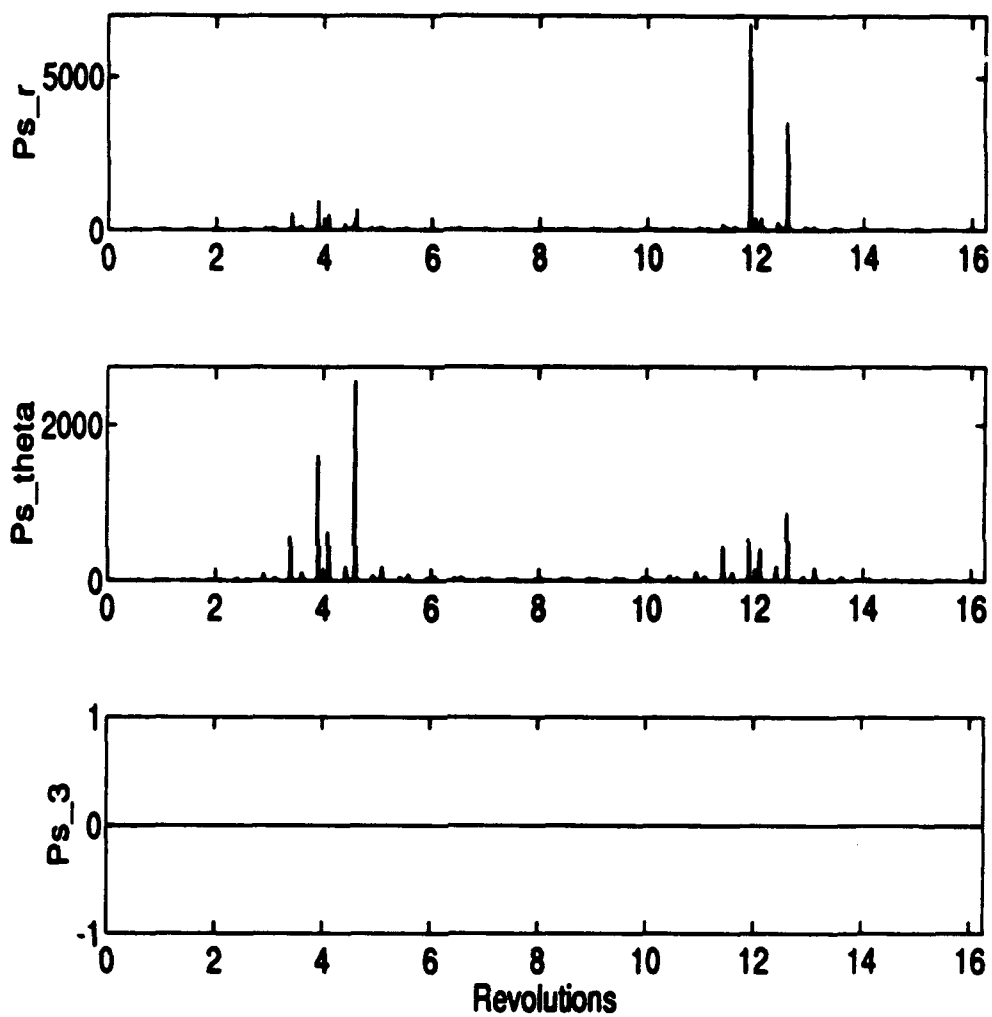


Figure 6. Case 1:  $P_r$  Profile (W/kg)

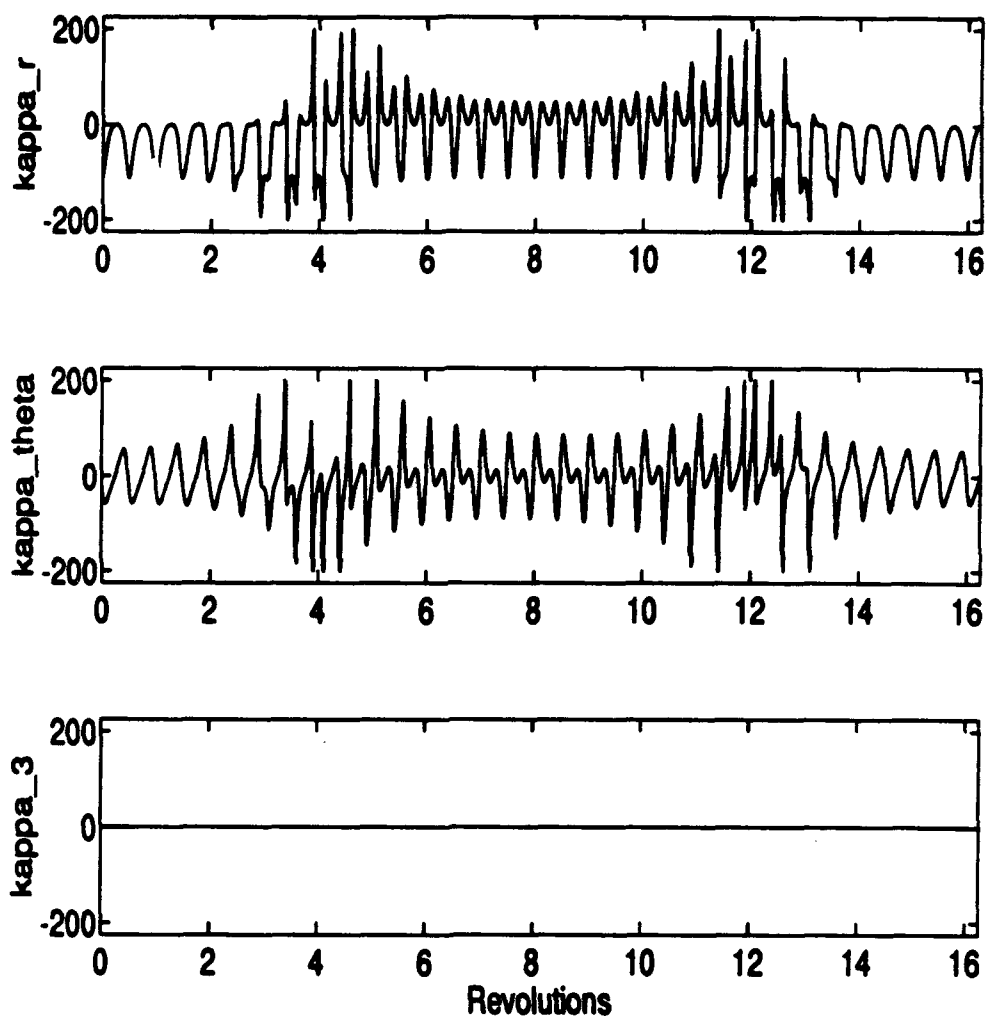


Figure 7. Case 2:  $\kappa$  Profile (Amp·m/kg)

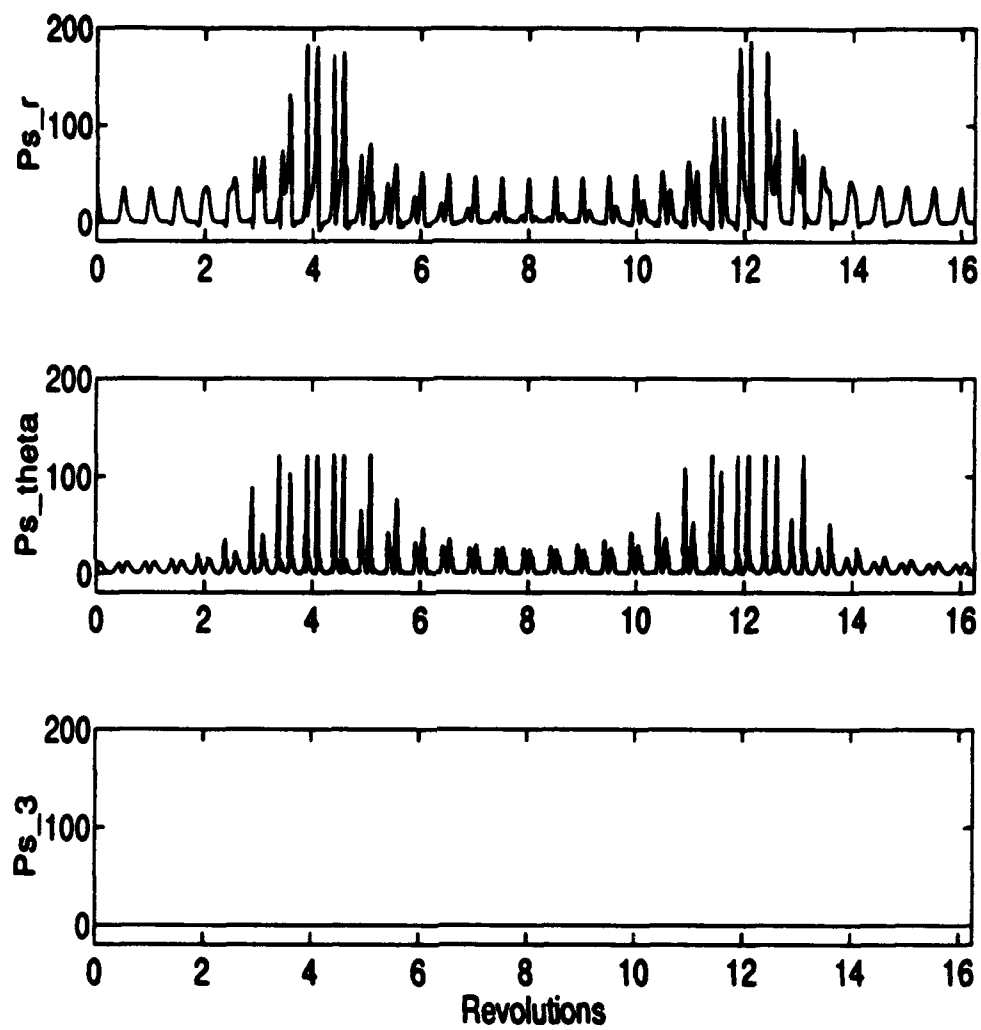


Figure 8. Case 2:  $P_r$  Profile (W/kg)

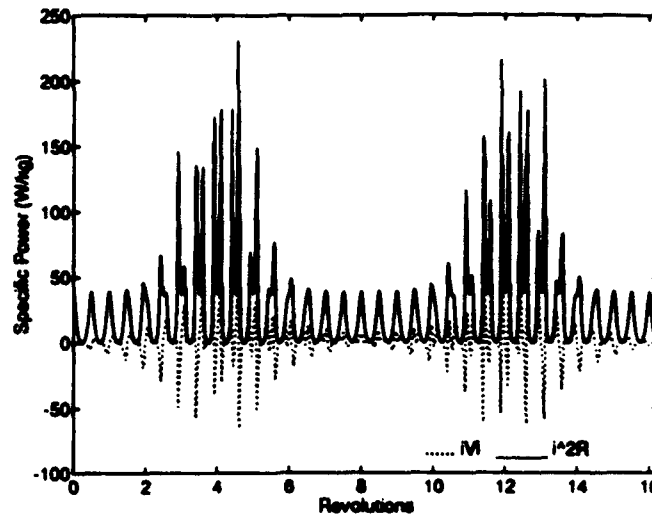


Figure 9. Case 2:  $i^2R$  and  $iV_i$  Power

$B_r$  and  $B_\theta$  are near zero compared to  $B_3$ . An example of such a point near revolution 4 is shown in Figure 11. In these instances,  $\underline{B}$  is nearly parallel to  $\underline{L}_4$ , thus Equation (57) becomes singular.

The unwanted  $f_r = \kappa_r B_3$  and  $f_\theta = -\kappa_\theta B_3$  accelerations rise and fall in phase with the relatively large  $B_3$  oscillations which occur twice per day as the geomagnetic poles revolve through the orbital plane, as shown in Figure 12. These accelerations manifest themselves in changes to  $a$ . In cases 1-5,  $a$  initially diverges and then returns to its initial value, resulting in no net change over the 24 hour period of interest. Figure 13 shows how  $a$  varies, and is typical of all the cases where  $I_o = 90^\circ$ . However, for  $I_o = 45^\circ$ ,  $a$  diverges and never returns to its initial value. Figure 14 shows  $a$  for case 6.

### 3.2 Right Ascension of the Ascending Node Change

There are two potential applications of  $\Delta\Omega$  maneuvers. The first involves a satellite at  $I = 90^\circ$  whose line of nodes is precessed with angular velocity equal to the Earth's mean angular velocity as it revolves around the sun, or  $\dot{\Omega} \approx 1^\circ/\text{day}$ .

The second application is to fine tune  $\Omega$ , such as might be required to maintain a specified angular separation between different orbital planes in a constellation. This

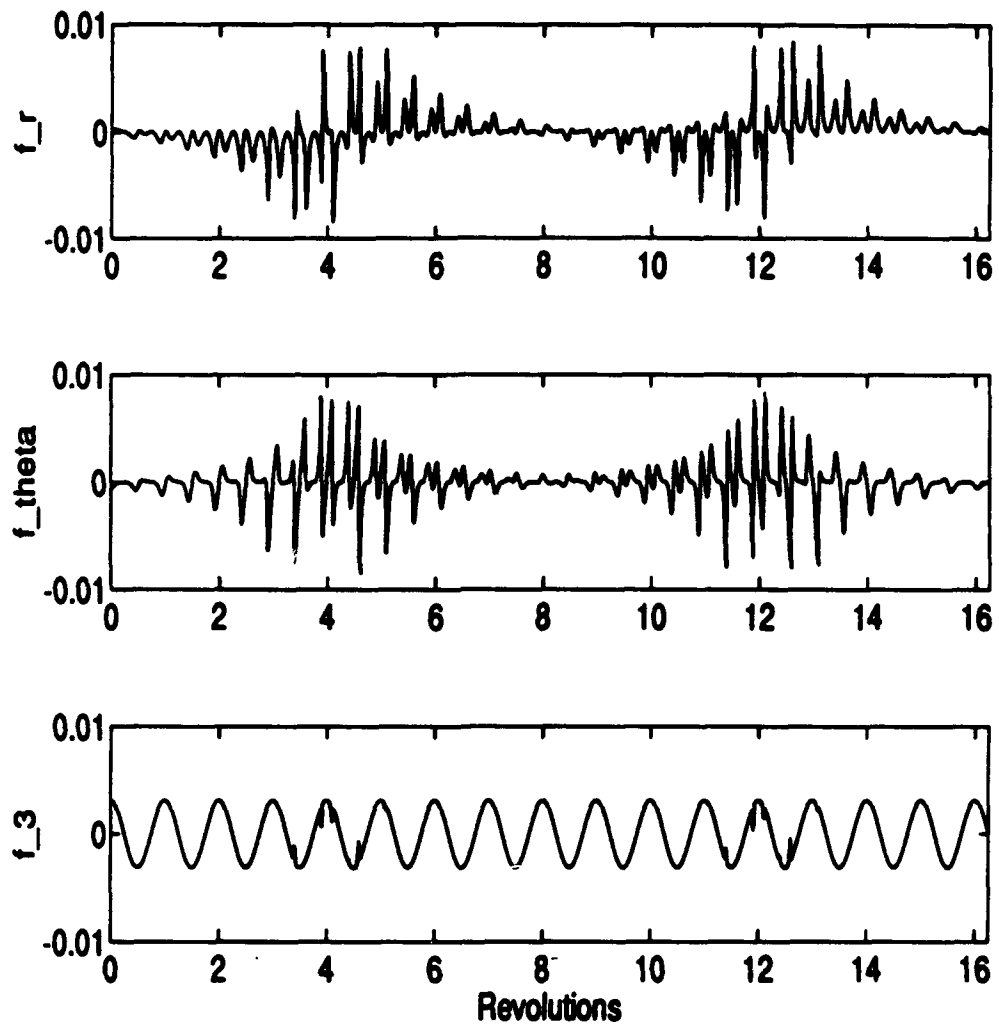


Figure 10. Case 2: Accelerations ( $\text{m/s}^2$ )

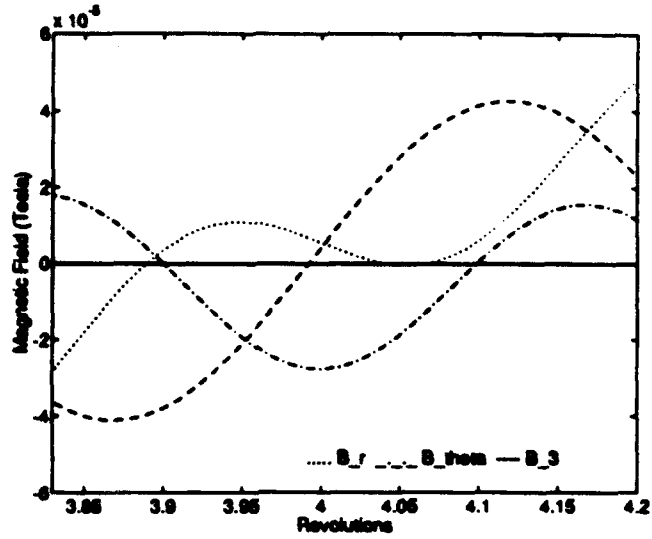


Figure 11. Case 2: Magnetic Field Near Revolution 4

would be an expensive fuel maneuver over the lifetime of a constellation of low Earth orbit satellites. Perhaps electrodynamic propulsion can perform small  $\Delta\Omega$  maneuvers at low power using renewable electrical energy.

**3.2.1 Right Ascension of the Ascending Node Forcing Function.** Development of a forcing function  $f_{3\Omega}$  will follow the same methodology as section 3.1. Simplifying Equation (12) for a circular orbit results in

$$\frac{d\Omega}{dt} = \frac{\sin u}{na \sin I} f_3$$

Again we find a sinusoid which eliminates a constant  $f_3$  from contention as a potential forcing function. Rather, assume  $f_{3\Omega}$  is of the form  $B_\Omega \sin u$ , where  $B_\Omega$  is a constant we find in the same manner as before:

$$\bar{\Omega} = \frac{1}{2\pi} \int_0^{2\pi} \frac{B_\Omega \sin^2 u}{na \sin I} du \quad (58)$$

$$= \frac{B_\Omega}{2\pi na \sin I} \int_0^{2\pi} \sin^2 u du \quad (59)$$

$$= \frac{B_\Omega}{2\pi na \sin I} \left( \frac{u}{2} - \sin u \cos u \right) \Big|_0^{2\pi} \quad (60)$$

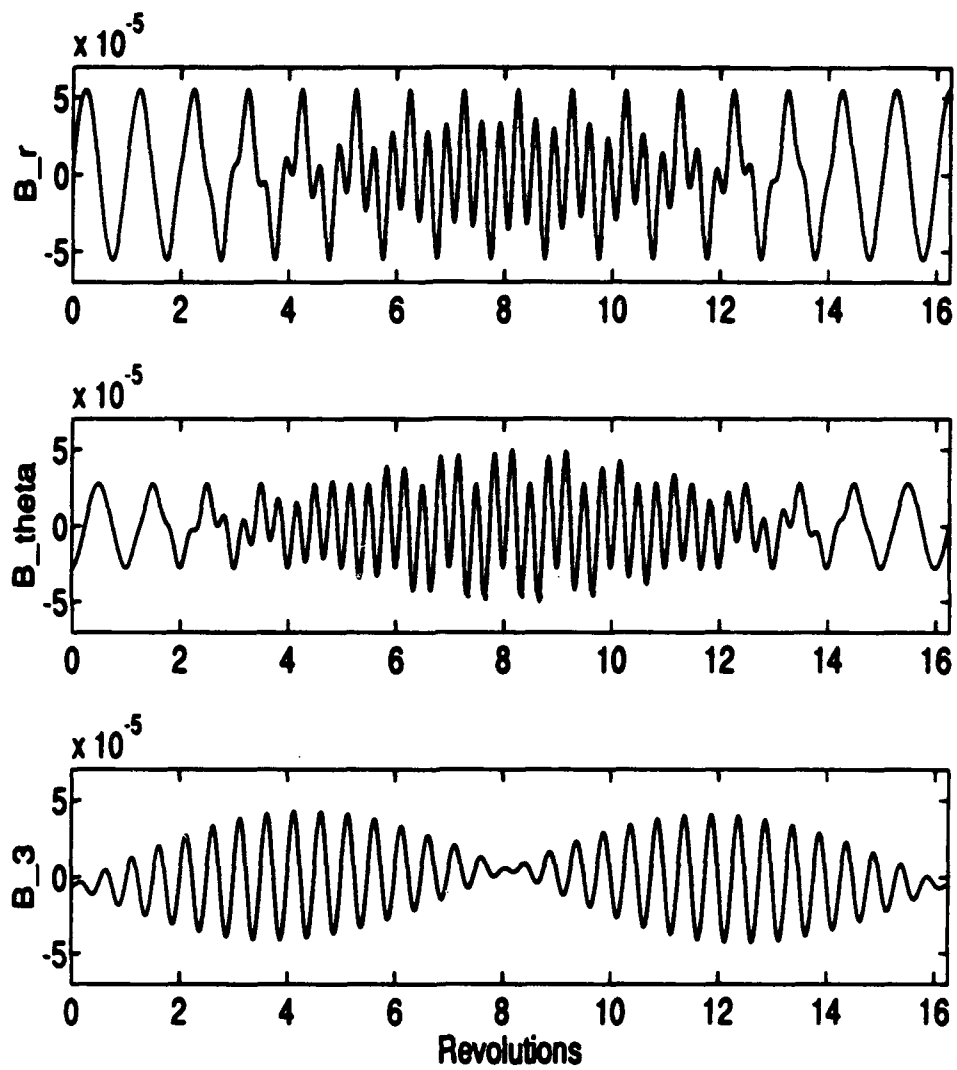


Figure 12. Magnetic Field Components (Tesla)

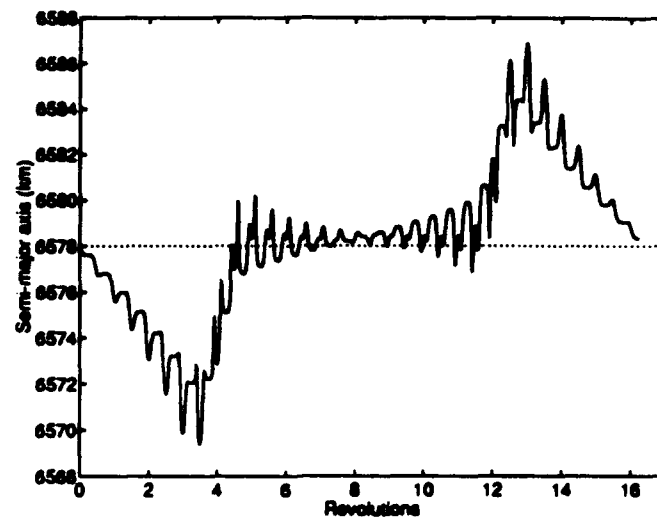


Figure 13. Case 2: Semi-major Axis Change

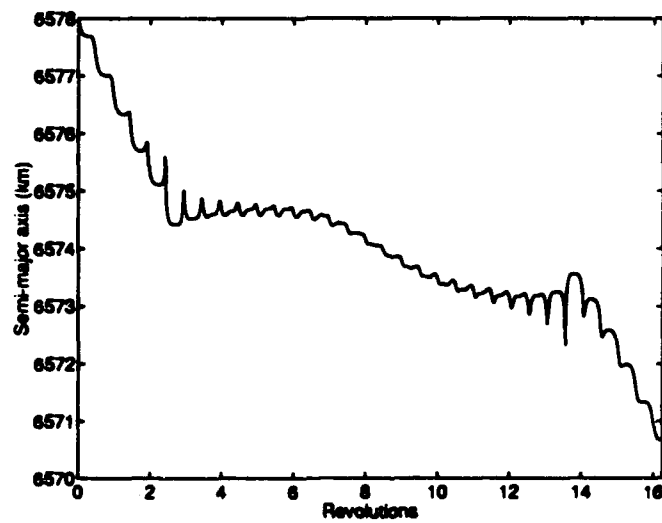


Figure 14. Case 6: Semi-major Axis Change

$$= \frac{B_{\Omega}}{2na \sin I} \quad (61)$$

$$B_{\Omega} = 2na\bar{\Omega} \sin I \quad (62)$$

$$f_{3\Omega} = 2na\bar{\Omega} \sin I \sin u \quad (63)$$

Equation (48) is revisited to see how  $f_{3\Omega}$  affects  $I$ :

$$\frac{dI}{dt} = \frac{\cos u}{na} f_3 \quad (64)$$

$$= \frac{\cos u}{na} (2na\bar{\Omega} \sin I \sin u) \quad (65)$$

$$= 2\bar{\Omega} \sin I \cos u \sin u \quad (66)$$

Again we treat  $I$  approximately constant with respect to  $u$  and find

$$\bar{I} = \frac{2\bar{\Omega} \sin I}{2\pi} \int_0^{2\pi} \cos u \sin u \, du = 0$$

as desired.

The methodology used in section 3.1 to find  $\underline{\kappa}$  also applies here. Define the desired force vector as  $\underline{f}_d = \{0 \ 0 \ f_{3\Omega}\}^T$ . Then

$$\hat{\kappa} = \frac{\underline{B} \times \underline{f}_d}{\|\underline{B} \times \underline{f}_d\|}$$

$$\kappa = \frac{f_{3\Omega}}{(B_\theta^2 + B_r^2)^{1/2}}$$

and  $\underline{\kappa} = \kappa \hat{\kappa}$ . As before we will see unwanted accelerations  $f_r$  and  $f_\theta$ , and we must limit the magnitude of  $\kappa$  the algorithm might demand when the denominator of  $\kappa$  goes to zero.

**3.2.2 Right Ascension of the Ascending Node Change Results.** Average  $\Omega$  change rates of  $\pm 1^\circ/\text{day}$  and  $\pm 0.1^\circ/\text{day}$  at initial inclinations  $I_o = 90^\circ$  and  $I_o = 45^\circ$  were studied. Results of each case are summarized in Table 2. To study the effects of the rotation of the  $\underline{B}$  field, the duration of each case was  $86\ 160^\circ$ . The other initial orbital elements of each

Table 2. Right Ascension of the Ascending Node Change Study Results

Case	1	2	3	4	5	6
$I_o$ (deg)	90	45	45	45	45	90
$\kappa_{limit}$ (A·m/kg)	200	200	200	200	200	200
Target $\dot{\Omega}$ (deg/day)	1.0	1.0	-1.0	.10	-.10	.10
$\mathcal{E}$ (J/kg $\times 10^4$ )	120	100	110	1.9	.81	1.5
$\overline{P}_s$ (W/kg)	14	12	11	.22	.094	.17
$\overline{P}_{push}$ (W/kg)	271	189	242	55	11	16
$\Delta a$ (km)	-1.59	5.93	-9.20	1.11	-1.08	-.531

case were

$$a = 6578 \text{ km}$$

$$h = 0$$

$$k = 0$$

$$\Omega = 0$$

$$u_o = 0$$

In each case we were able to obtain the desired secular change in  $\Omega$  with no net change in  $I$ . Figures (15 and (16 are representative of the performance of  $\Omega$  and  $I$  in each case.

Figures (17 and (18 show  $\overline{P}_s$  and  $\kappa$  for case 4, which is typical of the other five cases. In Table 2 we again see how the change in  $\dot{\Omega}$  from 1.0°/day to .1°/day results in two orders of magnitude change in  $\mathcal{E}$  and  $\overline{P}_s$ , bringing  $\overline{P}_s$  for the  $\Omega$  change maneuver below the four Watt/kg benchmark.

In comparing cases 1 and 6 in Table 2 to cases 2 and 4 in Table 1 we see how the variation in the  $\underline{B}$  field affects the total energy required for plane change of polar orbits. In Equation (31) we see  $B$  is twice as strong at  $\phi_m = 90^\circ$  than at  $\phi_m = 0$ . Since  $f_{3n} = B_n \sin u$  while  $f_{3l} = A_l \cos u$ , the  $f_{3n}$  function is able to take advantage of the stronger  $\underline{B}$  field near the poles. The  $f_{3l}$  function must expend more energy to achieve the same forces while thrusting over the equator.

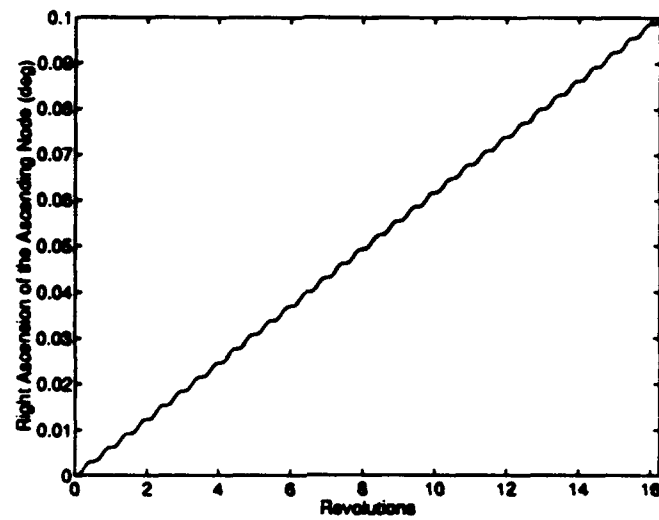


Figure 15. Case 4: Right Ascension of the Ascending Node Change

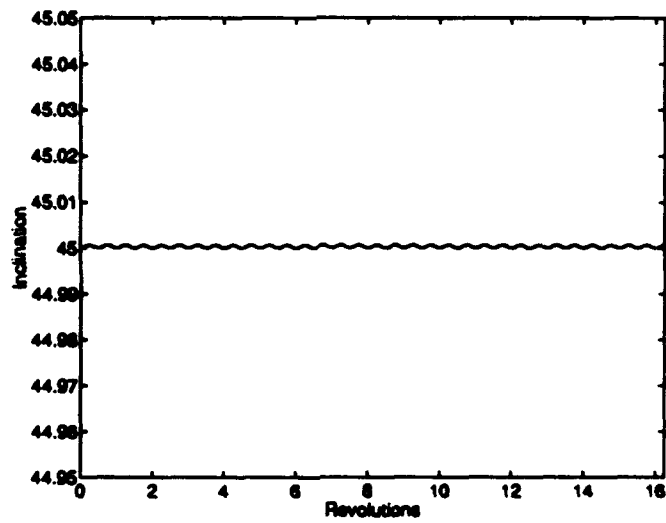


Figure 16. Case 4: Inclination Change

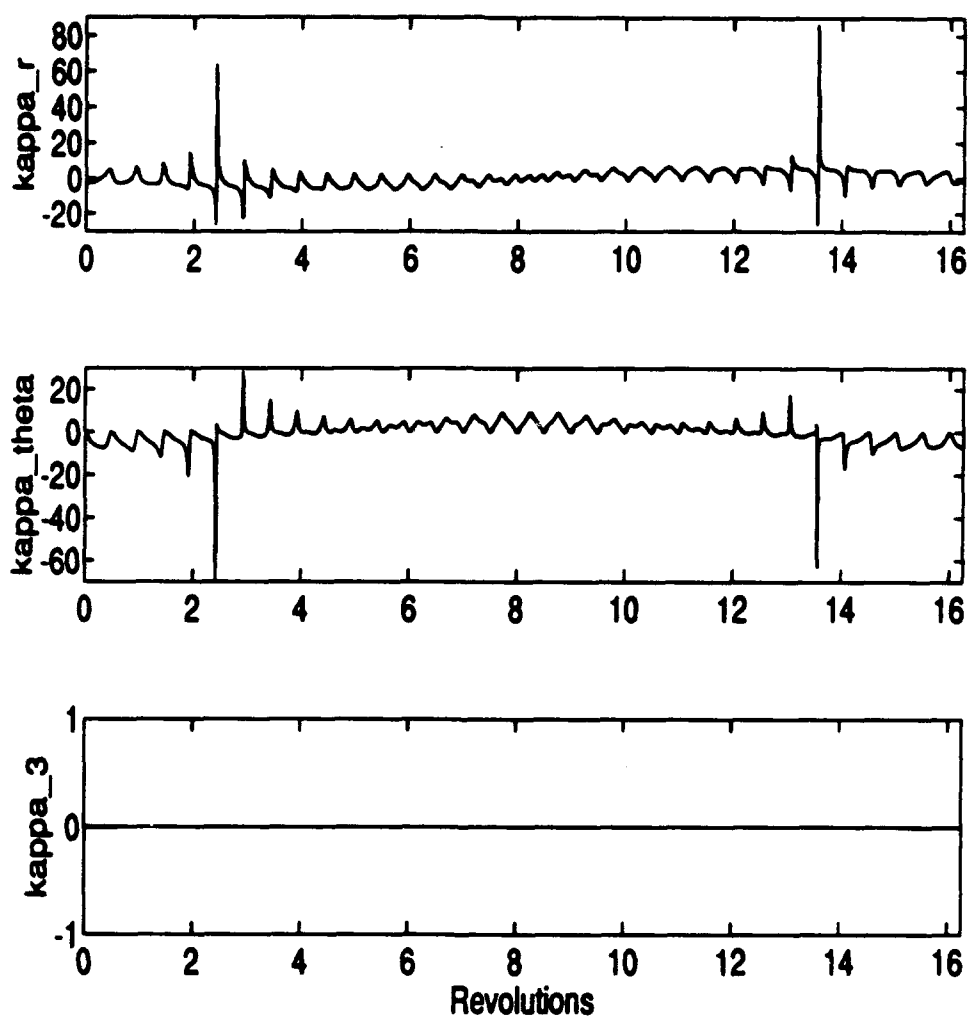


Figure 17. Case 4:  $\kappa$  Profile (Amp·m/kg)

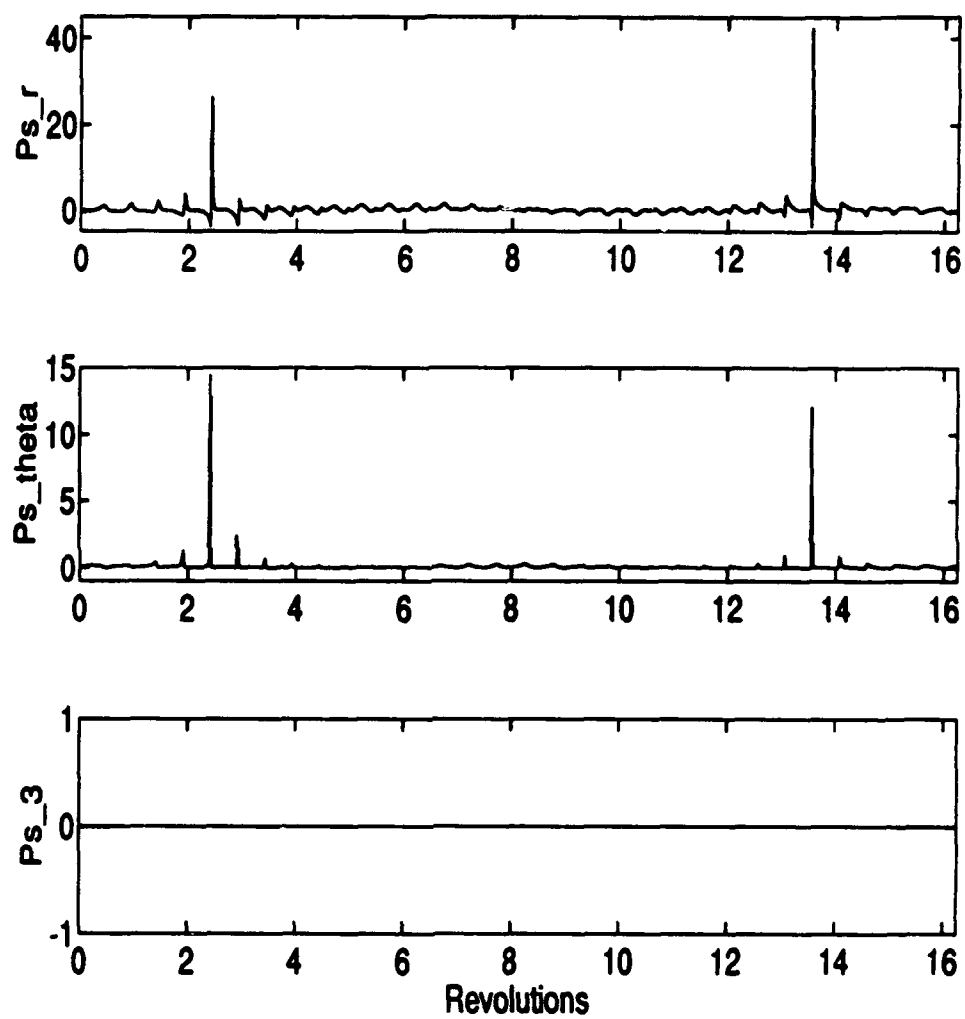


Figure 18. Case 4:  $P_s$  Profile (W/kg)

Table 3. Additional  $\Delta\Omega$  Cases

$\bar{\Omega}$ °/day	$iV_i/m$ (W/kg)	$i^2R/m$ (W/kg)	$\bar{P}_i$ (W/kg)
1.0	-0.0766	14.1202	14.0436
.9	-0.0604	11.7560	11.6957
.8	-0.0487	9.5775	9.5288
.7	-0.0464	7.5952	7.5487
.6	-0.0464	5.8287	5.7823
.5	-0.0522	4.2549	4.2026
.4	-0.0580	2.8389	2.7809
.3	-0.0638	1.6818	1.6179
.2	-0.0569	0.7950	0.7382
.1	-0.0279	0.1985	0.1706
0	0	0	0
-.1	0.0267	0.1985	0.2252
-.2	0.0511	0.7927	0.8438
-.3	0.0515	1.6783	1.7298
-.4	0.0371	2.8319	2.8691
-.5	0.0209	4.2375	4.2584
-.6	0.0001	5.8008	5.8010
-.7	-0.0174	7.5511	7.5337
-.8	-0.0325	9.5160	9.4835
-.9	-0.0429	11.6771	11.6342
-1.0	-0.0499	14.0204	13.9705

Figure 19 shows  $f_{3a}$  is a sine function, as desired, except for those times when the limit on  $\kappa$  is invoked. The unwanted  $f_r$  and  $f_\theta$  accelerations due to large  $B_3$  components again produce changes in  $a$ , as shown in Figure 20 for case 4.

The  $\Omega$  change cases were chosen for investigation of the affect the choice of  $\pi/m_e$  has on  $\bar{P}_i$ . In addition to case 6, 19 other cases were run at various  $\bar{\Omega}$  values and the  $\bar{P}_i$  due to the induced voltage and the  $\kappa_j^2$  terms were tabulated. Table 3 shows the results of these additional cases. All cases were run at  $I = 90^\circ$  and  $m/m_e = 10$ .

Figure 21 is a plot of the  $iV_i$  power, the  $i^2R$  power, and the total  $\bar{P}_i$  for all the cases shown in Table 3. At  $\bar{\Omega} = .1^\circ/\text{day}$ , the power (either expended or regenerated) due to the induced voltage is about 1/7 the power required to overcome the  $i^2R$  losses. At  $\bar{\Omega} = 1.0^\circ/\text{day}$ , the  $iV_i$  power is insignificant compared to the  $i^2R$  power. The 4 W/kg limit is exceeded near  $\bar{\Omega} = .5^\circ/\text{day}$

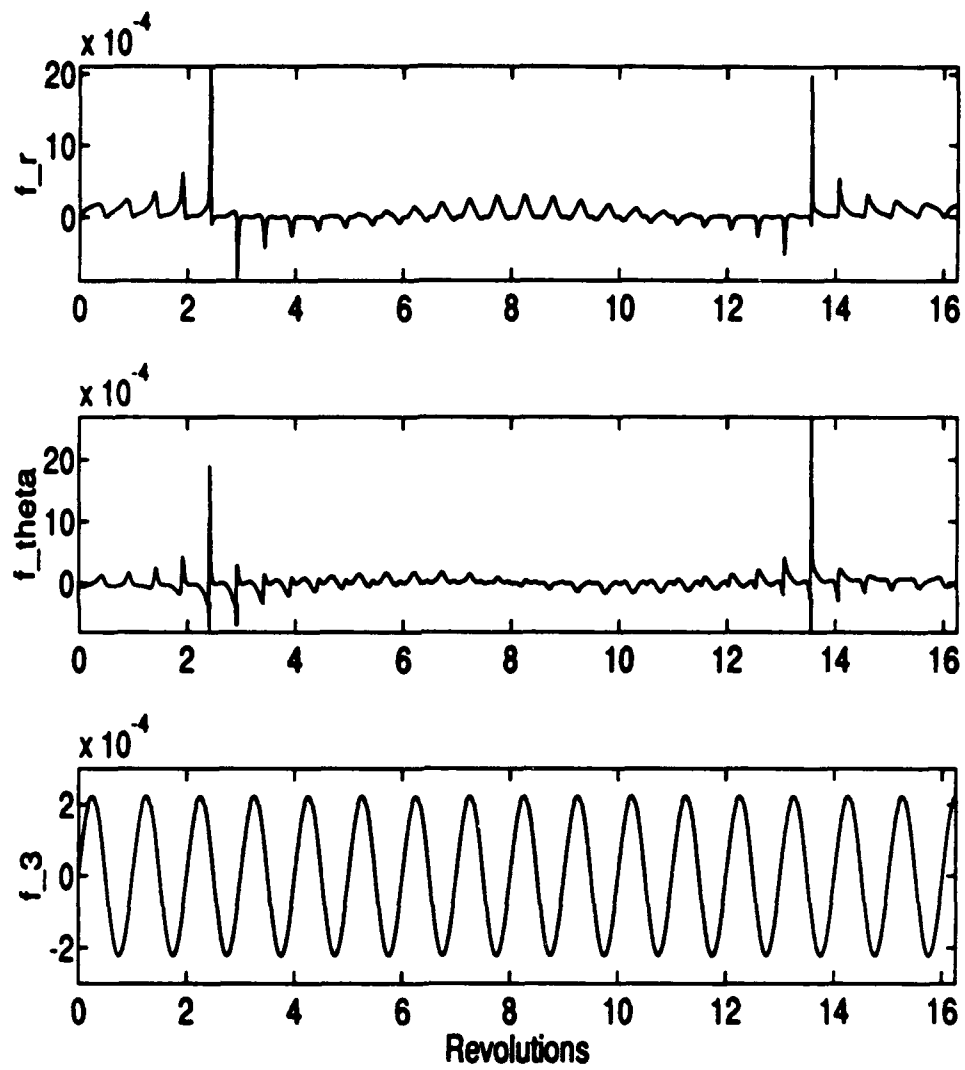


Figure 19. Case 4: Accelerations ( $\text{m/s}^2$ )

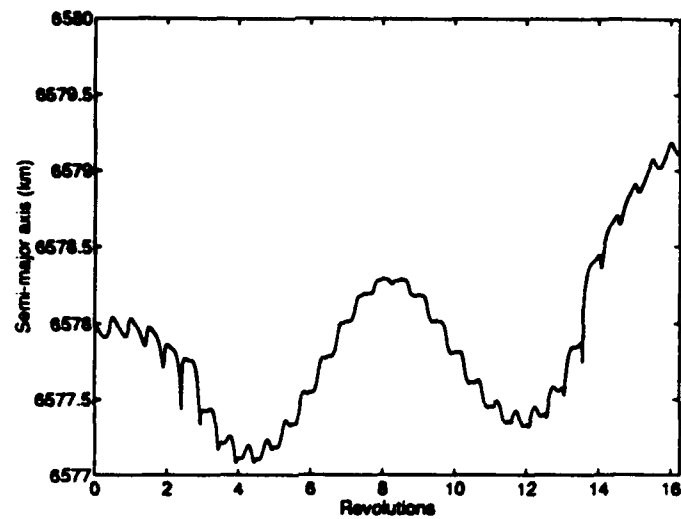


Figure 20. Case 4: Semi-major Axis Change

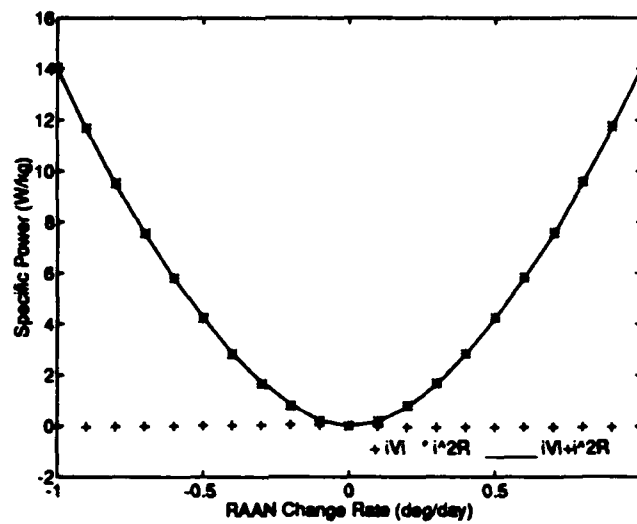


Figure 21.  $\bar{P}$ , Required for  $\Delta\Omega$  ( $m/m_c = 10$ )

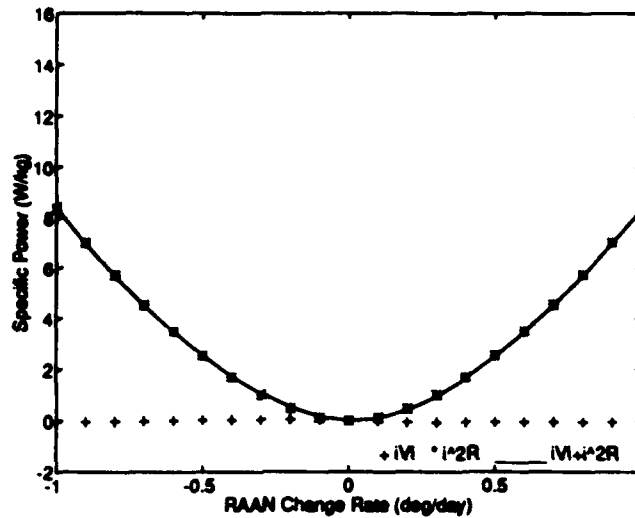


Figure 22.  $\bar{P}_s$  Required for  $\Delta\Omega$  ( $m/m_c = 6$ )

In Equation (47) we see the power dissipated as heat can be decreased by lowering  $m/m_c$  without changing the  $iV_i$  power. Lowering  $m/m_c$  implies more of the total vehicle mass is taken up by the conductor. In using  $m/m_c = 10$  and assuming three orthogonal conductors, 30% of the vehicle is conductor mass. The conductor mass can be increased to 50% of the vehicle mass by using  $m/m_c = 6$ . If we retain the three conductor configuration, the theoretical limit of  $m/m_c$  is 3, meaning the conductors account for 100% of the vehicle mass.

The existing data can be modified to study the effect of differing  $m/m_c$  values. For  $m/m_c = 6$ , the  $i^2R$  values of Table 3 are multiplied by .6 and added to the unchanged  $iV_i$  power to find a new  $\bar{P}_s$ . Likewise, multiplying the  $i^2R$  values by .3 results in a theoretical lower bound on  $\bar{P}_s$ . The modified data is plotted in Figures 22 and 23 for  $m/m_c = 6$  and  $m/m_c = 3$  respectively. Note the  $i^2R$  losses are still significant compared to the  $iV_i$  power. The  $1.0^\circ/\text{day}$  goal is almost in reach of the 4 W/kg power supply for  $m/m_c = 3$ , but further  $m/m_c$  reductions are not possible without invalidating many of the assumptions which went into the derivation of Equation (47). Although further power reductions might be found by deriving a more general form of Equation (47), a more promising way to reduce  $\bar{P}_s$  is to replace the aluminum conductor with a superconductor.

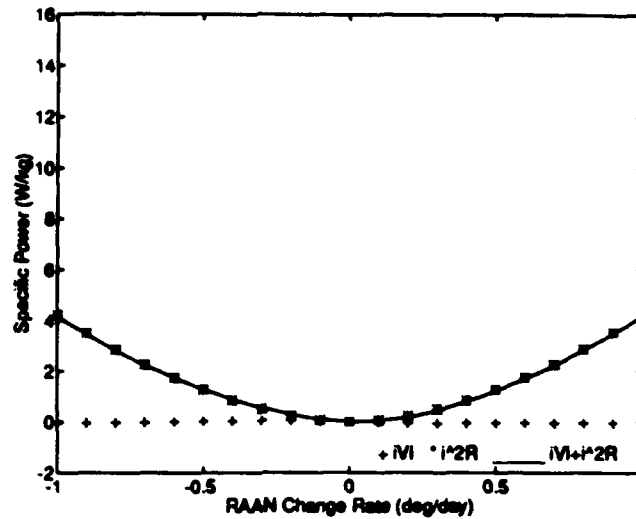


Figure 23.  $\bar{P}$ , Required for  $\Delta\Omega$  ( $m/m_c = 3$ )

### 3.3 Summary of Orbital Plane Change Results

In this section we summarize the results of the  $I$  and  $\Omega$  change maneuvers. We have developed an algorithm which allows us to use electrodynamic propulsion to change both  $I$  and  $\Omega$  as desired. However, the maneuvers can only be achieved with reasonable power requirements when the magnitude of the plane change is on the order of  $.4^\circ/\text{day}$ . Until spacecraft power technology advances, this eliminates electrodynamic propulsion from applications such as changing  $\Omega$  at  $1.0^\circ/\text{day}$  to produce a true polar sun synchronous orbit or relatively rapid  $\Delta I$  maneuvers.

At slower rates such as  $.10^\circ/\text{day}$ ,  $\Delta I$  maneuvers are feasible for polar orbits. Plane changes at lower inclinations may be feasible, provided the change in  $a$  can be negated.

Most of the power required to perform the maneuvers is dissipated as heat due to the resistance in the conductor. A larger conductor mass results in less power, but at the expense of payload capability. Superconductors should be investigated as a means to lower the power requirements.

Additional study should focus on constraining the change in  $a$  and incorporating a priori knowledge of the  $\underline{B}$  field into the forcing functions. Also, if the only desire is to

move  $\Omega$  from  $\Omega_1$  to  $\Omega_2$ , less energy may be required if  $I$  and  $\Omega$  change simultaneously so the angular momentum vector follows a great circle route, rather than simply precessing the line of nodes.

#### IV. Molniya Orbit Stationkeeping

Now we turn our attention to the application of electrodynamic propulsion to stationkeeping the argument of perigee of a polar Molniya orbit. A Molniya orbit is highly eccentric with a 12 or 24 hour period and large inclination. Thus if the argument of perigee is  $270^\circ$ , the apogee will remain over the northern latitudes of the Earth for a large portion of the 12 or 24 hour period. This provides multi-hour communications capability with minimum ground antenna tracking for those users who do not have visibility to equatorial geosynchronous communications satellites.

Janson has proposed a stationkeeping strategy for a 24 hour,  $90^\circ$  inclination Molniya orbit using electric thrusters (4:9). In this chapter we will look at effects of the Earth's oblateness on the Molniya orbit, develop a stationkeeping strategy, and compare our results with Janson's.

##### 4.1 Effects of the Earth's Oblateness

The first order approximation of the shape of the Earth is a sphere. The second order approximation is an oblate spheroid, with the polar diameter some 21 kilometers less than the equatorial diameter. Meirovitch derives the components of the disturbing acceleration  $^a\mathbf{f}$  due to oblateness in terms of the Earth's principal axis moments of inertia (9:457-459). They are

$$\begin{aligned} f_r &= -\frac{-3G(C_E - A_E)}{2r^4} (1 - 3\sin^2 u \sin^2 I) \\ f_\theta &= -\frac{-3G(C_E - A_E)}{2r^4} \sin 2u \sin^2 I \\ f_3 &= -\frac{-3G(C_E - A_E)}{2r^4} \sin u \sin 2I \end{aligned} \quad (67)$$

where  $G$  is the gravitational constant,  $C_E$  is the Earth's moment of inertia about the polar axis, and  $A_E$  is the Earth's moment of inertia about the orthogonal axes. If we substitute Equations (67) into Equation (13), which we repeat here for reference,

$$\frac{d\omega}{dt} = -\frac{\sqrt{1-e^2} \cos \nu}{nae} f_r + \frac{\sqrt{1-e^2}}{nae} \left(1 + \frac{1}{1+e \cos \nu}\right) \sin \nu f_\theta - \frac{r \cot I \sin u}{na^2 \sqrt{1-e^2}} f_3$$

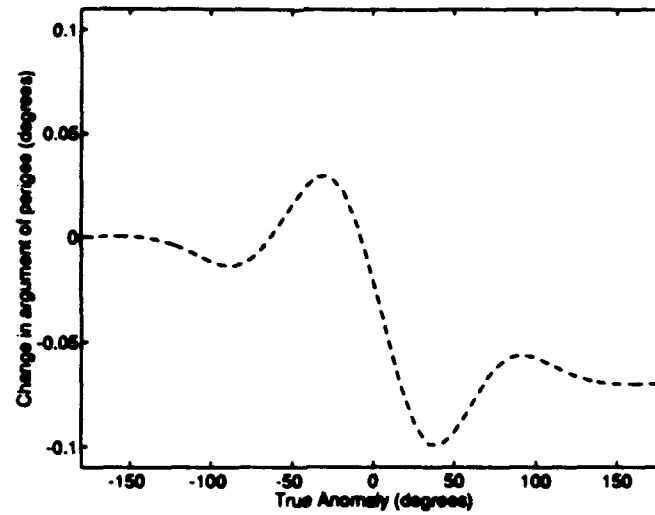


Figure 24. Effect of Earth Oblateness on 24 Hour Polar Molniya Orbit

we can see how the Earth's oblateness affects  $\omega$ . Our reference orbit is defined by

$$T = 86160'$$

$$e = .82501$$

$$\omega = 270^\circ$$

Figure 24 shows  $\Delta\omega_{oblate}$  due to the Earth's oblateness is approximately  $-.07^\circ$  after one revolution. Left unchecked,  $\omega$  will continue regressing until the apogee is no longer over the North pole, making the orbit unusable for polar communications. The goal is to drive  $\Delta\omega$  to 0.

#### 4.2 Desired Forcing Function

Finding a suitable forcing function to produce the desired  $\dot{\omega}$  is not as straightforward as it was for the plane change case. Equation (13) contains all three components of  $\underline{f}$ , so we have one equation and three unknowns. Even if we choose to neglect  $f_3$ , which is reasonable since the  $\cot I$  term negates its effect on  $\dot{\omega}$  for a  $90^\circ$  inclination orbit, we still

must find some combination of  $f_r$  and  $f_\theta$  to produce the desired  $\dot{\omega}$ . To solve this problem we call upon the method of Lagrange multipliers (9:54-55), in which we minimize one function subject to the constraint imposed by another function. From our experience with the plane change case we know the  $\kappa_j^2$  terms dominate Equation (47), so a function worth minimizing is

$$\mathcal{H}(\underline{\kappa}) \equiv \kappa_r^2 + \kappa_\theta^2 + \kappa_3^2 \quad (68)$$

The constraint we impose on  $\mathcal{H}$  comes from Equation (13). We require Equation (13) to produce  $-\Delta\omega_{oblate}$  during the thrust time  $\Delta t$ , and we define

$$\bar{\omega} = \frac{-\Delta\omega_{oblate}}{\Delta t}$$

We write the constraint function  $g$  as

$$g(\underline{\kappa}) = -k_1 \cos \nu f_r + k_1 k_2 \sin \nu f_\theta - \frac{r \cot I \sin u}{na^2 \sqrt{1-e^2}} f_3 - \bar{\omega} = 0$$

where

$$k_1 = \frac{\sqrt{1-e^2}}{nae}$$

and

$$k_2 = 1 + \frac{1}{1 + e \cos \nu}$$

We simplify  $g$  by neglecting the third term, since  $\cot I = \cot 90 = 0$ . Thus

$$g(\underline{\kappa}) = -k_1 \cos \nu f_r + k_1 k_2 \sin \nu f_\theta - \bar{\omega} = 0 \quad (69)$$

Last, we substitute in the definitions of  $f_r$  and  $f_\theta$  in terms of  $\underline{\kappa}$  from Equation (37):

$$\begin{aligned} f_r &= \kappa_\theta B_3 - \kappa_3 B_\theta \\ f_\theta &= \kappa_3 B_r - \kappa_r B_3 \end{aligned}$$

The result is

$$g = -k_1 \cos \nu (\kappa_\theta B_3 - \kappa_3 B_\theta) + k_1 k_2 \sin \nu (\kappa_3 B_r - \kappa_r B_3) - \bar{\omega} = 0 \quad (70)$$

Augment Equation (68) by multiplying  $g$  times the undetermined Lagrange multiplier  $\lambda$  so that

$$\bar{\mathcal{H}} = \mathcal{H} + \lambda g$$

$$\bar{\mathcal{H}} = \kappa_r^2 + \kappa_\theta^2 + \kappa_3^2 + \lambda (-k_1 \cos \nu (\kappa_\theta B_3 - \kappa_3 B_\theta) + k_1 k_2 \sin \nu (\kappa_\theta B_3 - \kappa_3 B_\theta) - \bar{\omega}) \quad (71)$$

Take the partial derivatives of  $\bar{\mathcal{H}}$  with respect to  $\kappa_r$ ,  $\kappa_\theta$ , and  $\kappa_3$ , set each equal to zero, and solve for  $\lambda$ :

$$\begin{aligned} \frac{\partial \bar{\mathcal{H}}}{\partial \kappa_r} &= 2\kappa_r - \lambda k_1 k_2 \sin \nu B_3 = 0 & \Rightarrow \lambda_1 &= \frac{2\kappa_r}{k_1 k_2 \sin \nu B_3} \\ \frac{\partial \bar{\mathcal{H}}}{\partial \kappa_\theta} &= 2\kappa_\theta - \lambda k_1 \cos \nu B_3 = 0 & \Rightarrow \lambda_2 &= \frac{2\kappa_\theta}{k_1 \cos \nu B_3} \\ \frac{\partial \bar{\mathcal{H}}}{\partial \kappa_3} &= 2\kappa_3 + \lambda (k_1 \cos \nu B_\theta + k_1 k_2 \sin \nu B_1) = 0 & \Rightarrow \lambda_3 &= -\frac{2\kappa_3}{k_1 \cos \nu B_\theta + k_1 k_2 \sin \nu B_1} \end{aligned}$$

Since  $\lambda = \lambda_1 = \lambda_2 = \lambda_3$ , we can solve for  $\kappa_r$  and  $\kappa_3$  in terms of  $\kappa_\theta$ :

$$\kappa_r = k_2 \tan \nu \kappa_\theta \quad (72)$$

$$\kappa_3 = -\frac{\kappa_\theta}{\cos \nu B_3} (\cos \nu B_\theta + k_2 \sin \nu B_r) \quad (73)$$

Finally, substitute  $\kappa_r$  and  $\kappa_3$  into Equation (70) and find  $\kappa_\theta$  is

$$\kappa_\theta = \frac{-\bar{\omega} B_3 \cos \nu}{B_3^2 (k_1 k_2^2 \sin^2 \nu + k_1 \cos^2 \nu) + k_1 (\cos \nu B_\theta + k_2 \sin \nu B_r)^2} \quad (74)$$

Substituting Equation (74) back into Equations (72) and (73) yields the complete solution for  $\underline{\kappa}$  required to obtained a desired  $\bar{\omega}$ .

As in Chapter 3, we have a completely analytical algorithm to determine  $\underline{\kappa}$  required to meet the stated objective. However, it has deficiencies also. Notice Equations (72) and (73) will call for infinite  $\kappa_r$  and  $\kappa_3$  at  $\nu = \pm 90^\circ$ . Like the plane change algorithm, this algorithm makes no assumptions about the  $\underline{B}$  field. Examine Equation (74) at  $\nu = 0$  and simplify to

$$\kappa_\theta = \frac{-\bar{\omega} B_3}{k_1 (B_3^2 + B_\theta^2)}$$

In Figure 25 we observe  $B_\theta$  and  $B_3$  both pass through zero at  $\nu = 0$ , making  $\kappa_\theta$  singular at that point.

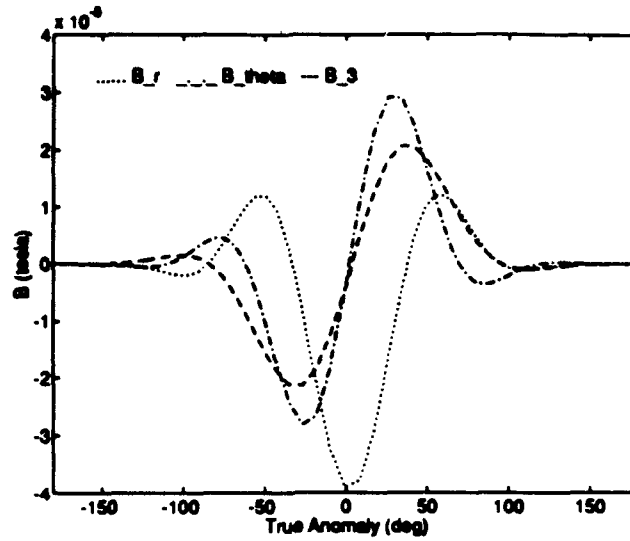


Figure 25. Geomagnetic Field Strength for 24 Hour Polar Molniya Orbit,  $\Omega_o = 141^\circ$

We compensate for the first problem by somewhat arbitrarily choosing to restrict our thrusting to the region where  $\cos \nu > .1$ , or  $-84.3^\circ < \nu < 84.3^\circ$ . This has the added benefit of not thrusting at higher altitudes where the magnitude of  $B$  drops off with the inverse cube of  $r$ , as shown in Equation (31). Another reason to not thrust over the whole orbit is the dipole model becomes suspect above 2000 km (10:2-21). Additionally, we will limit the magnitude of any component of  $\kappa$  to 500 Amp-m/kg throughout the thrust period. Thrusting near  $\nu = 0$  will not be restricted, but the magnitude will be subject to the above limit.

Earlier we defined

$$\bar{\omega} = \frac{-\Delta\omega_{oblate}}{\Delta t}$$

where  $\Delta t$  is a thrust time which can now be specified. To determine  $\Delta t$ , we find  $E$  and  $M$  at  $\cos \nu = .1$  from Equations (8) and (7), set  $M_o = -M$  at  $t_o$  and solve Equation (6) for  $\Delta t$ :

$$\begin{aligned} \cos E &= \frac{e + \cos \nu}{1 + e \cos \nu} \\ E &= .5662 \text{ rad} \end{aligned}$$

$$\begin{aligned}
M &= E - e \sin E \\
&= .4942 \text{ rad}
\end{aligned}$$

$$\begin{aligned}
M &= n\Delta t + M_0 \\
\Delta t &= \frac{2M}{n} \\
&= 3227'
\end{aligned}$$

We make two more points before analyzing the results. Even though our intent is to minimize  $\mathcal{H}$ , the method of Lagrange multipliers only guarantees we will find an extremum, not necessarily a minimum. To ensure  $\mathcal{H}$  is minimized, we must look at a point near the  $\underline{\kappa}_{sol}$  we solve for and verify  $\mathcal{H}(\underline{\kappa}_{sol}) < \mathcal{H}(\underline{\kappa}_{sol} + \delta \underline{\kappa}_{sol})$ . Also, we only chose to use a Lagrange multiplier solution to aid in solving for the three unknown components of  $\underline{f}$  with respect to one equation for  $\dot{\omega}$ . The fact that we somewhat optimized  $P_s$ , which is supposed to be beyond the scope of the thesis, is a side benefit.

### 4.3 Results

The energy required to stationkeep  $\omega$  depends on the initial right ascension of the ascending node ( $\Omega_0$ ). We see this in Figure 26, where we plot total energy versus initial  $\Omega$ . The minimum energy is  $2.4 \times 10^5$  J/kg at  $\Omega_0 = 214^\circ$ . There are several local minima with energies from  $2.6 \times 10^5$  to  $2.9 \times 10^5$  J/kg. Local maxima of  $5.3 \times 10^5$  J/kg exist at  $\Omega_0 = 89^\circ$  and  $\Omega_0 = 270^\circ$ . The wide variation in energy is caused by the  $11.5^\circ$  tilt of the magnetic field. Figure 27 shows the  $\underline{B}$  field for  $\Omega_0 = 89^\circ$ . Note the relative flatness of  $B_3$  in Figure 27 compared to  $B_3$  in Figure 25. Since  $B_3$  couples into both  $f_r$  and  $f_\theta$  in Equation (37), we can expect large values of  $\kappa_\theta$  and  $\kappa_r$  are required to generate the desired  $f_r$  and  $f_\theta$ . Hence the larger power requirement where  $\Omega_0$  results in a near zero  $B_3$ .

There is an unwanted side effect on  $a$ . Figure 28 shows how the forcing function affects  $a$  as a function of  $\Omega_0$ .  $a$  changes by as much as  $\pm 200$  km, which is undesirable. There are several places where  $\Delta a$  is 0. Unfortunately,  $\Omega_0 = 214^\circ$  is not one of them. However,  $\Delta a$  does cross zero at  $\Omega_0 = 141^\circ$ , which is near a local energy minimum at

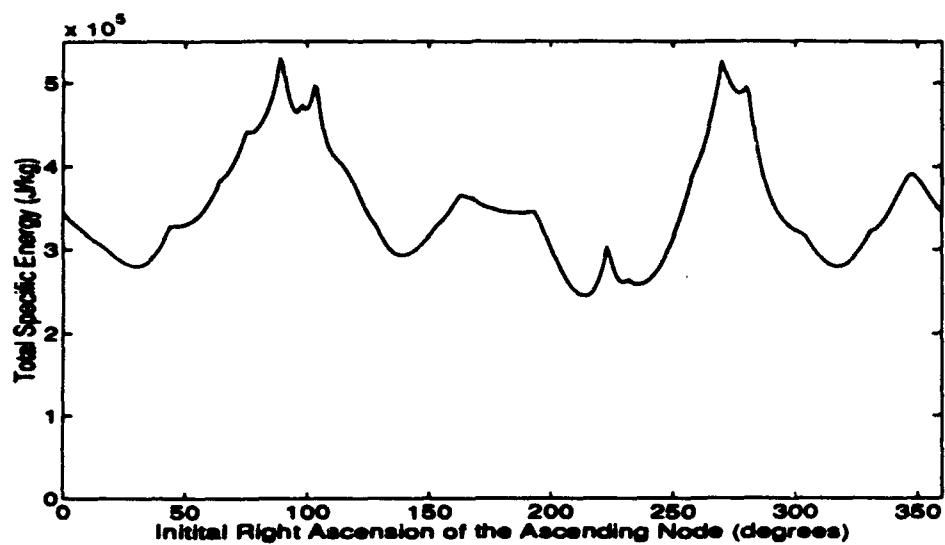


Figure 26. Specific Energy Required for Molniya Stationkeeping

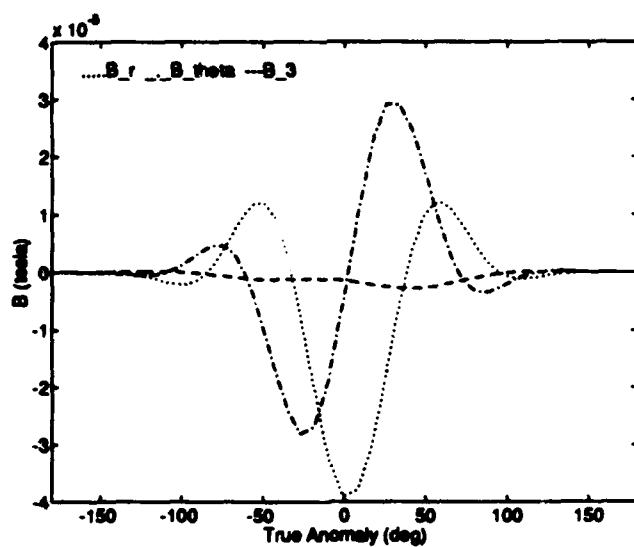


Figure 27. Geomagnetic Field Strength for 24 Hour Polar Molniya Orbit,  $\Omega_0 = 89^\circ$

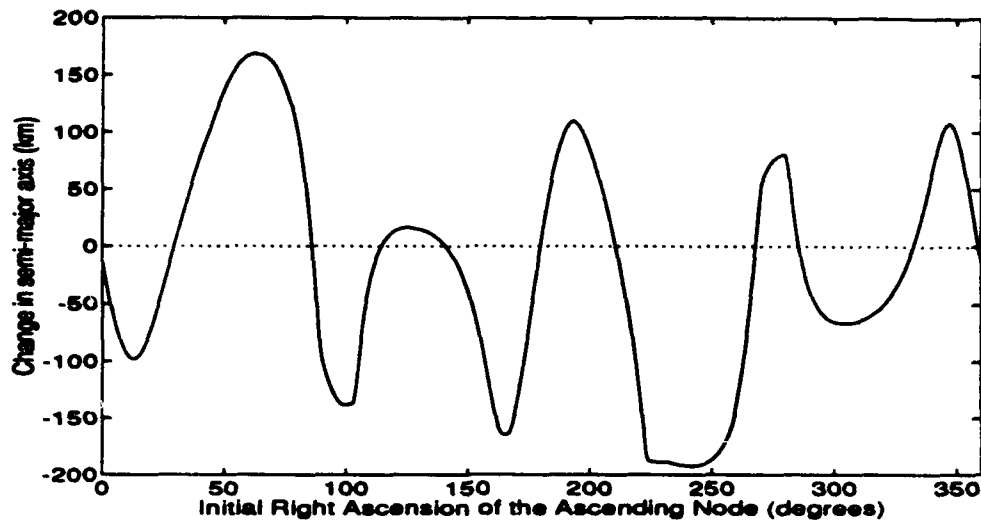


Figure 28. Change in Semi-major Axis Due to Molniya Stationkeeping

$\Omega_0 = 139^\circ$ . We choose to tradeoff an increase in energy for no change in  $a$ , and select the point  $\Omega_0 = 141^\circ$  for closer study.

Figure 29 shows how  $\omega$  varies over one orbit at  $\Omega_0 = 141^\circ$ . The algorithm produces  $\Delta\omega = -.0013^\circ$ , and we could make  $\Delta\omega$  smaller by fine tuning  $\bar{\omega}$ . Figures 30 and 31 show changes in  $I$  and  $\Omega$ . We can see what causes them by looking at Figure 32, which shows a large  $f_3$ .  $f_3$  doesn't contribute to  $\dot{\omega}$  because  $I = 90^\circ$ , but it does change  $I$  and  $\Omega$ . Although unexpected, these changes are acceptable within the scope of this analysis. Figures 33 and 34 show that by choosing  $\Omega_0 = 141^\circ$  we are able to keep  $\Delta a$  and  $\Delta e$  near 0, as desired. Finer selection of  $\Omega_0$  should drive  $\Delta a$  and  $\Delta e$  closer to 0.

The total specific energy required is  $2.94 \times 10^5$  J/kg. Figures 35 and 36 show the  $\kappa$  and  $P_t$  profiles respectively. Peak power is approximately 1000 W/kg, and occurs due to the large  $\kappa_3$  at the beginning of the thrust period.  $\kappa_3$  would be even larger if not for a limit of  $|\kappa_j|_{max} = 500$  Ampere-meters/kg. If we average the energy over  $\Delta t$  the average power  $\bar{P}_t$  is 91 W/kg, while averaging the energy over the entire orbital period  $T$  gives  $\bar{P}_t = 3.4$  W/kg.

Although restricting the beginning of the thrust period to  $\nu = -84.3^\circ$  solved the  $\cos \nu$  singularity in  $\kappa_3$ , it neglects the fact that  $B_3$  also goes through zero at  $\nu = 84.0^\circ$ , which is

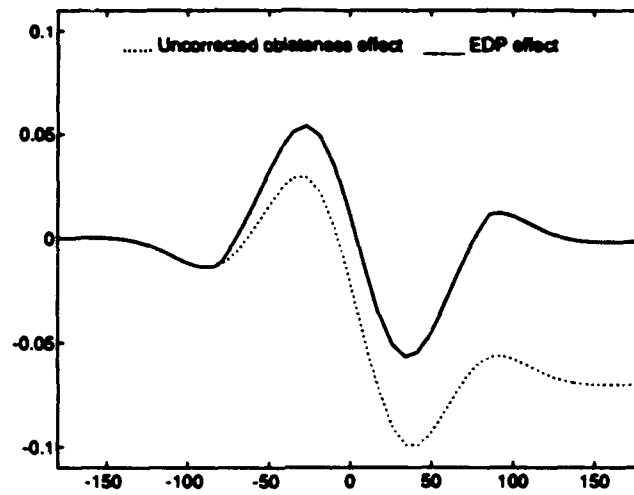


Figure 29. Change in Argument of Perigee for Molniya Stationkeeping

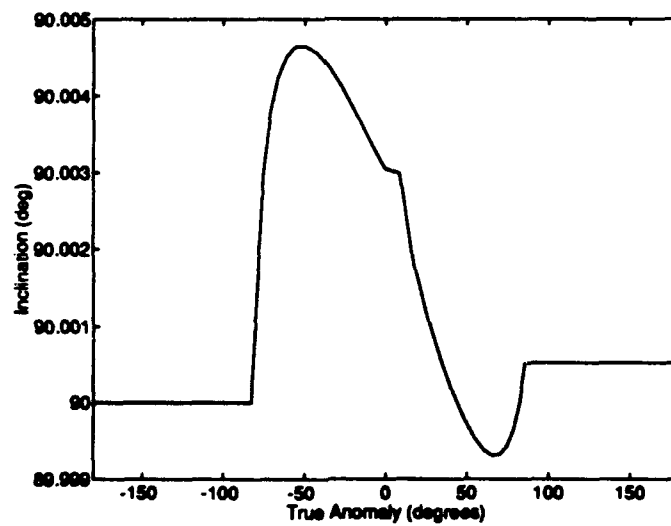


Figure 30. Change in  $I$  Due to Molniya Stationkeeping

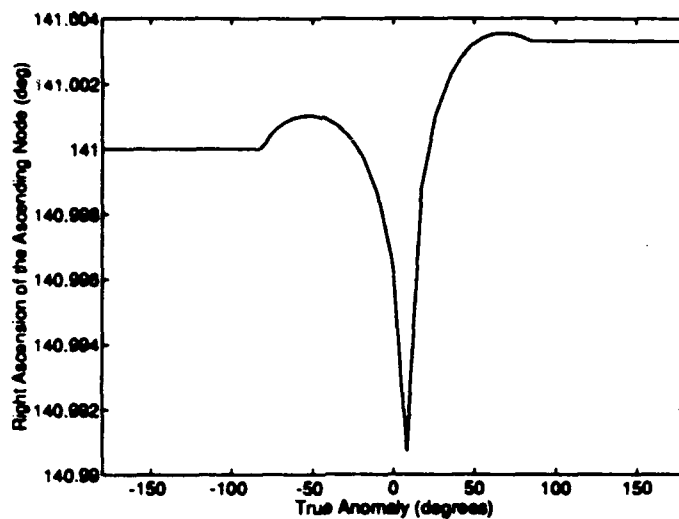


Figure 31. Change in  $\Omega$  Due to Molniya Stationkeeping

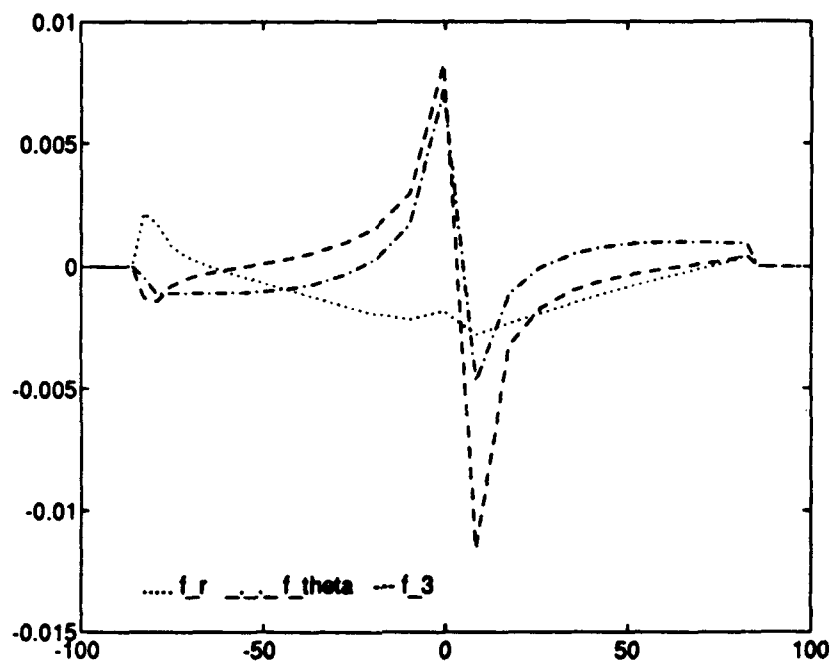


Figure 32. Electrodynamic Accelerations for Molniya Stationkeeping

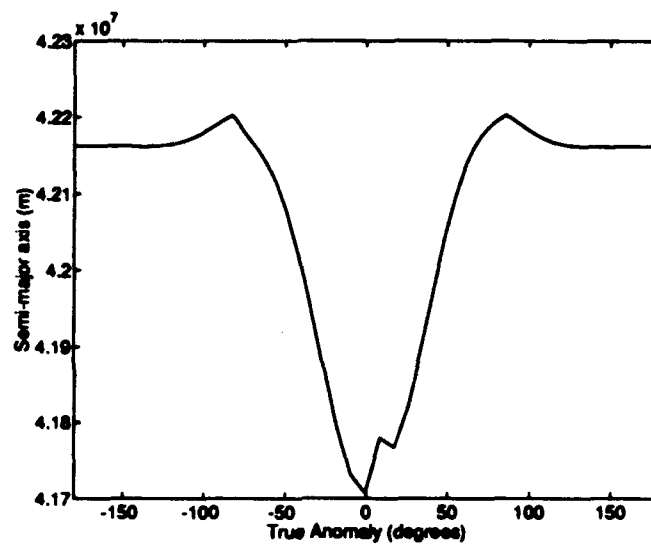


Figure 33. Change in  $a$  for Molniya Stationkeeping

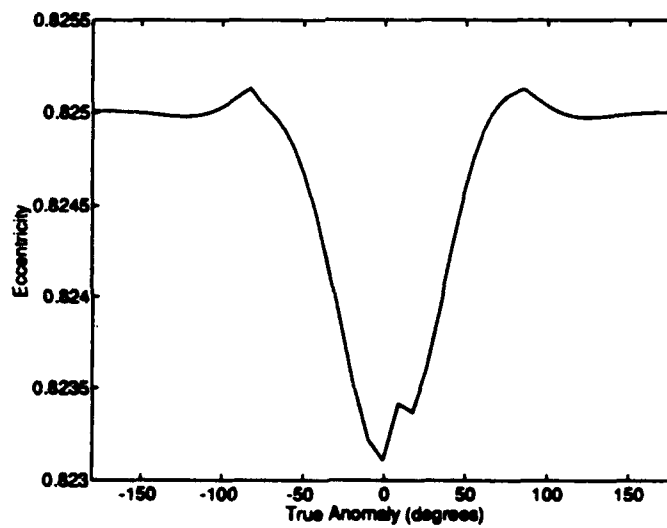


Figure 34. Change in  $e$  for Molniya Stationkeeping

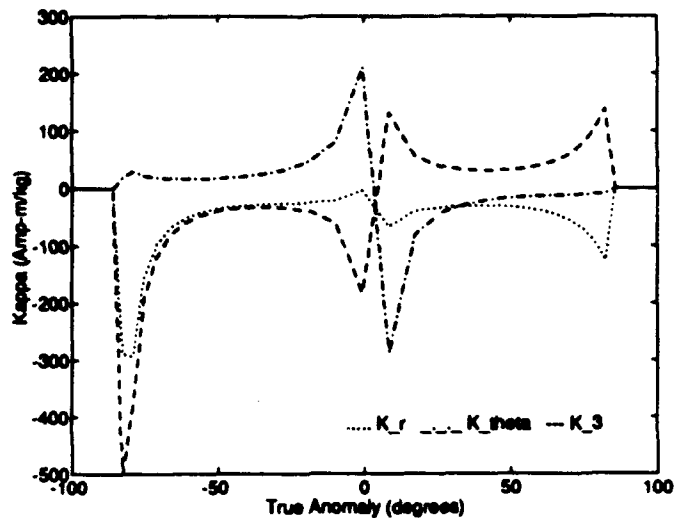


Figure 35.  $\kappa$  Profile for Molniya Stationkeeping

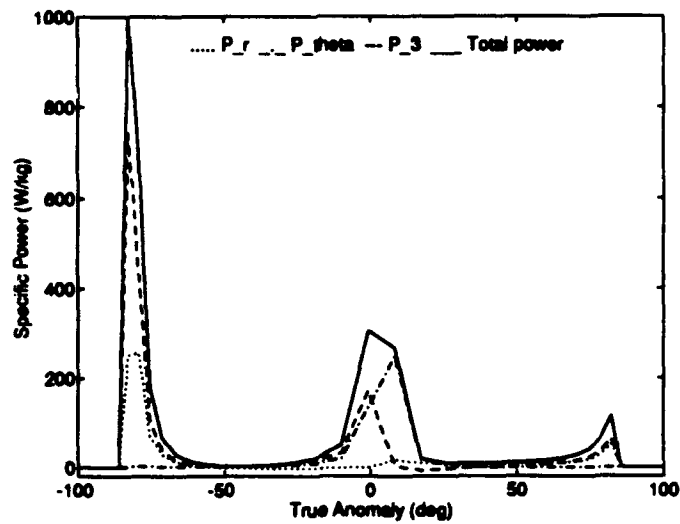


Figure 36. Power Profile for Molniya Stationkeeping

also shown in Figure 25. The peak near  $\nu = 0$  due to the weak  $B_\theta$  and  $B_3$  components is expected.  $B_3$  does not pass through zero again until  $\nu = 98^\circ$ , hence the asymmetry in the power profile. The  $\kappa$  and power levels are relatively small over the range  $20^\circ < |\nu| < 60^\circ$  where  $B_\theta$  and  $B_r$  are relatively large. This highlights the necessity to develop algorithms which incorporate some prior knowledge of the  $\underline{B}$  field. There is also some regenerative power in the each conductor at different times during the thrust period. However, it is negligible compared to the total energy required.

The check on  $\mathcal{H}(\underline{\kappa}_{old}) < \mathcal{H}(\underline{\kappa}_{old} + \delta \underline{\kappa}_{old})$  verified  $\mathcal{H}$  had in fact been minimized at every point. Although power is minimized at every point, this does not imply total energy is minimized. For instance, we can look closely at Equation (13) and see any energy expended near  $\nu = 0$  is wasted. First,  $f_3$  has no affect on  $\dot{\omega}$  due to the  $\cot I$  term. Likewise, the  $\sin \nu$  term negates the affect of  $f_\theta$ . An  $f_r$  would be useful, but we have already seen  $B_\theta$  and  $B_3$  are zero at  $\nu = 0$ .

Table 4 shows how these results compare with Janson's stationkeeping strategy for several conventional electric thrusters and a monopropellant system given a four year mission duration (4:9). Janson's approach to stationkeeping is to use a constant  $+f_r$  for six hours per day centered on apogee. Electrodynamic propulsion offers no advantage to electrical thrusters in terms of energy or power consumed. However, if the energy can be acquired from the sun and stored on board during the non-thrusting phase then no consumable fuel is required. If we treat the mass of the conductor as the analog of propellant mass for comparison purposes only, electrodynamic propulsion (EDP) can perform the mission for an unlimited time with only 30% 'propellant' mass, compared to the 38% required for a stationary plasma thruster (SPT).

There are several other advantages to using electrodynamic propulsion in this sceario compared to Janson's. Since all the thrusting is done near perigee when the payload would not be required for communications, strict attitude requirements which might not be met because of unwanted torques could be relaxed. Electrical power normally allocated to the payload could be diverted to the conductors. Any concerns about the possible adverse affects of the presence of a electrical thruster plume in the line of sight between the satellite and Earth would also be eliminated.

Table 4. Specific Power Requirements for a 24 Hour Polar Molniya Satellite

Thruster	Monopropellant	Arcjet	SPT	Ion	EDP
Energy (J/kg)	-	60,480	82,080	116,640	294,000
$P_p$ peak (W/kg)	-	2.8	3.8	5.4	997
$P_p$ ( $\mathcal{E}/\Delta t$ )	-	2.8	3.8	5.4	91
$P_p$ ( $\mathcal{E}/T$ )	-	.70	.95	1.35	3.4
Duty cycle ( $\Delta t/T$ )	-	.25	.25	.25	.0375
Propellant fraction	98%	73%	38%	23%	-

Even with the deficiencies in the forcing function algorithm which cause excessive energy and power requirements, the  $\bar{P}_p$  is feasible today. Incorporating knowledge of singularities and peaks in the  $\underline{B}$  field into the power, energy, and  $\dot{\omega}$  functions and approaching the problem with the goal of minimizing total energy should give electrodynamic propulsion a clear  $\bar{P}_p$  advantage over electric rocket propulsion.

## V. Rendezvous & Docking

In this chapter we will study the application of electrodynamic propulsion to rendezvous and docking. A unique feature of electrodynamic propulsion is there is no exhaust plume to impart momentum on the target as the chase vehicle approaches. Additionally, if we presume the electrical power comes from some renewable source, we should be able to thrust continuously and affect a *soft dock* such that the relative velocity and accelerations decay to zero as the chase vehicle approaches the target. This is in contrast to a conventional two burn maneuver, in which the chase vehicle arrives at the target with non-zero velocity and thruster firings are required to change the relative velocities to zero near-instantaneously.

For simplicity, we take the  $11.7^\circ$  tilt out of the magnetic field model and study a zero inclination reference orbit. In this scenario the  $\underline{B}$  field is perpendicular to the orbital plane, so out-of-plane thrusts are not possible. We further assume the chase vehicle is already in the same plane as the target. With these assumptions we will develop two different solutions to the Clohessy-Wiltshire equations and evaluate the trajectories and power requirements of each solution.

### 5.1 Solutions to the Clohessy-Wiltshire Equations

In section 2.5 we introduced the Clohessy-Wiltshire equations, Equations (25) and (26):

$$\ddot{x} - 2n\dot{y} - 3n^2x = f_r$$

$$\ddot{y} + 2n\dot{x} = f_\theta$$

Our approach to solving the forced Clohessy-Wiltshire equations is to specify a desired  $x$ ,  $y$ ,  $\dot{x}$ ,  $\dot{y}$ ,  $\ddot{x}$ , and  $\ddot{y}$ , then use Equations (25) and (26) to determine the necessary  $f_r$  and  $f_\theta$ .

**5.1.1 Decaying Solution.** One solution is to require  $x$  and  $y$  to behave as critically damped oscillators, i.e.

$$x = e^{pt}(b + ct) \quad (75)$$

Then the differential equation of the system is necessarily of the form

$$\ddot{x} + a_1\dot{x} + a_0x = 0 \quad (76)$$

Write the characteristic equation and solve it for critical damping:

$$p^2 + a_1p + a_0 = 0$$

$$p = \frac{-a_1 \pm \sqrt{a_1^2 - 4a_0}}{2}$$

Setting the radical equal to zero establishes critical damping:

$$a_1^2 - 4a_0 = 0$$

$$a_0 = \frac{1}{4}a_1^2$$

$$p = -\frac{a_1}{2}, -\frac{a_1}{2}$$

Next we return to Equation (77) and its derivative:

$$x = e^{pt}(b + ct)$$

$$\dot{x} = e^{pt}(pb + pct + c) \quad (77)$$

We can evaluate Equations (77) and (79) at  $t = 0$  and solve for  $b$  and  $c$  in terms of the initial conditions  $x_0$  and  $\dot{x}_0$ . We find  $b = x_0$  and  $c = \dot{x}_0 - px_0$ . Thus we can re-write Equations (77) and (79) as

$$x(t) = e^{pt}(x_0 + (\dot{x}_0 - px_0)t) \quad (78)$$

$$\dot{x}(t) = e^{pt}(\dot{x}_0 + p(\dot{x}_0 - px_0)t) \quad (79)$$

Similarly for  $y$ :

$$y(t) = e^{pt} (y_0 + (\dot{y}_0 - py_0)t) \quad (80)$$

$$\dot{y}(t) = e^{pt} (\dot{y}_0 + p(\dot{y}_0 - py_0)t) \quad (81)$$

To find  $f_r$  and  $f_\theta$  which will provide the desired performance, we set Equations (25) and (26) equal to Equation (78) and solve for  $f_r$  and  $f_\theta$ :

$$\begin{aligned} \ddot{x} - 2n\dot{y} - 3n^2x - f_r &= \ddot{x} + a_1\dot{x} + a_0x = 0 \\ f_r &= -2n\dot{y} - a_1\dot{x} - (a_0 + n^2)x \end{aligned} \quad (82)$$

$$\begin{aligned} \ddot{y} + 2n\dot{x} - f_\theta &= \ddot{y} + a_1\dot{y} + a_0y = 0 \\ f_\theta &= 2n\dot{x} - a_1\dot{y} - a_0y \end{aligned} \quad (83)$$

where  $x$ ,  $\dot{x}$ ,  $y$ , and  $\dot{y}$  are given by Equations (80-83) respectively. The value  $a_1$  will be chosen depending on the desired system performance.

**5.1.2 Polynomial Solution.** Another approach is to specify  $N$  boundary conditions and define functions  $x$  and  $y$  as  $(N - 1)$ th order polynomials in time. For instance, let

$$x = a_x + b_x t + c_x t^2 + d_x t^3 + e_x t^4 \quad (84)$$

$$\dot{x} = b_x + 2c_x t + 3d_x t^2 \quad (85)$$

$$\ddot{x} = 2c_x + 6d_x t \quad (86)$$

with boundary conditions

$$x(0) = x_o \quad x(t_f) = 0$$

$$\dot{x}(0) = \dot{x}_o \quad \dot{x}(t_f) = 0$$

$$\ddot{x}(t_f) = 0$$

If we evaluate Equations (86-88) at the boundary conditions we find

$$a_x = x_o$$

$$b_x = \dot{x}_o$$

$$c_x = \frac{-3\dot{x}_o}{t_f} - \frac{6x_o}{t_f^2}$$

$$d_x = \frac{3\dot{x}_o}{t_f^2} + \frac{8x_o}{t_f^3}$$

$$e_x = \frac{\dot{x}_o}{t_f^3} - \frac{3x_o}{t_f^4}$$

In a like manner

$$y = a_y + b_y t + c_y t^2 + d_y t^3 + e_y t^4 \quad (87)$$

$$\dot{y} = b_y + 2c_y t + 3d_y t^2 \quad (88)$$

$$\ddot{y} = 2c_y + 6d_y t \quad (89)$$

$$y(0) = y_0 \quad y(t_f) = 0$$

$$\dot{y}(0) = \dot{y}_0 \quad \dot{y}(t_f) = 0$$

$$\ddot{y}(t_f) = 0$$

$$a_y = y_0$$

$$b_y = \dot{y}_0$$

$$c_y = \frac{-3\dot{y}_0}{t_f} - \frac{6y_0}{t_f^2}$$

$$d_y = \frac{3\dot{y}_0}{t_f^2} + \frac{8y_0}{t_f^3}$$

$$e_y = \frac{\dot{y}_0}{t_f^3} - \frac{3y_0}{t_f^4}$$

Then  $f_r$  and  $f_\theta$  are given by substituting Equations (86-91) into Equations (25) and (26).

## 5.2 Methodology of the Rendezvous & Docking Study

The methodology of this study differs slightly from chapters 3 and 4 due to the simplifications we introduced at the beginning of the chapter. The first implication is  $\underline{B} = \{0 \ 0 \ B_3\}^T = \text{constant}$ . Then

$$\underline{f} = \underline{\kappa} \times \underline{B} = \begin{pmatrix} \kappa_\theta B_3 \\ -\kappa_r B_3 \\ 0 \end{pmatrix} \quad (90)$$

Solve Equation (92) for  $\underline{\kappa}$  and find

$$\kappa_r = -\frac{f_\theta}{B_3}$$

$$\kappa_\theta = \frac{f_r}{B_3}$$

$$\kappa_3 = 0$$

This simplifies the power expression also. In addition to the lack of  $\kappa_3$ ,  $B_r$ , and  $B_\theta$ , we can simplify the relative velocity equation to

$$\underline{v}_{rel} = (n - \omega_\oplus) r \hat{c}_\theta$$

Thus Equation (47) becomes

$$P_s = -\kappa_r (v_{rel} B_3) + 4 \frac{m}{m_c} \rho_n \rho_c (\kappa_r^2 + \kappa_\theta^2)$$

As in chapter 3,  $a = 6,578$  km for the reference orbit, which has a period  $T = 5,309^s$ . We choose one revolution as the time duration in which to perform the maneuver, and use  $t_f = 5,309^s$  in evaluating the constants of the polynomial solution.

An unlimited combination of initial conditions and time durations can be studied. The initial conditions we studied are those when the chase vehicle is in a circular orbit. In that case,  $\dot{x}_o = 0$  for any  $x_o$  and  $y_o$ . To find  $\dot{y}_o$  we revisit Equation (28):

$$x(t) = - \left( \frac{2\dot{y}_o}{n} + 3x_o \right) \cos nt + \frac{\dot{x}_o}{n} \sin nt + 4x_o + \frac{2\dot{y}_o}{n}$$

If  $x_o$  is specified, then we find  $\dot{y}_o$  by setting the coefficient of the  $\cos nt$  term equal to zero and solving for  $\dot{y}_o$  in terms of  $x_o$ :

$$\begin{aligned} \frac{2\dot{y}_o}{n} + 3x_o &= 0 \\ \dot{y}_o &= -\frac{3x_o n}{2} \end{aligned}$$

$a_1 = 3n$  is used in the decaying solution to ensure the positions, velocities, and electrodynamic accelerations sufficiently decay within  $t_f$ .  $a_1 = n$  and  $a_1 = 2n$  were also considered, but neither value produced  $x(t_f)$  and  $y(t_f)$  sufficiently close to zero to allow a valid comparison between the decaying solution and the polynomial solution. For example, the response at  $t_f$  of the decaying solution when  $a_1 = 2n$  for initial conditions  $(x_o, y_o) = (1, 1)$  km is  $x(t_f) = 14$  m and  $y(t_f) = -4$  m. In contrast,  $x(t_f) = 7\mu\text{m}$  and

Table 5. Rendezvous Power Results ( $m/m_c = 10$ )

Case	Solution	$x_0$ (km)	$y_0$ (km)	$\mathcal{E}$ (J/kg $\times 10^4$ )	peak $P_i$ (W/kg)	$\bar{P}_i$ (W/kg)
1	Decaying	1	0	6.04	234	11.5
2	Polynomial			8.65	38.3	16.5
3	Decaying	1	1	1.63	98.1	3.10
4	Polynomial			4.66	22.1	8.86
5	Decaying	0	1	1.47	14.5	2.80
6	Polynomial			.597	2.68	1.14
7	Decaying	-1	1	14.2	306	27.1
8	Polynomial			14.7	61.4	28.0
9	Decaying	-1	0	6.90	142	13.1
10	Polynomial			9.52	40.1	18.1
11	Decaying	-1	-1	2.49	52.1	4.74
12	Polynomial			5.52	23.7	10.5
13	Decaying	0	-1	1.47	60.6	2.80
14	Polynomial			.603	3.81	1.15
15	Decaying	1	-1	13.4	444	25.5
16	Polynomial			13.9	59.5	26.4

$y(t_f) = -9\mu\text{m}$  for the polynomial solution at the same initial conditions. If  $a_1 = 3n$ , then  $x(t_f) = 0.9\text{ m}$  and  $y(t_f) = 0.1\text{ m}$ , which we deem sufficiently close to zero to allow a valid comparison between the two solutions.

### 5.3 Results

Both solutions were evaluated at eight different starting positions on a  $1\text{ km} \times 1\text{ km}$  square centered on the  $x - y$  origin. The results of each case are summarized in Tables 5 and 6.

The decaying solution has the lowest energy and  $\bar{P}_i$  for all the trajectories except the two which start on the  $x$  axis. However, in every case the decaying solution has a higher peak  $P_i$  than the polynomial solution. If peak power is a concern, then the polynomial solution appears best, but the tradeoff is sometimes twice as much total energy and  $\bar{P}_i$ , depending on the initial conditions.

Table 6. Rendezvous Final Position and Velocity Results

Case	Solution	$x_f$ (m)	$y_f$ (m)	$\dot{x}_f$ (m/sec)	$\dot{y}_f$ (m/sec)
1	Decaying	.9254	-.8357	-.0015	.0013
2	Polynomial	7e-6	-2e-5	-3e-6	7e-6
3	Decaying	.9254	.0897	-.0015	-.0002
4	Polynomial	7e-6	-9e-6	-3e-6	4e-6
5	Decaying	0	.9254	0	-.0015
6	Polynomial	0	7e-6	0	-3e-6
7	Decaying	-.9254	1.7612	.0015	-.0028
8	Polynomial	-7e-6	23e-6	3e-6	-11e-6
9	Decaying	-.9254	.8357	.0015	-.0013
10	Polynomial	-7e-6	16e-6	3e-6	-8e-6
11	Decaying	-.9254	-.0897	.0015	.0002
12	Polynomial	-7e-6	9e-6	3e-6	-4e-6
13	Decaying	-.9254	.8357	.0015	-.0013
14	Polynomial	0	-7e-6	0	3e-6
15	Decaying	.9254	-1.7612	-.0015	.0028
16	Polynomial	7e-6	-23e-6	-3e-6	11e-6

Each solution has the desirable result of allowing a soft dock. The velocities and electrodynamic propulsion accelerations all go to zero as the chase vehicle approaches the target in every case.

Figures 37-40 show the trajectory, velocity, acceleration, and power profiles of each solution for cases 1-4. Note the peak  $P$ , occurs at the beginning of the thrust period for the decaying solution, and then quickly decays, as we expect. Both solutions cause large power discontinuities at  $t_0$ . In each case, the velocities and electrodynamic propulsion accelerations approach zero as the chase vehicle approaches the target. Figures 37-40 are also representative of cases 7-12, 15, and 16.

Cases 1-4 and 15-16 require less energy than their counterparts, cases 9-12 and 7-8. This is to be expected, since cases 7-12 are converting electrical energy into potential energy, while cases 1-4 and 15-16 are trading potential energy for electrical energy. In cases 1-4 and 15-16 we also see parts of the trajectory where the total power is negative, indicating the ability to regenerate power. There are even regions in the first quadrant ( $x_0 > 0, y_0 > 0$ ) where the total energy is zero, i.e. the entire maneuver can be done

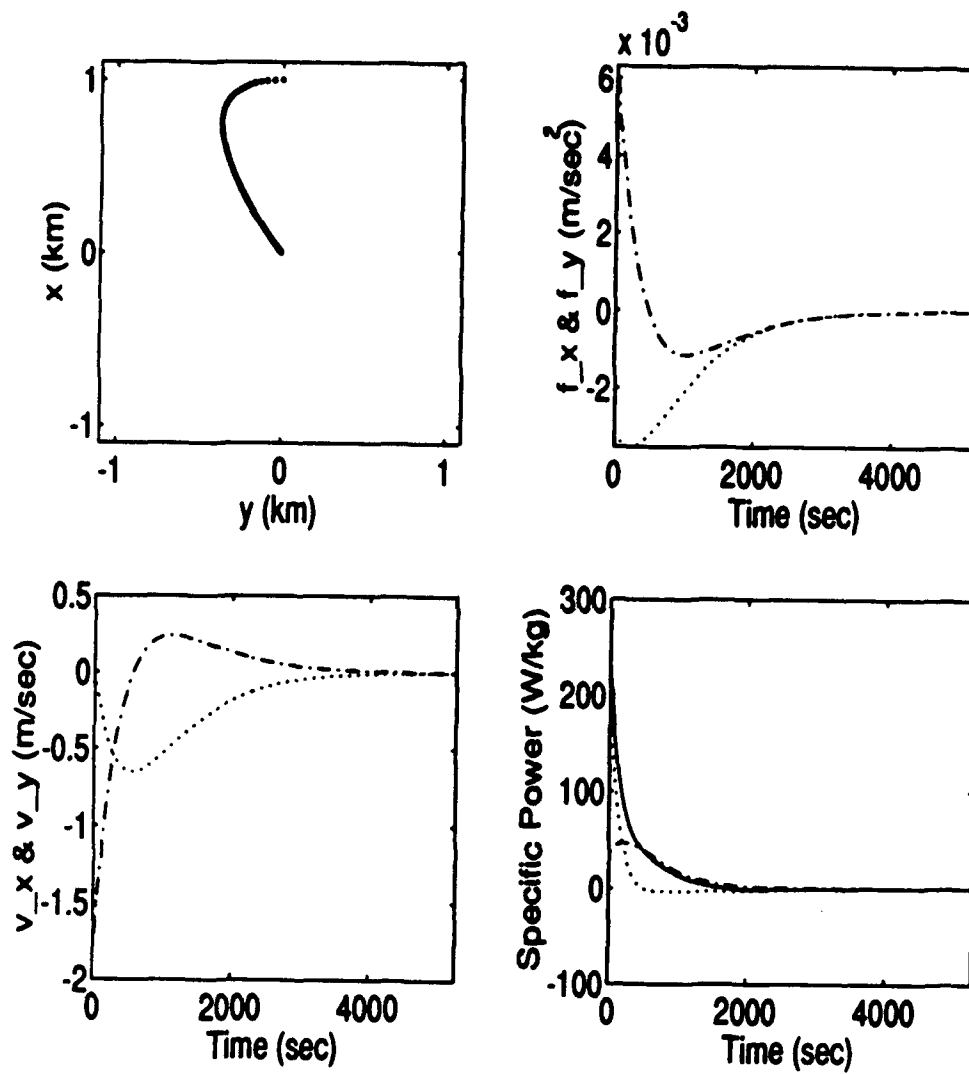


Figure 37. Case 1: Decaying Solution

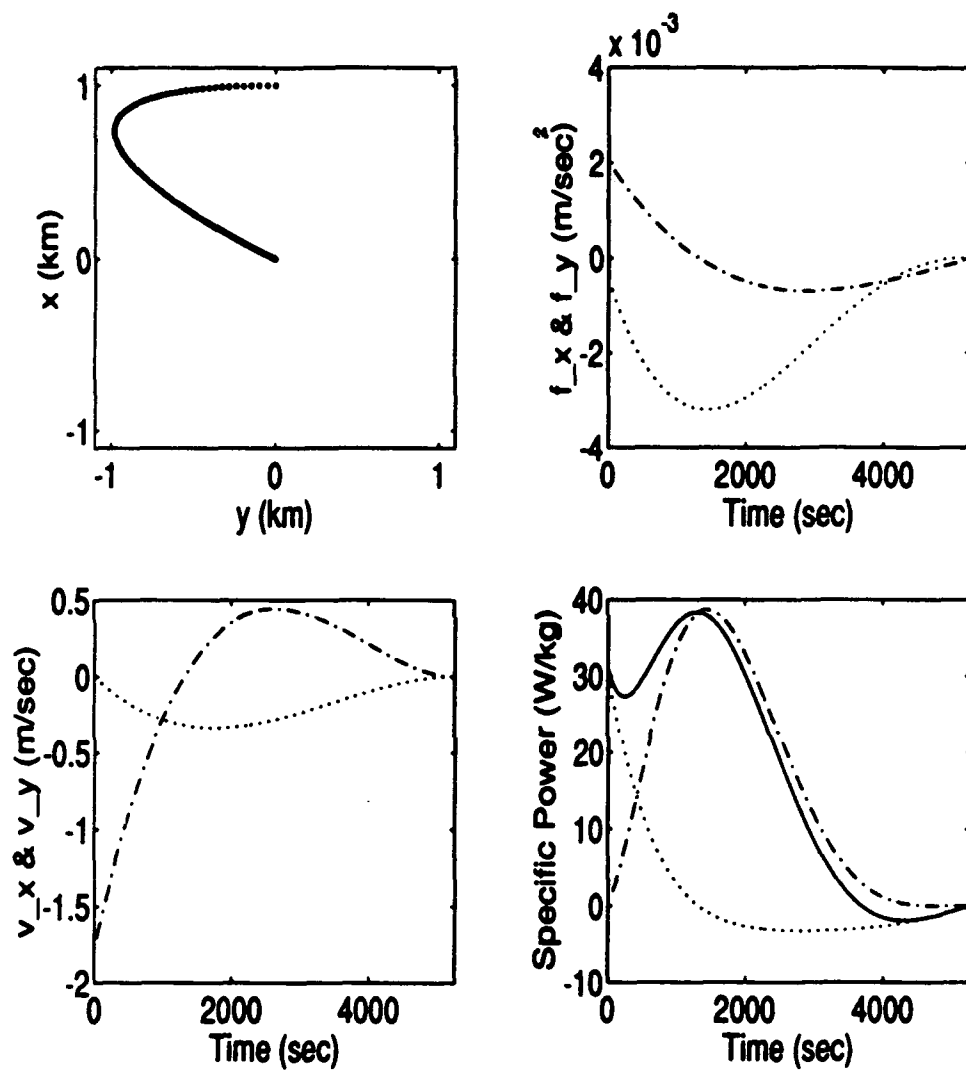


Figure 38. Case 2: Polynomial Solution

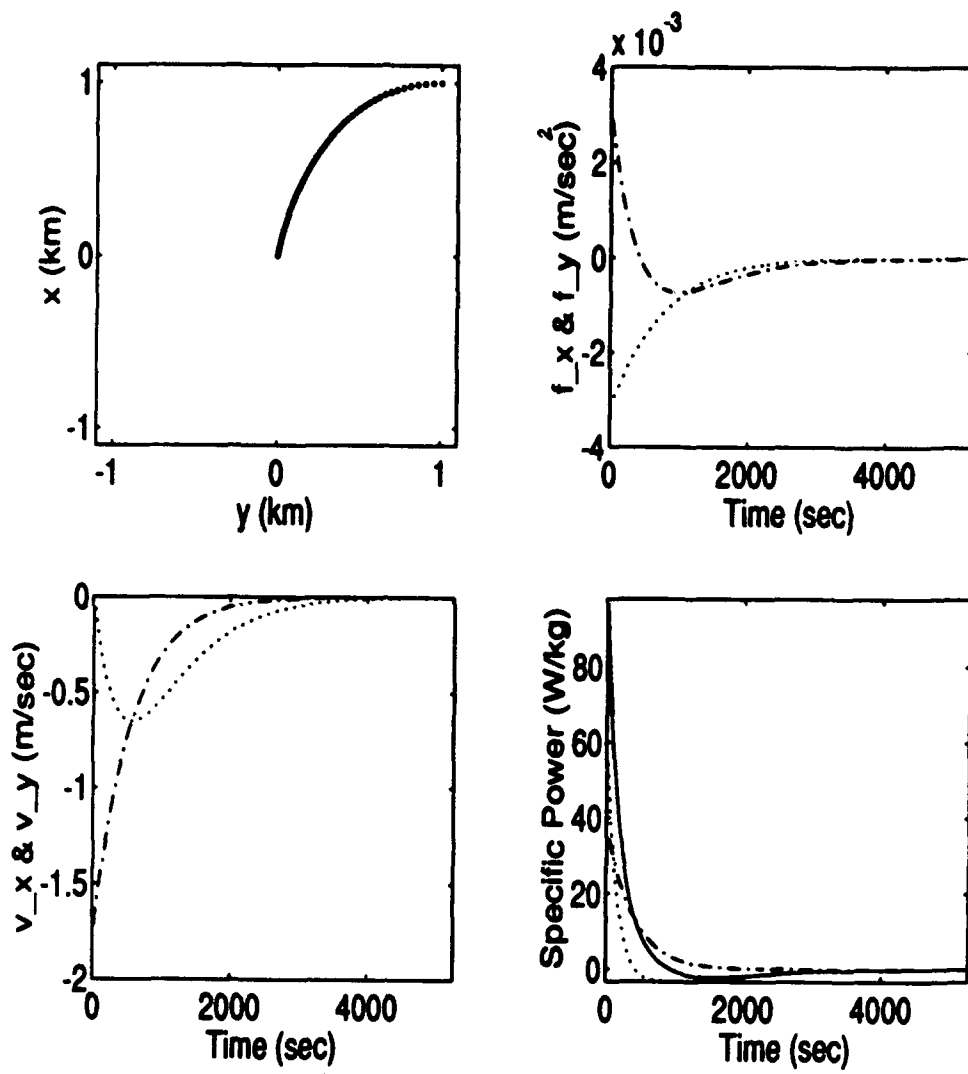


Figure 39. Case 3: Decaying Solution

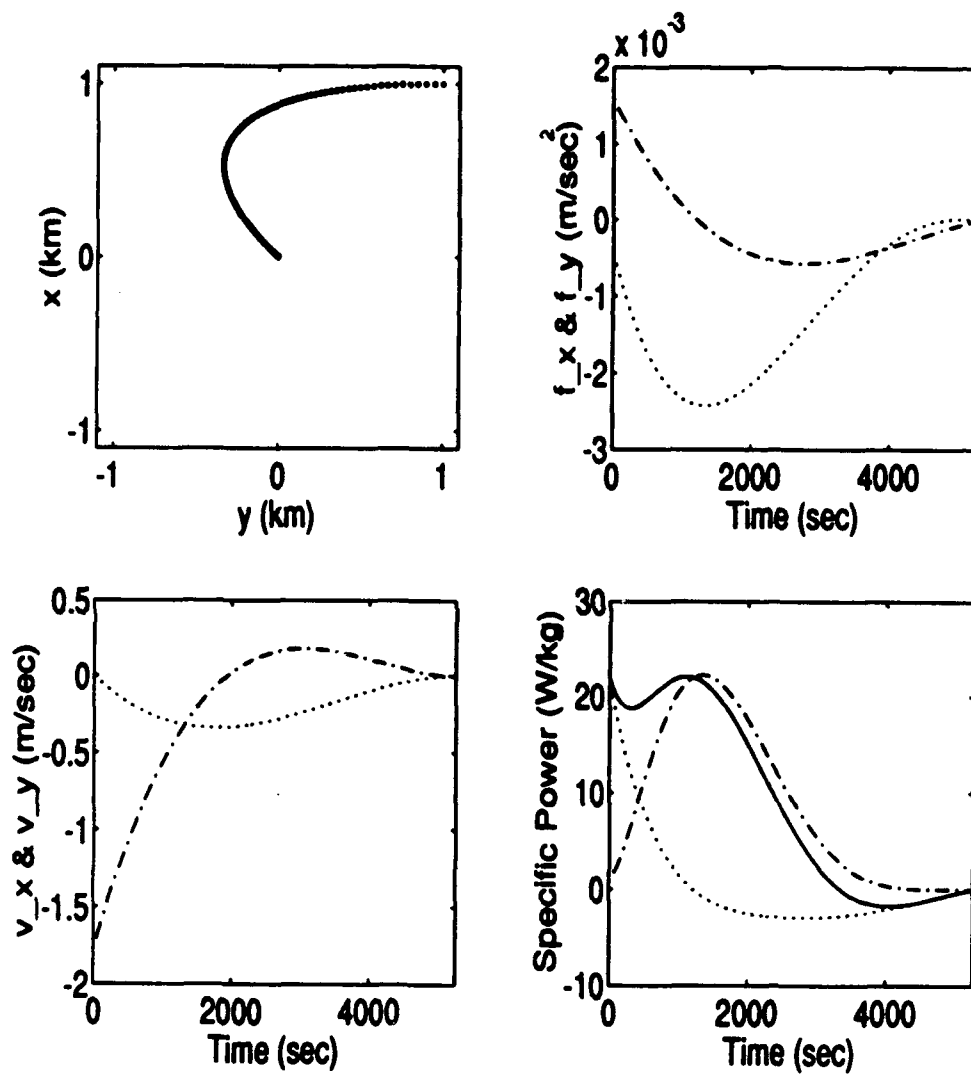


Figure 40. Case 4: Polynomial Solution

Table 7. Additional Rendezvous Power Results

Case	Solution	$m/m_c$	$\mathcal{E}$ (J/kg $\times 10^4$ )	peak $P_s$ (W/kg)	$P_s$ (W/kg)
7	Decaying	6	8.72	156	16.6
8	Polynomial	6	9.00	37.6	17.1
7	Decaying	3	4.57	43.6	8.7
8	Polynomial	3	4.72	20.2	8.98

with no net energy expenditure. This is consistent with what is already well known about electrodynamic propulsion: power generation creates a drag which lowers altitude (12:126). However, if a mission designer accepts the constraints on initial conditions which allow the maneuvers to be done with no net energy, then electrodynamic propulsion has near term application.

The worst case initial conditions, cases 7 and 8, were chosen for further evaluation at different conductor mass ratios. These results are summarized in Table 7. These results are consistent with the conclusions in Chapter 3: the  $\kappa_j^2$  terms dominate the power equation, so if larger conductors are used less power is required. This worst case initial condition is still beyond the 4 W/kg benchmark, even with the 'all conductor' ratio of  $m/m_c = 3$ .

Figures 41 and 42 show how either solution can be used to perform a V-BAR approach, where the chase vehicle approaches the target along  $\underline{y}$ .  $f_r$  and  $f_\theta$  are controlled to ensure in-track movement without any radial motion. Both trajectories are essentially the same, but the polynomial solution uses less energy.

A drawback of each solution is the power discontinuity at  $t_0$ . This can be solved with a new fifth order polynomial solution and the additional boundary conditions

$$\ddot{x}(0) = \ddot{x}_0$$

$$\ddot{y}(0) = \ddot{y}_0$$

Also, even though Equations (25) and (26) are coupled in  $x$  and  $y$ , neither the decaying nor polynomial solutions are coupled. If  $y$  can be specified as a function of  $x$  (or

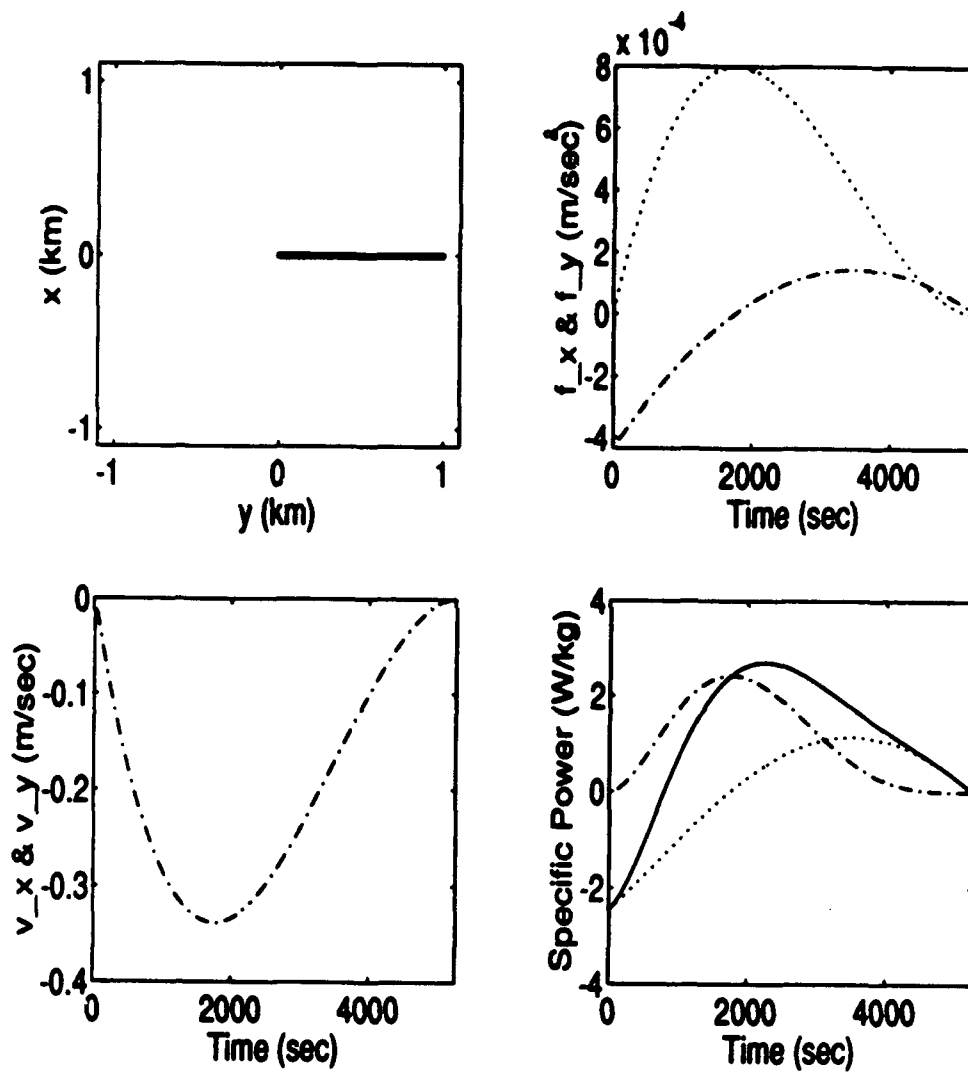


Figure 41. Case 6: V-BAR Approach with Polynomial Solution

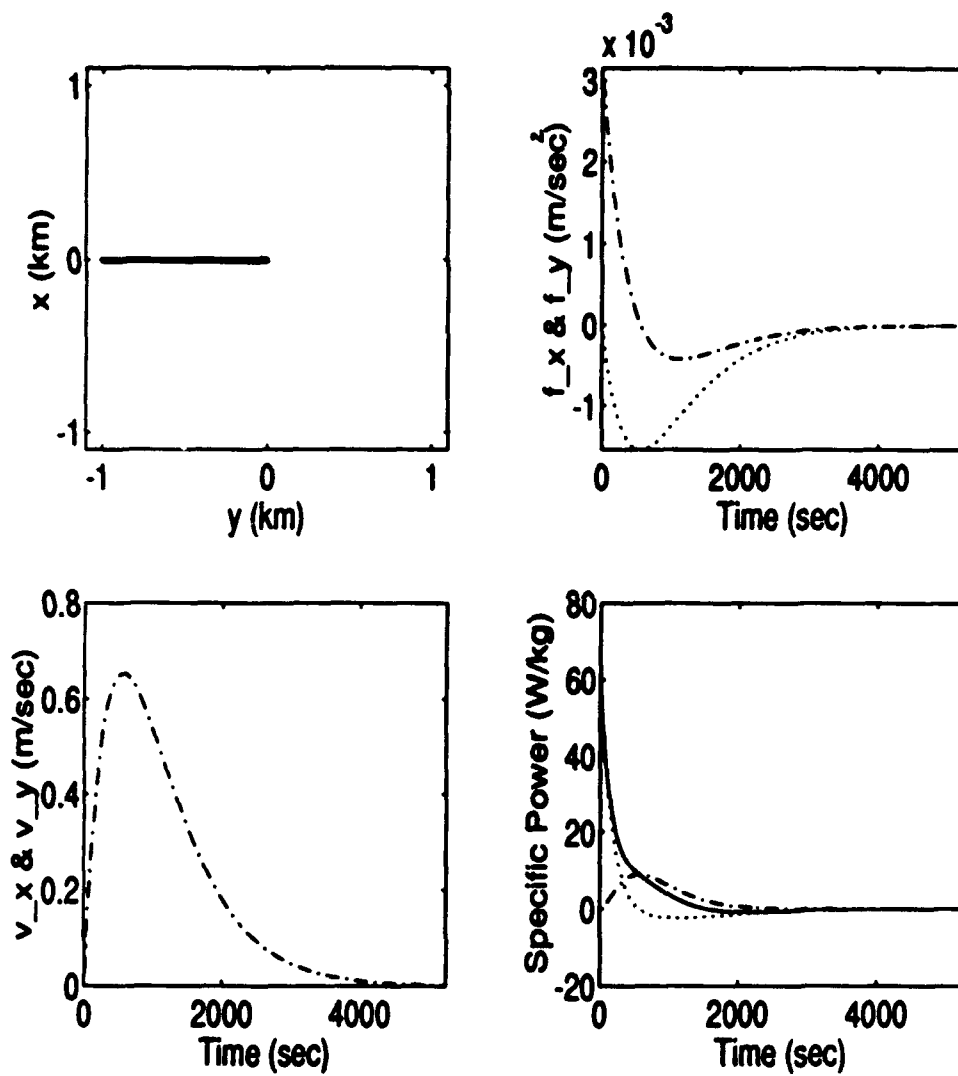


Figure 42. Case 13: V-BAR Approach with Decaying Solution

vice versa), then the angle of approach can be controlled. Such a coupled solution might also take advantage of the system's kinetic and potential energy in such a way as to lower the electrical energy requirement. Considerable effort was expended searching for such a solution without success.

Additional study should be performed to re-validate these results without the simplifying assumptions used here. Also, the initial conditions were very specific, and are not likely to be found in actual operations. Various initial conditions, especially a non-circular initial chase orbit, should be studied to ensure the conclusions still hold. Out of plane motion was not studied, and Lawrence has already shown undesired out of plane motion results even when  $z_o = 0$ ,  $\dot{z}_o = 0$ , and  $\ddot{z}_o = 0$  (8:E-15, E-17). Future work should re-incorporate this fact.

## *VI. Conclusions & Recommendations*

In this final chapter we summarize the major results of the thesis work and make recommendations for further research.

The two important results of the theoretical development were the definition of the vector  $\underline{g}$  and the subsequent derivation of the specific power equation. Together they allow the analysis to proceed without having to specify a detailed vehicle configuration; only designation of the conductor mass to total vehicle mass ratio and selection of a conductor metal need be made. The specific power equation clearly shows how these choices affect the power required. The total energy, found by integrating the power equation, is then useful in comparing different scenarios. If the conductor mass to total vehicle mass ratio is considered analogous to a classical propulsion system's propellant mass ratio, then the two parameters may be used as a basis for comparison between electrodynamic propulsion and classical propulsion systems, as we did in chapter 4. In the future, design engineers can use specified values of  $\kappa$  and  $P$ , to perform trade-off studies of current, conductor length, or number of conductor turns to determine the optimum configuration for a specific application.

Electrodynamic propulsion appears to be a feasible near term alternative to classical propulsion systems for small orbital plane changes. Plane changes are best done at relatively high inclinations due to the nature of the magnetic field. Constraining semi-major axis change may expand the plane change rate envelope.

Electrodynamic propulsion may also be used for stationkeeping the argument of perigee of a true polar Molniya satellite. The Molniya stationkeeping strategy developed here is very sensitive to the right ascension of the ascending node. A candidate for future research is to constrain the change in semi-major axis to eliminate this sensitivity.

For both plane change and Molniya stationkeeping, development of forcing function algorithms incorporating a priori knowledge of the magnetic field and application of optimization techniques to reduce power consumption or otherwise improve performance is recommended.

Electrodynamic propulsion is applicable to rendezvous and docking, although the relatively high power requirements limit near-term implementation to the V-BAR regime. If spacecraft specific power supplies can improve to approximately 25 W/kg then all the rendezvous cases studied in Chapter 5 become feasible. The ability to perform a soft dock has been demonstrated, which is advantageous compared to a two burn rendezvous and docking maneuver. We recommend these conclusions about rendezvous and docking be reconfirmed after incorporation of the tilt in the Earth's magnetic field into the geomagnetic field model and consideration of out of plane motion, as well as investigation of various other initial conditions. Further work is also warranted in developing solutions to the forced Clohessy-Wiltshire equations. Since the Clohessy-Wiltshire equations are coupled in  $x$  and  $y$ , we recommend investigating a solution which also couples  $x$  and  $y$ , and predict it will use less energy than our uncoupled solutions. It will have the additional benefit of allowing the approach angle to be controlled.

We have several general recommendations for future research. First, the feasibility of power supplies which can actually deliver the peak specific power and total energy in the ranges discussed in this thesis should be evaluated. Second, we reiterate Lawrence's recommendation that future studies be conducted with a more accurate geomagnetic field model. Third, electromagnetic compatibility is a concern for the integration of electrodynamic propulsion into any vehicle, and should be studied. A particular concern is the effect of the localized magnetic field caused by the current in the closed circuit conductor on the geomagnetic field, especially if the vehicle is using magnetometers to measure the magnetic field.

The most feasible near term realization of electrodynamic propulsion may be a combination of chemical and electrodynamic thrusters applied to rendezvous and docking. The chemical thrusters could be used to reduce the range to a point where electrodynamic propulsion can take over and perform the terminal docking maneuver within reasonable power limits. Perhaps someday electrodynamic thrusters can even be incorporated into manned maneuvering units, allowing astronauts to work in close proximity without concern for thruster plume impingement on each other.

## Appendix A. File Listings

This appendix contains the MATLAB script and function files used to generate the data in Chapters 3-5

The script inc.m was used for the inclination change study.

```
% variable names in square brackets are the names of the variables
% used in the main body of the thesis.
tic
% -----Get started -----

i=1; % Counter for matrices at end
n=1.18339e-3; % Mean motion (rad/sec)
alfao=0.; % Inertial longitude of Greenwich
%meridian at beginning of time span
% (rad) [theta_g_0]
alfadot=7.292462056e-5; % Rotational rate of Earth (rad/sec)
% [omega_o+]
r=6578000; % Initial radius (m)
Mag=8.05e15; % Magnetic moment [script M]
% (kg/m^3-coul-sec)
RAAN=0; % Right ascension of ascending node
% [cap Omega] (rad)
a=r; % Semi-major axis (m)
e=0.; % Eccentricity
w=0.; % Argument of perigee (rad)
% [little omega]
Mo=0; % Mean anomaly at epoch (rad) [M_o]
rhor=2.8e-8; % Conductor resistivity (ohm-m)
% [rho_R]
rhoc=2700; % Conductor mass density (kg/m^3)
% [rho_c]
mass=1; % Total vehicle mass (kg) [m]
Mu=3986012e14; % Gravitational parameter of the
% Earth (m^2/s^2) [mu]
mmc=10; % Conductor mass ratio [m/m_c]
idotbar=2.0257e-7;I=pi/2; % idotbar is desired average
% inclination change rate (rad/sec)
% [bar over dot over I]
% I is inclination (rad)
% 1 deg/day
% I=45 deg, -1 deg/day
% .1 deg/day, I=90
% -.1 deg/day, I=45

%idotbar=-2.0257e-07;I=pi/4;
%idotbar=2.0257e-8;I=pi/2;
%idotbar=-2.0257e-08;I=pi/4;
```

```

p1=0; % Equinoctial element [h]
p2=0; % Equinoctial element [k]
M=0; % Mean anomaly (rad)
v=0; % Argument of latitude (rad)[u]

% -----Initialize magnetic field rotation matrix -----

phio=pi/2-78.3*pi/180;
lamo=69*pi/180;

Rmag=[cos(lamo)*cos(phio) -sin(lamo)*cos(phio) -sin(phio)
      sin(lamo) cos(lamo) 0
      cos(lamo)*sin(phio) -sin(lamo)*sin(phio) cos(phio)];

% Note: Rmag rotates from Earth's cartesian frame to magnetic cartesian
%frame Rmag=[R^gb]

% ----- Here is the main loop -----

for t=to:ts:tf % t is the time (sec)
               % ts is the time step (sec)
               % tf is the final time (sec)

    p=a*(1-e^2); % Semi-latus rectum (m)

    %if rem(i,10)==0 % This puts out a message to let you
    %[v*180/pi w*180/pi] % know where the program is if you
    %end % want it to

    r=p/(1+e*cos(v));

    alfa=alfao+alfadot*t; % Rotates the Earth

% ----- Create rot matrix from orbital frame to cart inert -----
r11=cos(RAAN)*cos(v)-sin(RAAN)*cos(I)*sin(v);
r12=-cos(RAAN)*sin(v)-sin(RAAN)*cos(I)*cos(v);
r13=-sin(RAAN)*sin(I);

r21=sin(RAAN)*cos(v)+cos(RAAN)*cos(I)*sin(v);
r22=-sin(RAAN)*sin(v)+cos(RAAN)*cos(I)*cos(v);
r23=-sin(I)*cos(RAAN);

r31=sin(v)*sin(I);
r32=sin(I)*cos(v);

```

```

r33=cos(I);

Ro2ci=[r11 r12 r13           % [R-ia]
       r21 r22 r23
       r31 r32 r33];

% ----- Rotate [r 0 0] in sperical coord into [x y z] inertial -----
xyzi=Ro2ci*[r 0 0]';

% ----- Rotate xyzi into xyzE -----
Rci2cE=rot(0,alfa-alfao);      % Rci2cE rotates from cartesian
                                % inertial frame to Earth's
                                % rotating cartesian frame [R-gi]

xyzE=Rci2cE*xyzi;

% ----- rotate xyzE into magnetic cartesian frame -----
xyzm=Rmag*xyzi;

% ----- Compute lat and long in mag frame -----
phim=atan2(xyzm(3),(xyzm(1)^2+xyzm(2)^2)^.5);
lamm=atan2(xyzm(2),xyzm(1));

% ----- Compute magnetic field components -----

z=2*Mag*sin(phim)/r^3;          % Radial component (kg/coul-sec)
h=-Mag*cos(phim)/r^3;          % Transverse component (toward
                                % north pole) (kg/coul-sec)

% -Compute rot matrix to go from spherical magnetic to cartesian magnetic-
Rsm2cm=rot(phim,lamm);          % [R-bm]

% ----- Rotate [z 0 h] into cartesian magnetic frame -----
Bcm=Rsm2cm*[z 0 h]';           % (kg/coul-sec)

% ----- Rotate Bcm into Earth's rotating cartesian frame -----
BcE=Rmag'*Bcm;

```

```

% ----- Rotate BcE into cartesian inertial frame -----

Bci=Rci2cE'*BcE; % (kg/coul-sec)
xyzI=Rci2cE'*xyzE; % Debug code: xyzI=xyzi if all
                    % rotations are correct

% ----- Rotate Bci into orbital frame -----

B=Ro2ci'*Bci; % (kg/coul-sec)

rtp=Ro2ci'*xyzI; % Debug code - rtp=[r 0 0] if all
                  % rotations are correct;

% ----- Compute kappa vector -----
b=B/norm(B);
d=[b(2) -b(1) 0]/sqrt(b(2)^2+b(1)^2); % kappa unit vector [kappa hat]

a3=idotbar*2*n*r*cos(v); % Out of plane acceleration
                           % (m/sec^2) [f_3]

ilm=a3/sqrt(B(1)^2+B(2)^2); % Scalar il/m (A-m/kg) [kappa]

ILM=ilm*d; % IL/m vector [kappa vector]

if max(abs(ILM))>200 % Sorry, no infinite kappa
    ILM=200*ILM/max(abs(ILM));
end

% ----- Power requirements -----
vmagE=[-alfadot*xyzE(2) alfadot*xyzE(1) 0]'; % B field velocity [v_B]
                                              % in the g frame

vmagi=Rci2cE'*vmagE; % v_B in the i frame

vmago=Ro2ci'*vmagi; % v_B in the a frame

vrel=[r*e*sin(v)*n/(1+e*cos(v)) r*n 0]'-vmago; % v_rel

Pxi=-(vrel(2)*B(3)-vrel(3)*B(2)); % iVi radial
Pyi=-(vrel(3)*B(1)-vrel(1)*B(3)); % iVi in-track
Pzi=-(vrel(1)*B(2)-vrel(2)*B(1)); % iVi out of plane
Pxr=4*rhor*rhoc*mmc*ILM(1)^2; % i^2R radial
Pyr=4*rhor*rhoc*mmc*ILM(2)^2; % i^2R in-track
Pzr=4*rhor*rhoc*mmc*ILM(3)^2; % i^2R out of plane
Pwri=Pxi+Pyi+Pzi; % total iVi

```

```

Pwrr=Pxr+Pyr+Pzr; % total  $1^{-2}R$ 

sumP=(Pwri+Pwrr); % total [P_s]

% ----- Cross product for forces -----

Fr=ILM(2)*B(3)-ILM(3)*B(2); % radial force (kg-m/sec^2)
Fu=ILM(3)*B(1)-ILM(1)*B(3); % In-track force (kg-m/sec^2)
F3=ILM(1)*B(2)-ILM(2)*B(1); % out-of-plane force (kg-m/sec^2)

% ----- Collect output -----

%          1      2-4      5      6      7-9  10  11  12
data(i,:)= [v*180/pi xzi' phi*180/pi lam*180/pi B' Fr Fu F3];

%          1      2-4  5-7
datab(i,:)= [lamm*180/pi Bcm' Bci'];

%          1      2-4      5      6
datam(i,:)= [v*180/pi xyzm' lamm*180/pi phim*180/pi];

%dttest(i,:)= [v*180/pi xzi' xziI']; % Debug code
%dttest(i,:)= [v*180/pi 1 0 0 rtp']; % Debug code

%          1      2  3  4  5-7  8
dat(i,:)= [v*180/pi Fr Fu F3 ILM ilm];

%          1      2  3      4      5      6      7
elem(i,:)= [v*180/pi a e I*180/pi RAAN*180/pi atan2(p1,p2)*180/pi M*180/pi];
A3(i,1)=a3;

P(i,:)= [Pxi Pyi Pzi Pxr Pyr Pzr Pwri Pwrr sumP];
% ----- Propagate elements -----

lagrange; % Subroutine Lagrange integrates
          % Lagrange's planetary equations

i=i+1; % Update matrix index
end
toc

subplot(2,2,1)
plot(elem(:,1),P(:,1),':',elem(:,1),P(:,2),'-.',elem(:,1),P(:,3),'--',
% elem(:,1),P(:,4),'-') % This line is a continuation of the
                        % previous one

```

```

ylabel('Specific power (W/kg)')

subplot(2,2,2)
plot(elem(:,1),elem(:,4))
ylabel('Inclination')

subplot(2,2,3)
plot(elem(:,1),dat(:,2),'y',elem(:,1),dat(:,3),'r',elem(:,1),dat(:,4),'g',
% elem(:,1),A3,'w') % This line is a continuation of the
% previous one.
%plot(dat(:,1),dat(:,4),dat(:,1),A3)
ylabel('Acceleration (m/sec^2)')

subplot(2,2,4)
plot(elem(:,1),dat(:,5),elem(:,1),dat(:,6),'r',elem(:,1),dat(:,7),'g')
ylabel('IL/m')

m=size(P,1); % Number of rows in P
energy=(.5*(P(1,4)+P(m,4))+sum(P(2:m-1,4)))*ts % Trapezoidal integration
maxP=max(P)
avgP=energy/(tf-to) % [bar over P_s] (W/kg)
da=a-6578000 % Change in a (m)
I=I+180/pi
disp('hit a key')
pause
subplot(2,2,1)
plot(elem(:,1),elem(:,5))
ylabel('RAAN')

subplot(2,2,2)
plot(elem(:,1),debug(:,4))
ylabel('h')

subplot(2,2,3)
plot(elem(:,1),elem(:,2))
ylabel('semi-major axis')

subplot(2,2,4)
plot(elem(:,1),elem(:,3))
ylabel('k')

```

The script raan.m was used for  $\Omega$  change study.

```
% variable names in square brackets are the names of the variables
% used in the main body of the thesis.
tic
% -----Get started -----

i=1; % Counter for matrices at end
n=1.18339e-3; % Mean motion (rad/sec)
alfao=0.; % Inertial longitude of Greenwich
% meridian at beginning of time span
% (rad) [theta_g_0]
alfadot=7.292462056e-5; % Rotational rate of Earth (rad/sec)
% [omega_o+]
r=6578000; % Initial radius (m)
Mag=8.05e15; % Magnetic moment [script M]
% (kg/m^3-coul-sec)
RAAN=0; % Right ascension of ascending node
% [cap Omega] (rad)
a=r; % Semi-major axis (m)
e=0.; % Eccentricity
w=0.; % Argument of perigee (rad)
% [little omega]
Mo=0; % Mean anomaly at epoch (rad) [M_o]
rhor=2.8e-8; % Conductor resistivity (ohm-m)
% [rho_R]
rhoc=2700; % Conductor mass density (kg/m^3)
% [rho_c]
mass=1; % Total vehicle mass (kg) [m]
Mu=3986012e14; % Gravitational parameter of the
% Earth (m^2/s^2) [mu]
mmc=10; % Conductor mass ratio [m/m_c]
RAANDotbar=2.0257e-7; I=pi/2; % RAANDotbar is desired average
% RAAN change rate (rad/sec)
% [bar over dot over Omega]
% I is inclination (rad)
% True polar sun synchronous case
% I=45 deg sun synchronous
% .1 deg/day, I=90
% -.1 deg/day, I=45
% Equinoctial element [h]
% Equinoctial element [k]
% Mean anomaly (rad)
% Argument of latitude (rad)[u]

%RAANDotbar=-2.0257e-07; I=pi/4;
%RAANDotbar=2.0257e-8; I=pi/2;
%RAANDotbar=-2.0257e-08; I=pi/4;
p1=0;
p2=0;
M=0;
v=0;

% -----Initialize magnetic field rotation matrix -----
```

```

phio=pi/2-78.3*pi/180;
lamo=69*pi/180;

Rmag=[cos(lamo)*cos(phio) -sin(lamo)*cos(phio) -sin(phio)
      sin(lamo)           cos(lamo)           0
      cos(lamo)*sin(phio) -sin(lamo)*sin(phio) cos(phio)];

% Note: Rmag rotates from Earth's cartesian frame to magnetic cartesian
% frame Rmag=[R^gb]

% ----- Here is the main loop -----

for t=to:ts:tf                                % t is the time (sec)
                                                % ts is the time step (sec)
                                                % tf is the final time (sec)

p=a*(1-e^2);                                  % Semi-latus rectum (m)

%if rem(i,10)==0                               % This puts out a message to let you
%[v*180/pi w*180/pi]                          % know where the program is if you
%end                                             % want it to

r=p/(1+e*cos(v));

alfa=alfao+alfadot*t;                         % Rotates the Earth

% ----- Create rot matrix from orbital frame to cart inert -----
r11=cos(RAAN)*cos(v)-sin(RAAN)*cos(I)*sin(v);
r12=-cos(RAAN)*sin(v)-sin(RAAN)*cos(I)*cos(v);
r13=-sin(RAAN)*sin(I);

r21=sin(RAAN)*cos(v)+cos(RAAN)*cos(I)*sin(v);
r22=-sin(RAAN)*sin(v)+cos(RAAN)*cos(I)*cos(v);
r23=-sin(I)*cos(RAAN);

r31=sin(v)*sin(I);
r32=sin(I)*cos(v);
r33=cos(I);

Ro2ci=[r11 r12 r13                            % [R^-1a]
      r21 r22 r23
      r31 r32 r33];

```

```

% ----- Rotate [r 0 0] in sperical coord into [x y z] inertial -----
xyzi=Ro2ci*[r 0 0]';

% ----- Rotate xyzi into xyzE -----

Rci2cE=rot(0,alfa-alfao);           % Rci2cE rotates from cartesian
                                     % inertial frame to Earth's
                                     % rotating cartesian frame [R^gi]

xyzE=Rci2cE*xyzi;

% ----- rotate xyzE into magnetic cartesian frame -----

xyzm=Rmag*xyzi;

% ----- Compute lat and long in mag frame -----

phim=atan2(xyzm(3),(xyzm(1)^2+xyzm(2)^2)^.5);
lamm=atan2(xyzm(2),xyzm(1));

% ----- Compute magnetic field components -----

z=2*Mag*sin(phim)/r^3;                % Radial component (kg/coul-sec)
h=-Mag*cos(phim)/r^3;                % Transverse component (toward
                                     % north pole) (kg/coul-sec)

% -Compute rot matrix to go from spherical magnetic to cartesian magnetic-

Rsm2cm=rot(phim,lamm);                % [R^bm]

% ----- Rotate [z 0 h] into cartesian magnetic frame -----

Bcm=Rsm2cm*[z 0 h]';                 % (kg/coul-sec)

% ----- Rotate Bcm into Earth's rotating cartesian frame -----

BcE=Rmag'*Bcm;

% ----- Rotate BcE into cartesian inertial frame -----

Bci=Rci2cE'*BcE;                     % (kg/coul-sec)
xyzi=Rci2cE'*xyzE;                   % Debug code: xyzi=xyzi if all
                                     % rotations are correct

```

```

% ----- Rotate Bci into orbital frame -----

B=Ro2ci'*Bci;                                % (kg/coul-sec)

rtp=Ro2ci'*xyzI;                             % Debug code - rtp=[r 0 0] if all
                                              % rotations are correct;

% ----- Compute kappa vector -----
b=B/norm(B);
d=[b(2) -b(1) 0]/sqrt(b(2)^2+b(1)^2); % kappa unit vector [kappa hat]

a3=RAANdotbar*2*n*a*sin(I)*sin(v);          % Out of plane acceleration
                                              % (m/sec^2) [f_3]

ilm=a3/sqrt(B(1)^2+B(2)^2);                  % Scalar il/m (A-m/kg) [kappa]

ILM=ilm*d;                                    % IL/m vector [kappa vector]

if max(abs(ILM))>200                          % Sorry, no infinite kappa
    ILM=200*ILM/max(abs(ILM));
end

% ----- Power requirements -----
vmagE=[-alfadot*xyzE(2) alfadot*xyzE(1) 0]'; % B field velocity [v_B]
                                              % in the f frame

vmagi=Rci2cE'*vmagE;                         % v_B in the i frame

vmago=Ro2ci'*vmagi;                          % v_B in the a frame

vrel=[r*e*sin(v)*n/(1+e*cos(v)) r*n 0]'-vmago; % v_rel

Pxi=-(vrel(2)*B(3)-vrel(3)*B(2));             % iVi radial
Pyi=-(vrel(3)*B(1)-vrel(1)*B(3));             % iVi in-track
Pzi=-(vrel(1)*B(2)-vrel(2)*B(1));             % iVi out of plane
Pxr=4*rhor*rhoc*mmc*ILM(1)^2;                % i^2R radial
Pyr=4*rhor*rhoc*mmc*ILM(2)^2;                % i^2R in-track
Pzr=4*rhor*rhoc*mmc*ILM(3)^2;                % i^2R out of plane
Pwri=Pxi+Pyi+Pzi;                            % total iVi
Pwrr=Pxr+Pyr+Pzr;                            % total i^2R

sumP=(Pwri+Pwrr);                            % total [P_s]

% ----- Cross product for forces -----

```

```

Fr=ILM(2)*B(3)-ILM(3)*B(2);           % radial force (kg-m/sec^2)
Fu=ILM(3)*B(1)-ILM(1)*B(3);           % In-track force (kg-m/sec^2)
F3=ILM(1)*B(2)-ILM(2)*B(1);           % out-of-plane force (kg-m/sec^2)

% ----- Collect output -----

%           1       2-4       5       6       7-9  10  11  12
data(i,:)=[v*180/pi xyzi' phi*180/pi lam*180/pi B' Fr Fu F3];

%           1       2-4  5-7
datab(i,:)=[lamm*180/pi Bcm' Bci'];

%           1       2-4       5       6
datam(i,:)=[v*180/pi xyzm' lamm*180/pi phim*180/pi];

%dttest(i,:)=[v*180/pi xyzi' xyzI'];   % Debug code
%dttest(i,:)=[v*180/pi 1 0 0 rtp'];     % Debug code

%           1       2   3  4 5-7  8
dat(i,:)=[v*180/pi Fr Fu F3 ILM ilm];

%           1       2 3   4       5       6       7
elem(i,:)=[v*180/pi a e I*180/pi RAAN*180/pi atan2(p1,p2)*180/pi M*180/pi];
A3(i,1)=a3;

P(i,:)=[Pxi Pyi Pzi Pxr Pyr Pzr Pwri Pwrr sumP];
% ----- Propagate elements -----

lagrange;                               % Subroutine Lagrange integrates
                                         % Lagrange's planetary equations

i=i+1;                                   % Update matrix index
end
toc

subplot(2,2,1)
plot(elem(:,1),P(:,1),'-',elem(:,1),P(:,2),'-.',elem(:,1),P(:,3),'--',
% elem(:,1),P(:,4),'-')                % This line is a continuation of the
                                         % previous one
ylabel('Specific power (W/kg)')

subplot(2,2,2)
plot(elem(:,1),elem(:,4))
ylabel('Inclination')

```

```

subplot(2,2,3)
plot(elem(:,1),dat(:,2),'y',elem(:,1),dat(:,3),'r',elem(:,1),dat(:,4),'g',
% elem(:,1),A3,'w') % This line is a continuation of the
% previous one
%plot(dat(:,1),dat(:,4),dat(:,1),A3)
ylabel('Acceleration (m/sec^2)')

subplot(2,2,4)
plot(elem(:,1),dat(:,5),elem(:,1),dat(:,6),'r',elem(:,1),dat(:,7),'g')
ylabel('IL/m')

m=size(P,1); % Number of rows in P
energy=(.5*(P(1,4)+P(m,4))+sum(P(2:m-1,4)))*ts % Trapezoidal integration
maxP=max(P)
avgP=energy/(tf-to) % [bar over P_s] (W/kg)
da=a-6578000 % Change in a (m)
I=I+180/pi
disp('hit a key')
pause
subplot(2,2,1)
plot(elem(:,1),elem(:,5))
ylabel('RAAN')

subplot(2,2,2)
plot(elem(:,1),debug(:,4))
ylabel('h')

subplot(2,2,3)
plot(elem(:,1),elem(:,2))
ylabel('semi-major axis')

subplot(2,2,4)
plot(elem(:,1),elem(:,3))
ylabel('k')

```

The script `lagrangeir.m` is called by `inc.m` and `raan.m`. It evaluates Lagrange's planetary equations and integrates the orbital elements used in the plane change studies.

```
% This file implements Lagrange's planetary equations
% Square brackets denote the nomenclature used in the thesis writeup

adot=2*e*sin(v)/(n*sqrt(1-e^2))*Fr/mass+2*a*sqrt(1-e^2)/(n*r)*Fu/mass;
Idot=((r*cos(w+v))/(n*a*a*sqrt(1-e^2)))*F3/mass;
RAANdot=((r*sin(w+v))/(n*a*a*sqrt(1-e^2)*sin(I)))*F3/mass;

dM=n-2*Fr/(a*n*mass)-sin(theta)*F3/(tan(I)*a*n*mass); % This is [ds/dt]

% p1 is [h]
% Next line is first two terms of the h dot eqtn
pidotru=-cos(theta)*Fr/(n*a*mass)+(p1*r+(r+a)*sin(theta))*Fu/(n*a^2*mass);

% Next line is the last term of the h dot eqtn
pidot3=-p2*r*sin(theta)*F3/(n*a^2*tan(I));

pidot=pidotru+pidot3; % This is all three terms

% p2 is [k]
% Next line is the first two terms of the k dot eqtn
p2dotru=sin(theta)*Fr/(n*a*mass)+((r+a)*cos(theta)+p2*r)*Fu/(n*a^2*mass);

% Next line is the third term of the k dot eqtn
p2dot3=p1*r*sin(theta)*F3/(n*a^2*tan(I));

p2dot=p2dotru+p2dot3; % This is all three terms

%dn=-1.5*sqrt(Mu/a^5)*adot;

% Next lines are the Euler integration of elements
p1=p1+pidot*ts;
p2=p2+p2dot*ts;
a=a+adot*ts;
e=sqrt(p1^2+p2^2);
v=dM*ts+v; % This is [s]
I=I+Idot*ts;
RAAN=RAAN+RAANdot*ts;

debug(i,:)= [i t rem(v*180/pi,360) p1 p2 sqrt(p1^2+p2^2)]; % Debug data
% collection
```

The script molniya.m was used for the Molniya stationkeeping study:

```
tic
% Variable names in square brackets are those used in the main body of
% the thesis.
% This is the file used to investigate the following designer orbit:

% inclination: 90 deg
% period: 86160 s (~24 hr)
% rotation of argument of perigee: 0 deg/day

% -----Get started -----

i=1;                                % Counter for matrices at end
n=2*pi/86160      ;                % Mean motion (rad/sec)
alfao=0.;          % Inertial longitude of Greenwich
                                % meridian at beginning of time span
                                % (rad) [little omega_o plus_o]
alfadot=7.292462056e-5;            % Rotational rate of Earth (rad/sec)
                                % [little omega_o plus]
Mag=8.05e15;                  % Magnetic moment (kg-m^3/coul-sec)
                                % [script M]
I=pi/2;                      % Inclination (rad)
mass=1;                      % mass (kg) [m]
Mu=3.986012e14;              % gravitational parameter (m^3/s^2);
e=.82501;                    % Eccentricity
w=1.5*pi;                    % Argument of perigee (omega) [rad]
M=pi;                        % Mean anomaly (rad)
ke=-2.67542e25;              % term for Earth's oblateness equal
                                % to G times mass of the Earth
                                % see section 4.1 (units?)
                                % omega change rate (rad/sec)
wdot=0;                      % omega change rate (rad/sec)
rhor=2.8e-8;                  % Conductor resistivity (ohm-m)
rhoc=2700;                    % Conductor mass density (kg/m^3)
wdotbar=-3.8e-7              % Desired omega change rate
                                % (rad/sec). This value has to be
                                % adjusted to obtain the desired
                                % change in omega. The nominal value
                                % is wdotbar=-5.406e-7 rad/sec
                                % RAANo is initial RAAW (rad)
RAANo=RAAN

% -----Init mag field rotation matrix -----

phio=pi/2-78.3*pi/180;
lamo=69*pi/180;
```

```

Rmag=[cos(lam0)*cos(phio) -sin(lam0)*cos(phio) -sin(phio)
      sin(lam0)           cos(lam0)           0
      cos(lam0)*sin(phio) -sin(lam0)*sin(phio) cos(phio)];

% Note: Rmag rotates from Earth's cartesian frame to magnetic cartesian
% frame. Rmag is [R^gb]

% ----- Here is the main loop -----

for t=to:ts:tf                                % t is the time (sec)
                                                % ts is the time step (sec)
                                                % tf is the final time (sec)

p=a*(1-e^2);                                  % Semi-latus rectum (m)

%if rem(i,10)==0                               % This puts out a message to let you
%[v*180/pi w*180/pi]                          % where the program is if you want
%end                                             % it to

Eo=M;                                           % Begin algorithm to solve for E
E=kepler(M,Eo,e);
for j=1:10
if abs(E-Eo)>1.0E-9
Eo=E;
E=kepler(M,E,e);
else end
end                                             % End algorithm to solve for E

v=acos((e-cos(E))/(e*cos(E)-1));              % True anomaly from E

if sin(M)<0                                     % Quadrant check
v=-v;
end

r=p/(1+e*cos(v));                             % r calculation
vsat=[e*sin(v)*sqrt(Mu/p) (1+e*cos(v))*sqrt(Mu/p) 0]; % velocity in a frame

alfa=alfao+alfadot*t;                        % Rotates the Earth

% ----- Create rot matrix from orbital frame to cart inert -----
r11=cos(RAAN)*cos(v+w)-sin(RAAN)*cos(I)*sin(v+w);
r12=-cos(RAAN)*sin(v+w)-sin(RAAN)*cos(I)*cos(v+w);

```

```

r13=-sin(RAAN)*sin(I);

r21=sin(RAAN)*cos(v+w)+cos(RAAN)*cos(I)*sin(v+w);
r22=-sin(RAAN)*sin(v+w)+cos(RAAN)*cos(I)*cos(v+w);
r23=-sin(I)*cos(RAAN);

r31=sin(v+w)*sin(I);
r32=sin(I)*cos(v+w);
r33=cos(I);

Ro2ci=[r11 r12 r13
        r21 r22 r23
        r31 r32 r33];          % [R^-ia]

% ----- Rotate [r 0 0] in sperical coord into [x y z] inertial -----
xyzi=Ro2ci*[r 0 0]';

% ----- Rotate xyzi into xyzE -----
Rci2cE=rot(0,alfa-alfao);      % Rci2cE rotates from cartesian
                                % inertial frame to Earth's rotating
                                % cartesian frame [R^-gi]

xyzE=Rci2cE*xyzi;

% ----- Compute lat and long in g frame -----
phiE=atan2(xyzE(3),(xyzE(1)^2+xyzE(2)^2)^.5); % latitude (rad)
lamE=atan2(xyzE(2),xyzE(1));               % longitude (rad)

% ----- rotate xyzE into magnetic cartesian frame -----
xyzm=Rmag*xyzi;

% ----- Compute lat and long in mag frame -----
phim=atan2(xyzm(3),(xyzm(1)^2+xyzm(2)^2)^.5);
lamm=atan2(xyzm(2),xyzm(1));

% ----- Compute magnetic field components -----
z=2*Mag*sin(phim)/(r^3);          % Radial component (kg/coul-sec)

```

```

h=-Mag*cos(phim)/(r^3);                                % Transverse component (toward
                                                         % north pole) (kg/coul-sec)
                                                         % See Tascione for details

%- Compute rot matrix to go from spherical magnetic to cartesian magnetic -

Rsm2cm=rot(phim,lamm);                                % [R^bm]

% ----- Rotate [z 0 h] into cartesian magnetic frame -----
Bcm=Rsm2cm*[z 0 h]';                                % (kg/coul-sec)

% ----- Rotate Bcm into Earth's rotating cartesian frame -----
BcE=Rmag'*Bcm;

% ----- Rotate BcE into cartesian inertial frame -----
Bci=Rci2cE'*BcE;                                % (kg/coul-sec)
xyzI=Rci2cE'*xyzE;                                % Debug code: xyzI=xyzi if all
                                                         % rotations are correct

% ----- Rotate Bci into orbital frame -----
B=Ro2ci'*Bci;                                % (kg/coul-sec)
rtp=Ro2ci'*xyzI;                                % Debug code - rtp=[r 0 0] if all
                                                         % rotations are correct;

% ----- Compute kappa vector -----
fr=(ke*(1-3*(sin(w+v)*sin(I))^2))/(r^4); % radial acceleration (m/sec^2)
fu=(ke*sin(2*(w+v))*(sin(I)^2))/(r^4); % in-track acceleration (m/sec^2)
fl=ke*sin(w+v)*sin(2*I)/(r^4); % out of plane acceleration (m/s^2)

sub_wdoto                                % Calculates the effect of the
                                                         % Earth's oblateness

% ----- Compute IL/m vector -----
ILM=[0 0 0]';

if cos(v)>0.1;                                % Limit thrusting to this region

a1=sqrt(1-e^2)/(n*a*e);                                % [k_1]
b1=1+1/(1+e*cos(v));                                % [k_2]

```

```

% Next two lines are [kappa_theta]
ILM(2)=-wdotbar/(-a1*b1^2*sin(v)^2*B(3)/cos(v)-a1*cos(v)*B(3)-
a1*(cos(v)*B(2)+b1*sin(v)*B(1))^2/(cos(v)*B(3)));

ILM(1)=b1*tan(v)*ILM(2); % [kappa_r]
ILM(3)=-ILM(2)*(cos(v)*B(2)+b1*sin(v)*B(1))/(cos(v)*B(3)); % [kappa_3]

ILMck=1.01*ILM; % Check to ensure function has been
if norm(ILMck)-norm(ILM)<0 % minimized
disp('Warning - non-minimum power at')
[i t v*180/pi]
end

if max(abs(ILM))>500 % Limit magnitude of kappa if
ILM=500*ILM/max(abs(ILM)); % necessary
end

end

% ----- Cross product for forces -----

F1=ILM(2)*B(3)-ILM(3)*B(2); % radial force (kg-m/sec^2)
F2=ILM(3)*B(1)-ILM(1)*B(3); % In-track force (kg-m/sec^2)
F3=ILM(1)*B(2)-ILM(2)*B(1); % out-of-plane force (kg-m/sec^2)

Fr=F1+fr; % Combines effects of Earth
Fu=F2+fu; % oblateness and thrusting
Fl=F3+fl; % fr, fu, and fl come from
%Fu=2*fu; % sub_wdoto

% ----- Power requirements -----
vmagE=[-alfadot*xyzE(2) alfadot*xyzE(1) 0]'; % B field velocity [v_B]
% in the g frame
vmagi=Rci2cE'*vmagE; % v_B in the i frame
vmago=Ro2ci'*vmagi; % v_B in the a frame

vrel=vsat'-vmago; % v_rel

% Next two lines are the power due to the induce voltage
Pi=-((vrel(2)*B(3)-vrel(3)*B(2))*ILM(1)+(vrel(3)*B(1)-vrel(1)*B(3))*ILM(2)
+(vrel(1)*B(2)-vrel(2)*B(1))*ILM(3));

% Next 3 lines are the power due to resistance in the radial, in-track,
% and out of plane conductors respectively

```

```

Px=-(vrel(2)*B(3)-vrel(3)*B(2))*ILM(1)+4*rhor*rhoc*mmc*ILM(1)^2;
Py=-(vrel(3)*B(1)-vrel(1)*B(3))*ILM(2)+4*rhor*rhoc*mmc*ILM(2)^2;
Pz=-(vrel(1)*B(2)-vrel(2)*B(1))*ILM(3)+4*rhor*rhoc*mmc*ILM(3)^2;
sumP=(Px+Py+Pz);

% ----- Collect output -----

%           1           2-4           5           6           7-9           10           11 12 13
data(i,1:13)=[v*180/pi xyzi' phiE*180/pi lamE*180/pi B' theta*180/pi Fr Fu F3];

%           1           2-4 5-7
datab(i,1:7)=[lamm*180/pi Bcm' Bci'];

%           1           2-4           5           6
datam(i,1:6)=[v*180/pi xyzm' lamm*180/pi phim*180/pi];
dtest(i,1:7)=[v*180/pi xyzi' xyzI']; % Debug code
dtest(i,1:7)=[v*180/pi 1 0 0 rtp'/r]; % Debug code

P(i,:)= [Pi Px Py Pz sumP];
%           1           2           3           4           5           6 7 8
dat(i,1:8)=[v*180/pi t I*180/pi RAAN*180/pi (1.5*pi-w)*180/pi Fr Fu F3];

%           1           2           3           4           5 6 7 8 9 10 11
angles(i,1:4)=[ t v*180/pi M*180/pi E*180/pi];
kep(i,1:8)=[ t v*180/pi a e I RAAN w Mo];
forces(i,1:11)=[t v*180/pi fr fu fl F1 F2 F3 Fr Fu Fl];
current(i,1:5)=[t v*180/pi ILM'];
Wdot(i,1:3)=[wdot wdoto wdot+wdoto];
elem(i,:)= [t a e I*180/pi RAAN*180/pi]; % w*180/pi; % Mo*180/pi];
% ----- Propagate elements -----

lagrange;
i=i+1; % Update matrix index

end % End of the integration
toc
% m=size(P,1);
energy=(.5*(P(347,5)+P(373,5))+sum(P(348:372,5)))*ts % Trapezoidal int.
P100=energy/tf % Power averaged over entire orbit
pbar=energy/3240 % Power average over thrust period

dw=(w-1.5*pi)*180/pi % Change in argument of perigee
dI=(I-pi/2)*180/pi % Change in I
dRAAN=(RAAN-RAANo)*180/pi % Change in RAAN
da=(a-42162862)/1000 % Change in a

```

de=e-.82501

% Change in e

elem(:,1)=dat(:,1);

elem(1,1)=-180;

dat(1,1)=-180;

subplot(2,2,1)

plot(dat(:,1),dat(:,5))

ylabel('delta argument of perigee')

subplot(2,2,2)

plot(dat(:,1),forces(:,6),'y',dat(:,1),forces(:,7),'r',dat(:,1),forces(:,8),  
'g')

ylabel('Acceleration (m/sec<sup>2</sup>)')

subplot(2,2,3)

plot(elem(:,1),current(:,3),elem(:,1),current(:,4),'r',elem(:,1),current(:,  
5),'g')

ylabel('IL/m (A-m/kg)')

subplot(2,2,4)

plot(dat(:,1),P(:,1),'',dat(:,1),P(:,2),'y',dat(:,1),P(:,3),'r',dat(:,1),P  
(:,4),'g',dat(:,1),P(:,5),'b')

ylabel('Specific power (W/kg)')

%disp('Hit any key to continue')

%pause

subplot(2,2,1)

plot(elem(:,1),elem(:,4))

ylabel('Inclination')

subplot(2,2,2)

plot(elem(:,1),elem(:,5))

ylabel('RAAN')

subplot(2,2,3)

plot(elem(:,1),elem(:,2))

ylabel('semi-major axis')

subplot(2,2,4)

plot(elem(:,1),elem(:,3))

ylabel('eccentricity')

The script `lagrangem.m` is called by `molniya.m`. It evaluates Lagrange's planetary equations and integrates the orbital elements used in the Molniya stationkeeping study.

```
% This file integrates the orbital elements according to Lagrange's
% planetary equations
```

```
adot=2*e*sin(v)/(n*sqrt(1-e^2))*Fr/mass+2*a*sqrt(1-e^2)/(n*r)*Fu/mass;
edot=sqrt(1-e^2)*sin(v)/(n*a)*Fr/mass+sqrt(1-e^2)/(n*a^2*e)*(a^2*(1-e^2)/r
-r)*Fu/mass;
Idot=((r*cos(w+v))/(n*a*a*sqrt(1-e^2)))*F3/mass;
RAANdot=((r*sin(w+v))/(n*a*a*sqrt(1-e^2)*sin(I)))*F3/mass;
wdot1=-(sqrt(1-e^2)/(n*a*e))*(cos(v)*Fr/mass);           % 1st term
wdot3=-r*(1/tan(I))*sin(w+v)*F3/(n*a*a*sqrt(1-e^2)*mass); % 2nd term
wdot2=(sqrt(1-e^2)/(n*a*e))*(1+1/(1+e*cos(v)))*sin(v)*Fu/mass; % 3rd term
wdot=wdot1+wdot2+wdot3;           % All 3 terms of eqtn 13
```

```
dM=n-(2*r/a-(1-e^2)*cos(v)/e)*Fr/(mass*n*a)
-(1-e^2)*(1+r/(a*(1-e^2)))*sin(v)*Fu/(n*a*e*mass);           % Eqtn 17
```

```
% Euler integration
a=a+adot*ts;
e=e+edot*ts;
M=dM*ts+M;
w=w+wdot*ts;
I=I+Idot*ts;
RAAN=RAAN+RAANdot*ts;
```

```
% Debug data collection
debug(i,:)= [i t v*180/pi wdot1 wdot2 wdot3 wdot];
```

Function `kepler.m` solves Kepler's equation. It is called by `molniya.m`.

```
function E=kepler(M,Eo,e)
E=Eo-(Eo-e*sin(Eo)-M)/(1-e*cos(Eo));
```

```
% This function is used to iteratively find E from M and e.
% Eo is a guess of E. Repeat the function until Eo converges to E.
```

Function `rotate.m` generates a rotation matrix given two rotation angles. It is called by `inc.m`, `raan.m`, and `molniya.m`.

```
function [R] = rot (phi,lam)
R=[cos(lam)*cos(phi) -sin(lam) -cos(lam)*sin(phi)
sin(lam)*cos(phi) cos(lam) -sin(lam)*sin(phi)
sin(phi) 0 cos(phi)];
```

```
% This function calculates a rotation matrix based on the two rotation
% angles phi and lam
```

Script decaya1.m was used to study the decaying solution to the rendezvous study.

```
% This is the file used to investigate the decaying solution of the
% rendezvous problem
rhor=2.8e-8;          % Resistivity (Ohm-m) [rho_R]
rhoc=2700;            % Conductor mass density (kg/m^3)
                        % [rho_c]
mmc=10;               % Conductor mass ratio [m/m_c]
r=6578000;            % Radius of target (m)
n=1.1834e-03;         % Mean motion (rad/sec)
alfadot=7.292462056e-5; % Angular velocity of the Earth's
                        % rotation (rad/sec)
xdo=0;ydo=-3*xo*n/2;  % Calculate initial velocities as a
                        % function of initial position
tf=.99*2*pi/n          % tf is the time period in which the
                        % rendezvous is to be performed.
                        % See the file for the polynomial
                        % solution for an explanation of the
                        % .99 value.

B=[0 0 -2.8282e-05];  % B field vector

ao=(a1^2)/4;          % The ao coefficient
s=a1/2;               % This is [p] in chapter 5
bx=xo;                % More constants
x=xdo+s*xo;
by=yo;
cy=ydo+s*yo;

j=0;
for i=0:30:tf          % Integrates the equations. The time
                        % step is 30 sec.

t=i;

x=exp(-s*t)*(bx+cx*t); % x soln
xd=exp(-s*t)*(-s*bx-s*cx*t+cx);

y=exp(-s*t)*(by+cy*t); % y soln
yd=exp(-s*t)*(-s*by-s*cy*t+cy);

fx=-2*n*yd-a1*xd-(ao+3*n^2)*x; % radial acceleration
fy=2*n*xd-a1*yd-ao*y;          % in-track acceleration
X(j+1,:)=[x y xd yd t];

u(j+1,:)=[fx fy];
```

```

IL1=-fy/B(3);
IL2=fx/B(3);
IL3=0;
vy=(n-alfadot)*r;
Pi=-IL1*vy*B(3);
Px=4*rhor*rhoc*mmc*IL1^2;
Py=4*rhor*rhoc*mmc*IL2^2;
sumP=Pi+Px+Py;

% [kappa_r]
% [kappa_theta]
% [kappa_3]
% v_rel
% power due to induced voltage
% radial i^2R power
% in-track i^2R power
% total power

IL(j+1,:)=[IL1 IL2 IL3];
P(j+1,:)=[Pi Pi+Px Py sumP];

dat(j+1,1)=t;
j=j+1;
end

subplot(2,2,1)
plot(X(:,2)/1000,X(:,1)/1000,'.')
axis([-1.1 1.1 -1.1 1.1])
xlabel('y (km)')
ylabel('x (km)')

subplot(2,2,3)
plot(dat(:,1),X(:,3),':',dat(:,1),X(:,4),'-');
ylabel('v_x & v_y (m/sec)')
ax=axis;
axis([ax(1) 5256 ax(3:4)]);
xlabel('Time (sec)');

subplot(2,2,2)
plot(dat(:,1),u(:,1),':',dat(:,1),u(:,2),'-');
%ax=axis;axis([0 180 ax(1,3) ax(1,4)])
ylabel('f_x & f_y (m/sec)')
xlabel('Time (sec)')
ax=axis;
axis([ax(1) 5256 ax(3:4)]);

subplot(2,2,4)
plot(dat(:,1),P(:,2),':',dat(:,1),P(:,3),'-',dat(:,1),P(:,4));
ylabel('Specific Power (W/kg)')
ax=axis;
axis([ax(1) 5256 ax(3:4)]);
xlabel('Time (sec)');

```

```

m=size(P,1);
energy=(.5*(P(1,:)+P(m,:))+sum(P(2:m-1,:)))*30 % Trapezoidal integration
Pmax=max(P)
Pbar=energy/tf % Average power

```

Script poly.m was used to study the polynomial solution to the rendezvous study.

% This is the file used to study the polynomial solution to the rendezvous  
% and docking problem

```

rhor=2.8e-8; % Resistivity (Ohm-m) [rho_R]
rhoc=2700; % Conductor mass density (kg/m^3)
% [rho_c]
mmc=10; % Conductor mass ratio [m/m_c]
r=6578000; % Radius of target vehicle (m)
n=1.1834e-03; % Mean motion (rad/sec)
alfadot=7.292462056e-5; % Angular velocity of Earth's
% rotation (rad/sec)
xdo=0;ydo=-3*xo*n/2; % Initial conditions based on xo
% and yo
tf=.99*2*pi/n % This is the time span you want to
% perform the rendezvous in. 99% of
% the orbital period is used so
% comparison can be made to a 2 burn
% rendezvous, like the example in
% Kaplan (pp 114-115). If the exact
% orbital period is used, Kaplan's
% eqtns 3.54 and 3.55 become
% singular.

B=[0 0 -2.8282e-05]; % B field vector. It is constant for
% the assumptions made in Ch 5.

j=0;

ax=xo; % Constants for the x soln
bx=xdo;

```

```

cx=-3*xdo/tf-6*xo/tf^2;
dx=3*xdo/tf^2+8*xo/tf^3;
ex=-xdo/tf^3-3*xo/tf^4;

ay=yo;
by=ydo;
cy=-3*ydo/tf-6*yo/tf^2;
dy=3*ydo/tf^2+8*yo/tf^3;
ey=-ydo/tf^3-3*yo/tf^4;

for i=0:30:tf

t=i;

x=ax+bx*t+cx*t^2+dx*t^3+ex*t^4;
xd=bx+2*cx*t+3*dx*t^2+4*ex*t^3;
xdd=2*cx+6*dx*t+12*ex*t^2;

y=ay+by*t+cy*t^2+dy*t^3+ey*t^4;
yd=by+2*cy*t+3*dy*t^2+4*ey*t^3;
ydd=2*cy+6*dy*t+12*ey*t^2;

X(j+1,:)=[x y xd yd t];

fx=xdd-2*n*yd-3*n^2*x;
fy=ydd+2*n*xd;

u(j+1,:)=[fx fy];

IL1=-fy/B(3);
IL2=fx/B(3);
IL3=0;
vy=(n-alfadot)*r;
Pi=-IL1*vy*B(3);
Px=4*rhorrhoc*mmc*IL1^2;
Py=4*rhorrhoc*mmc*IL2^2;
sumP=Pi+Px+Py;

IL(j+1,:)=[IL1 IL2 IL3];

P(j+1,:)=[Pi Pi+Px Py sumP];

dat(j+1,1)=t;

```

% Constants for the y soln  
 % Integrates the equations. Note the  
 % time step is 30 sec.  
 % x soln  
 % y soln  
 % Collect the position and velocity  
 % data  
 % Compute the accelerations  
 % [kappa\_r]  
 % [kappa\_theta]  
 % [kappa\_3]  
 % v\_rel  
 % power due to induced voltage  
 % radial i^2R power  
 % in-track i^2R power  
 % total power

```
j=j+1;
end
```

```
subplot(2,2,1)
plot(X(:,2)/1000,X(:,1)/1000,'.')
axis([-1.1 1.1 -1.1 1.1])
xlabel('y (km)')
ylabel('x (km)')
```

```
subplot(2,2,3)
plot(dat(:,1),X(:,3),':',dat(:,1),X(:,4),'-');
ylabel('v_x & v_y (m/sec)')
ax=axis;
axis([ax(1) 5256 ax(3:4)]);
xlabel('Time (sec)');
```

```
subplot(2,2,2)
plot(dat(:,1),u(:,1),':',dat(:,1),u(:,2),'-');
%ax=axis;axis([0 180 ax(1,3) ax(1,4)])
ylabel('f_x & f_y (m/sec)')
xlabel('Time (sec)')
ax=axis;
axis([ax(1) 5256 ax(3:4)]);
```

```
subplot(2,2,4)
plot(dat(:,1),P(:,2),':',dat(:,1),P(:,3),'-',dat(:,1),P(:,4));
ylabel('Specific Power (W/kg)')
ax=axis;
axis([ax(1) 5256 ax(3:4)]);
xlabel('Time (sec)');
```

```
m=size(P,1);
energy=(.5*(P(1,:)+P(m,:))+sum(P(2:m-1,:)))*30 % Trapezoidal integration
Pmax=max(P)
Pbar=energy/tf % Average power
```

### *Appendix B. Survey of Conducting Metals*

Equation (47) was derived in section 2.6.3. The last term includes the product  $\rho_R \rho_c$ , where  $\rho_R$  is the resistivity of the conducting material in Ohm-meters and  $\rho_c$  is the conductor mass density in kilograms/meter<sup>3</sup>. To minimize the last term of Equation (47), it is desirable to use a conductor with a low  $\rho_R \rho_c$  product. To find such a conductor we compile  $\rho_R$  and  $\rho_c$  values for common conducting metals (3:1324-1325) and compute  $\rho_R \rho_c$ :

Metal	$\rho_R$ (Ohm·m × 10 <sup>-8</sup> )	$\rho_c$ (kg/m <sup>3</sup> × 10 <sup>3</sup> )	$\rho_R \rho_c$ (Ohm·kg/m <sup>2</sup> × 10 <sup>-5</sup> )
Aluminum	2.66	2.7	7.2
Copper	1.68	8.9	15.0
Gold	2.42	19.3	46.7
Silver	1.63	10.5	17.1

Aluminum is the worst conductor in terms of resistivity, but its low mass density makes it the best overall conductor for electrodynamic propulsion.

### *Bibliography*

1. Bate, Roger R. and others. Fundamentals of Astrodynamics. New York: Dover Publications, 1971.
2. Battin, R. H. An Introduction to the Mathematics and Methods of Astrodynamics. New York: American Institute of Aeronautics and Astronautics, 1987.
3. Eshbach, Ovid W. and Mott Souders. Handbook of Engineering Fundamentals (Third Edition). New York: John Wiley & Sons, 1974
4. Janson, S.W. "The On-Orbit Role of Electric Propulsion." AIAA/SAE/ASME/ASEE 29th Joint Propulsion Conference and Exhibit, June 28-30 1993, Monterey CA.
5. Kaplan, Marshall H. Modern Spacecraft Dynamics & Control. New York: John Wiley & Sons, 1976.
6. Kreyszig, Erwin. Advanced Engineering Mathematics (Sixth Edition). New York: John Wiley & Sons, 1988.
7. Ladouceur, Richard J.R. Feasibility Study of Electrodynamic Propulsion in Space Using a Closed Loop Circuit. MS thesis, AFIT/GSO/ENY/93D-6, School of Engineering, Air Force Institute of Technology (AU), Wright-Patterson AFB OH, December 1993.
8. Lawrence, Richard E. An Electromagnetically-Controlled Precision Orbital Tracking Vehicle (POTV). MS thesis, AFIT/GA/ENY/92D-05. School of Engineering, Air Force Institute of Technology (AU), Wright-Patterson AFB OH, December 1992.
9. Meirovitch, Leonard. Methods of Analytical Dynamics. New York: McGraw Hill, 1970.
10. National Aeronautics and Space Administration. Space and Planetary Environment Criteria Guidelines for Use in Space Vehicle Development, 1982 (Volume 1). NASA Technical Memorandum 82478. January 1983.
11. Orear, Jay. Physics. New York: Macmillan Publishing Company, 1979.
12. Penzo, Paul A. and Paul W. Ammann. National Aeronautics and Space Administration. Tethers in Space Handbook (Second Edition). Contract Number: NASW-4341, May 1989.
13. PRO-MATLAB. Sun Workstation. Computer Software. The Mathworks Inc. 1990.
14. Spenny, C.H. and Lawrence, R.E. "A Precision Orbital Tracking Vehicle (POTkV)." AIAA/SAE/ASME/ASEE 29th Joint Propulsion Conference and Exhibit, June 28-30 1993, Monterey CA.
15. Tascione, Thomas F. Introduction to the Space Environment. Malabar FL: Orbit Book Company, 1988.
16. United States Naval Observatory. The Astronomical Almanac for the Year 1993. Washington: GPO, May 1991.
17. Wertz, James R. Spacecraft Attitude Determination and Control. Dordrecht Holland: D. Reidel Publishing Company, 1978.

18. Wiesel, William E. Class handout, MECH 636, Advanced Astrodynamics. School of Engineering, Air Force Institute of Technology, Wright-Patterson AFB OH, 4 Jan 1993.

### *Vita*

Captain Troy Irwin was born August 6, 1961 in San Antonio, Texas. He graduated from Pleasanton High School in Pleasanton, Texas in 1979 and attended The University of Texas. Upon graduation with a Bachelor of Science in Aerospace Engineering degree in May 1983, he was commissioned in the United States Air Force through the Reserve Officer Training Corps and assigned to the Air Force Satellite Control Facility at Sunnyvale Air Force Station, California. He served as a Satellite Operations Manager from 1983 to 1986, and as Chief, Computer Systems Engineering from 1986 to 1988 for Program E. In addition, he earned a Master of Science in Systems Management degree from the University of Southern California in 1986. In 1988 he was reassigned as the Milstar Flight Operations Manager in the Milstar Joint Program Office at Los Angeles Air Force Base, California, where he served until entering the Graduate School of Engineering, Air Force Institute of Technology, in May 1992. Upon graduation in December 1993, he was assigned to the 45th Spacecraft Operations Squadron, Cape Canaveral Air Force Base, Florida. Troy and his wife Vicki were married in May, 1991.

Permanent address: Rt 1, Box 138-A  
Pleasanton, Texas 78064

# REPORT DOCUMENTATION PAGE

1. AGENCY USE ONLY (Leave blank)		2. REPORT DATE December 1993		3. REPORT TYPE AND DATES COVERED Master's Thesis	
4. TITLE AND SUBTITLE ORBITAL APPLICATIONS OF ELECTRODYNAMIC PROPULSION				5. FUNDING NUMBERS	
6. AUTHOR(S) Troy Irwin					
7. PERFORMING ORGANIZATION NAME(S) AND ADDRESS(ES) Air Force Institute of Technology, WPAFB OH 45433-6583				8. PERFORMING ORGANIZATION REPORT NUMBER AFIT/GA/ENY/93D-4	
9. SPONSORING MONITORING AGENCY NAME(S) AND ADDRESS(ES) Mr Franklin Meade OLAC-PL/RKFE 9 Antares Rd Edwards AFB, CA 93524-7680				10. SPONSORING MONITORING AGENCY REPORT NUMBER	
11. SUPPLEMENTARY NOTES					
12a. DISTRIBUTION AVAILABILITY STATEMENT Distribution Unlimited				12b. DISTRIBUTION CODE	
13. ABSTRACT (Maximum 200 words) Electrodynamic propulsion (EDP) uses forces resulting from electric currents in conductors as a spacecraft travels through a magnetic field. A vehicle-independent expression for the specific power required for any maneuver is derived and used to assess EDP feasibility. Analytical expressions for the accelerations and combined current-conductor vector required to change the orbital plane or the argument of perigee are developed based on Lagrange's planetary equations. Solutions to the forced Clohessy-Wiltshire equations are developed to study in-plane rendezvous. Results show EDP can change inclination or right ascension of the ascending node at approximately 0.4 degrees/day with current spacecraft specific power technology. The effects of the Earth's oblateness on a 24 hour, 90 degree inclination Molniya orbit can be negated. Rendezvous is possible with EDP, and approaches along the target velocity vector with no altitude change are possible with current spacecraft specific power. Approaches involving altitude changes will be possible when modest spacecraft power improvements are made. EDP allows a soft dock - velocities and accelerations decay to zero as the chase vehicle approaches the target - and there is no thruster plume to impart momentum or contaminate the target.					
14. SUBJECT TERMS Electric propulsion, electrodynamic propulsion, orbital plane change, Molniya orbit, rendezvous, inclination, right ascension of the ascending node				15. NUMBER OF PAGES 123	
				16. PRICE CODE	
17. SECURITY CLASSIFICATION OF REPORT UNCLASSIFIED	18. SECURITY CLASSIFICATION OF THIS PAGE UNCLASSIFIED	19. SECURITY CLASSIFICATION OF ABSTRACT UNCLASSIFIED	20. LIMITATION OF ABSTRACT UL		